Extremely Loosely Coupled Near-Field Magneto-Inductive Ranging System : Modeling and Applications

Vighnesh Gharat

UNIVERSITÉ PARIS-EST

UNIVERSITÉ PARIS-EST

ÉCOLE DOCTORALE MSTIC

Thèse pour obtenir le grade de **docteur de l'Université Paris-Est**

Spécialité : **Electronique, Optronique et Systèmes**

Soutenue et présentée publiquement par

Vighnesh GHARAT

Dirigée par **Geneviève Baudoin** et co-encadrée par **Elizabeth Colin**

Extremely Loosely Coupled Near-Field Magneto-Inductive Ranging System: Modeling and Applications

Composition du jury :

M. LAHEURTE Jean-Marc Professeur, ESYCOM, Université Gustave Eiffel	Président
Mme. RENAUDIN Valérie Directrice de recherche, Laboratoire GEOLOC, Université Gustave Eiffel	Rapporteur
M. EL HILLALI Yassin Maître de conférences, IEMN, Université Polytechnique Hauts-de-France	Rapporteur
M. SAMAMA Nel Professeur, Samovar, Telecom SudParis, Institut Polytechnique de Paris	Examinateur
Mme. COLIN Elizabeth Professeure Associée, EFREI Paris, Allianstic	Co-encadrant de thèse
M. IVALDI Paul ELA Innovation	Co-encadrant de thèse
Mme. BAUDOIN Geneviève Professeure émérite, ESYCOM, ESIEE Paris, Université Gustave Eiffel	Directeur de thèse
M. BONZON Pierre ELA Innovation	Invité
M. RICHARD Damien VAILLANT Group	Invité

Title:

Extremely Loosely Coupled Near-Field Magneto-Inductive Ranging System: Modeling and Applications

Abstract

Low-Frequency (LF) magneto-quasistatic fields are less affected by multipath and shadow fading from obstacles when compared to the radio signals with higher frequencies, thus enabling better range estimation performance in strong multipath and Non-Line-of-Sight (NLOS) environments. Traditional near-field RFID systems based on inductive coupling suffer from the low range of operation and thus are limited in use cases. Although increasing the loop sizes increases the operational range of inductively coupled systems, this solution is not suitable where compact and easy-to-deploy systems are needed. Considering these aspects, a dual-frequency-RFID system for ranging and positioning based on Near-Field Magneto Inductive (NFMI) communication is presented. This system makes use of magnetic field strength for range estimation.

The presented dual-frequency-RFID system relies on 125 kHz signal for range estimation while the data communication is handled at 433 MHz. The system consists of LF transmitters which generate magneto-quasistatic fields, active RFID tags which serve as LF receiver and Ultra-High-Frequency (UHF) transmitter, and UHF readers which capture the magnetic field strength information and identification data of the LF transmitters and the tags. The LF receiver on the tag measures the magnetic field strength which can be used for range estimation. This kind of architecture increases the use cases of the system and enables various range-estimation based application scenarios for the system such as access control, security, and real-time localization. As the presented work is a part of the ANRT CIFRE research partnership contract, it is carried out considering the industrial needs and constraints.

The main contributions made by the presented work are:

1. Modelization of inductive coupling in extremely loosely coupled systems
2. Optimization of the system for large operational range and compactness

3. Evaluation of the influence of tag orientation for a 3D antenna with simplified processing

4. Evaluation of the influence of ferromagnetic materials on the signal produced by the system

5. Evaluation of the performance of the presented system in terms of distance-estimation-based applications and comparing it with existing solutions based on UHF and Ultra-Wide Band (UWB) technologies.

Keywords

Ranging, LF, NFMI, extremely loosely coupled systems, quasi-static magnetic fields, magnetic field strength measurements.

Titre :

Système magnéto-inductif d'estimation de distance en champ proche très faiblement couplé : modélisation et applications

Résumé

Les champs magnéto-quasistatiques à basse fréquence (BF) sont moins affectés par les trajets multiples et les effets de masquage dus aux obstacles que les signaux radioélectriques à fréquences plus élevées, ce qui permet de meilleures performances d'estimation de la distance dans les environnements de propagation à trajets multiples et sans trajet direct (*NLOS - Non-Line-of-Sight*). Les systèmes RFID traditionnels en champ proche basés sur le couplage inductif couvrent une plage de fonctionnement limitée. Bien que l'augmentation de la taille des boucles augmente la plage opérationnelle des systèmes à couplage inductif, cette solution ne convient pas lorsque des systèmes compacts et faciles à déployer sont nécessaires. Compte tenu de ces aspects, un système bi-fréquence-RFID basé sur la communication *NFMI* (*Near-Field Magneto Inductive*) est présenté. Ce système utilise l'intensité du champ magnétique pour l'estimation de la distance.

Le système bi-fréquence-RFID présenté utilise un signal de fréquence 125 kHz pour l'estimation de la distance, tandis que la communication des données s'effectue à 433 MHz. Le système comprend des émetteurs BF générant des champs magnéto-quasistatiques, des étiquettes RFID actives servant de récepteur BF et d'émetteur UHF, enfin, des lecteurs UHF qui reçoivent les informations d'intensité de champ magnétique et les données d'identification des émetteurs BF ainsi que des étiquettes. Le récepteur BF de l'étiquette mesure l'intensité du champ magnétique pouvant être utilisé pour l'estimation de la distance. Ce type d'architecture augmente les cas d'utilisation du système et permet différents scénarios d'application basés sur une estimation de la distance, tels que le contrôle d'accès, la sécurité et la localisation en temps réel. Le travail présenté s'est effectué dans le cadre d'un partenariat de recherche ANRT CIFRE, il a été réalisé en tenant compte des besoins et des contraintes de l'entreprise.

Les principales contributions apportées par le travail présenté sont :

1. Modélisation du couplage inductif dans des systèmes à couplage extrêmement lâche,

2. Optimisation du système pour une plage opérationnelle étendue et et une meilleure compacité,

3. Evaluation de l'influence de l'orientation du tag pour une antenne 3D et un traitement simplifié,

4. Évaluation de l'influence des matériaux ferromagnétiques sur le signal produit par le système,

5. Évaluation des performances du système présenté et comparaison à des solutions existantes basées sur les technologies *UHF* et *UWB*.

Mots Clés

Estimation de distance, BF, *NFMI*, systèmes très faiblement couplé, champs magnétiques quasi-statiques, mesures d'intensité de champ magnétique.

Abbreviations

2D ..... Two Dimensional

3D ..... Three Dimensional

AC ..... Alternating Current

AGC ..... Automatic Gain Control

AOA ..... Angle of Arrival

AP ..... Access Point

ASK ..... Amplitude Shift Keying

BLE ..... Bluetooth Low Energy

CL ..... Centroid Localization

COTS ..... Commercial off the Shelf

CPS ..... Cyber Physical Systems

CSI ..... Channel State Indicator

DC ..... Direct Current

EKF ..... Extended Kalman Filter

ELF ..... Extremely Low Frequency

EMI ..... Electromagnetic Interference

FMM ..... Fast Multiple Method

FSI ..... Field Strength Indicator

GNSS ..... Global Navigation Satellite System

GPS ..... Global Positioning System

HF ..... High Frequency

IMU ..... Inertial Measurement Units

IOT ..... Internet of Things

IR ..... Infra-Red

LBS ..... Location Based Service

LED ..... Light Emitting Diode

LF ..... Low Frequency

LOS ..... Line-of-Site

LQI ..... Link Quality Indicator

MEMS ..... Microelectromechanical Sensors

MI ..... Magneto Inductive

MM ..... Map Matching

MOM ..... Method of Moments

NFMI ..... Near Field Magneto Inductive

NLOS ..... Non Line-of-Site

NN ..... Neural Networks

PAN ..... Personal Area Network

PDOA ..... Phase Difference of Arrival

PDR ..... Pedestrian Dead Reckoning

PIR ..... Passive Infra-Red

PKE ..... Passive Keyless Entry

RF ..... Radio Frequency

RFID ..... Radio Frequency Identification

RSS ..... Received Signal Strength

RSSI ..... Received Signal Strength Indicator

RTLS ..... Real-Time Location System

RTT ..... Round-Trip Time

SIG ..... Special Interest Group

SNR ..... Signal to Noise Ratio

SVM ..... Support Vector Machines

TDOA ..... Time Difference of Arrival

TOF ..... Time of Flight

TWR ..... Two-Way Ranging

UHF ..... Ultra-High Frequency

UWB ..... Ultra-Wide Band

VGA ..... Variable Gain Amplifier

VLC ..... Visible Light Communication

VLF ..... Very Low Frequency

WURx ..... Wake-Up-Receiver

WCL ..... Weighted Centroid Localization

WLAN ..... Wireless Local Area Network

WPT ..... Wireless Power Transfer

WSN ..... Wireless Sensor Network

Notations

$\times$ ..... Vector cross product

$\cdot$ ..... Vector dot product

$\ll$ ..... Extremely less than

∇ ..... Del or Nabla operator

D ..... Maximum physical dimension of the system

$\overrightarrow{J}$ ..... Vector Current Density

$\overrightarrow{B}$ ..... Vector Magnetic field

$\overrightarrow{A}$ ..... Vector Magnetic potential

$\overrightarrow{m}$ ..... Vector Magnetic moment

Φ ..... Magnetic flux

c ..... Velocity of light

λ ..... Wavelength

Contents

Introduction

Context

The work of this thesis is in the context of an ANRT-CIFRE [1] research partnership with the company ELA Innovation [2] and the two research laboratories, ESYCOM (UMR 9007 CNRS) [3] and AlliansTIC [4]. This collaboration offered the ability to manage this work in academic and business context. The research work carried out during this thesis is in direct connection with the business needs of ELA Innovation.

Over the past decade, ELA Innovation have been developing a wide range of industrial wireless beacons and readers based upon long-range active Ultra-High Frequency (UHF) Radio Frequency Identification (RFID) technology. UHF-RFID beacons or tags from ELA Innovation feature various sensors which provide information such as temperature, humidity, movement, luminosity, etc. The UHF-RFID readers from ELA Innovation can read information transmitted by the tags at around 30-50 m in indoor environments and around 100-200 m in outdoor environments. These products from ELA Innovation offer various application scenarios such as telematics, inventory, security, etc.

Over past few years, there is an ever-growing need for tracking solutions within the environments such as manufacturing plants, warehouses, public buildings, etc. where Wireless Sensor Networks (WSN) are mostly deployed and the demand for real-time indoor tracking solutions has been growing rapidly. Real-Time Locating Systems (RTLS) automatically identify and find the location of objects or people in real time, usually in a building or other confined area. RTLS solutions are being used in a growing number of sectors, including supply chain management, healthcare, retail and postal services, security for people in risk-prone areas, etc. The demand for tracking of tools, pallets, and

persons within the environments such as manufacturing plants, warehouses, tunnels, underground mines, construction sites, is rapidly growing. Context-aware localization solutions are important for protection of workers from the danger of industrial accidents. There is a great demand for automated access control solutions within confined environments. All these applications are concerned with reliable localization solutions within confined or indoor environments which produce harsh conditions for radio signal propagation.

Keeping these demands in mind, ELA Innovation participated in a research project called TROUVE (Annex A) funded by the French national research agency ANR [5]. In this project related to indoor localization, ELA Innovation produced a prototype based on dual-frequency-RFID system. The work of this thesis is an extension of the work carried out during the TROUVE project. One of the goals of this work was to enhance the applicability of the indoor positioning system produced by ELA Innovation.

System Description

This section intends to give a simple introduction to the dual-frequency-RFID system built by ELA Innovation, named as DOT system. This system was designed by ELA Innovation before the work for this thesis had been started. In this section, the state of this system before the beginning of this work is presented along with its limitations in that state.

System Topology

The DOT system basically consists of three types of devices, 1) LF transmitters operating at 125 kHz referred as LF-activators, 2) DOT tags, each containing a LF receiver and an UHF transponder operating at 433 MHz and 3) UHF receivers referred as IP2 readers. Basic architecture and system topology for the DOT system is shown in figure 1.

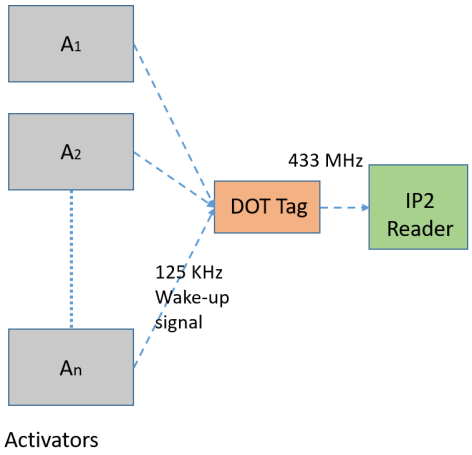

Figure 1: Topology of the DOT system

LF-activator

LF-activator (figure 2) consists of LF transmitter circuit with 12 V power supply and can be connected to two LF transmitter coils or the LF transmitter antenna. The LF signal transmission through the LF-activator is not continuous and it can be configured to transmit LF signal at a transmission period with the minimum being 200 milliseconds. The LF activator can be assigned with a 11 bits identifier including a different identifier for each antenna. The input current to the LF transmitter antennas can be controlled which defines the operational range of that antenna. In addition to stationary installations, LF-activator can also be installed on vehicles and can be powered using onboard battery. LF-activator enables the operation of the DOT tag within its operational range with its LF transmission.

DOT tag

DOT tag (figure 2) is a battery-operated portable device with small form factor. It consists of a LF Wake-Up-Receiver (WURx), a control unit, and a UHF transponder. When the DOT tag is inside the operational range of the LF-activator and the LF signal generated by the LF-activator is received by LF WURx, the tag is activated, and it starts its predefined operation. The received strength of the LF signal referred as LF Field Strength Indicator (FSI) is measured and sent to the IP2 reader using a UHF transmission triggered by the activation of the tag. The DOT tag can have a 16-bits identifier.

IP2 reader

IP2 reader (figure 2) consists of UHF receiver circuitry in addition to the components required to transfer this information to the centralized data accumulation block where the system has been deployed. In other words, the IP2 readers are gateways passing the information generated by the DOT system. A single packet of information passed by a IP2 reader contains its own identifier, identifier of a DOT tag, identifier of the LF-activator which has activated that tag and LF-FSI value measured by the tag. IP2 reader is powered by a 12 V power supply and like the LF-activator, it can be installed on stationary on mobile entities. The IP2 reader also has an 8-bits identifier.

LF Operation and Ranging

The DOT system makes use of NFMI communication [6], which is a relatively short-range wireless communication technology with low power consumption and ability to operate reliably in harsh propagation environments. NFMI technology makes use of near-field magnetic flux created by the LF transmitter in order to communicate with the LF receiver inside the NFMI bubble of the transmitter. With the help of inductive coupling, energy from one circuit is transferred to the other through mutual inductance between the two circuits. Inductively coupled systems operate in near-field region making use of quasi-static magnetic fields. When there is enough coupling between the transmitter coil and the receiver coil, a voltage is induced in the receiver coil which enables the tag operation. In the near field, the magnetic field strength decays rapidly as the inverse cube ($1/r^3$) of the distance between the transmitter antenna and the receiver. LF-FSI value measured by DOT tag corresponds to the strength of the magnetic field due to the transmitter at the point of measurement. This LF-FSI value can be used as the means of estimating the distance between the transmitter and the receiver.

Limitations of the DOT system

The default operational range of the system is limited to 5-6 m. A panel antenna increases the operational range to 15-16 m. However, the form factor of the panel antenna makes it difficult to deploy. The resolution of the LF wake-up receiver is only

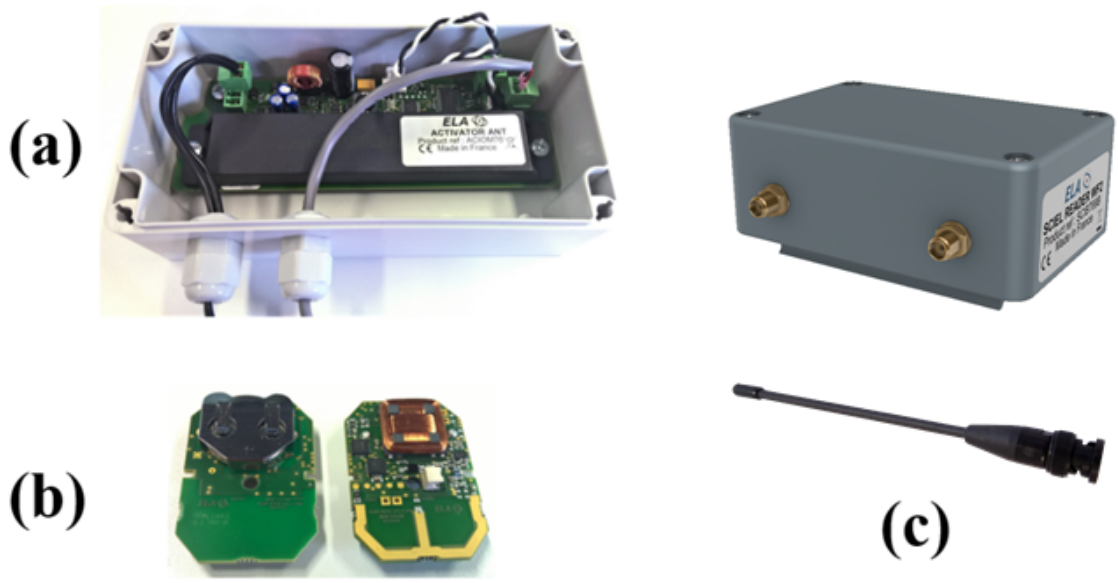

Figure 2: Components of system DOT (a) LF-activator with default transmitter antenna (b) DOT tag (c) IP2 reader with UHF antenna.

5 bits, that means the LF-FSI value generated by the tag is represented by 32 integers (0-31). This makes it difficult for DOT system to precisely relate the LF-FSI value to the distance and obtain very high accuracy in ranging and positioning.

Motivation

We want to design a system that achieves high operational range while keeping the size of the transmitter and receiver coils small compared to existing dual-frequency RFID systems. The DOT system intends to tackle the problems faced by MI based ranging and positioning systems and offer a ranging and localization solution with greater operational range, good accuracy while keeping its complexity and cost low. It should achieve a good trade-off between coil sizes and operational range. In order to obtain this trade-off, optimization of parameters was performed based on the system modeling.

Modeling the physical features of the system helps to define the optimum parameters for the transmitter coil. Use of ferrite, length of winding, inductance of winding, are some parameters which affect the mutual inductance between the transmitter and receiver coil and eventually the operational range. Thus, these parameters are important in optimization of the system for compact size and high operational range. In addition

to this, some parameters must be chosen by taking into consideration the market availability of ferrite rods of standard dimension and the availability of tuning capacitors as only standard values are available which can introduce design constraints. Modeling of the system depending on the coil sizes, ferrite sizes, quality factor, transmitter current, allows to optimize the system for operational range and compactness.

Summary of contributions

A compact near-field dual frequency RFID system with its LF component operating at 125 kHz is presented along with the study concerning improvements in operational range. Theoretical analysis of the system is supported by measurements and simulations. Range estimation and localization performance is evaluated by experimental work. Further improvements to the system are discussed. The main contributions made by the presented work are as follows:

1. Modeling of inductive coupling in extremely loosely coupled systems: The main contribution of this work is modeling of the MI based part of the DOT system which relies on extremely low amount of coupling between LF transmitter and receiver.

2. Guidelines for optimizing the system for large operational range, compactness and consistent performance in presence of obstacles: Various measurements using the DOT system are presented and the behavior of the signal produced by the system is analyzed in comparison to the modeling.

3. The impact on the signal of the ferromagnetic obstacles in different configurations is presented. Based on the observation some guidelines are provided in order to optimize the performance of the system.

4. Evaluation of the influence of tag orientation for a 3D antenna with simplified processing.

5. Evaluation the performance of the presented system in terms of ranging and positioning applications: Ranging and positioning based experiments using the DOT system are presented.

6. Comparing the system performance of the presented system with existing solutions based on Ultra-High Frequency (UHF) and Ultra-Wide Band (UWB): Ranging and positioning performance of the DOT system is benchmarked against UHF and UWB technologies.

Organization of the Thesis

The rest of this manuscript is organized as follows:

Chapter 1 provides an overview of indoor positioning techniques, and technologies and applications. This chapter discusses different criterions which render certain indoor positioning method or technology suitable for a certain type of application.

In chapter 2 MI technology and its theoretical background is presented. Ranging and positioning applications of the MI technology are discussed, approaches and problems of the MI based ranging and positioning systems are discussed. Physical modeling of the DOT system is presented in this chapter.

In chapter 3, characteristics of MI signal produced by DOT system are studied using different sets of measurements. The measurements are analyzed with respect to the physical modeling. Experiments and simulation intended to validate the physical modeling are presented in this chapter. The guidelines regarding the deployment of the DOT system are discussed.

Chapter 4 presents the ranging and positioning methodology utilized by the DOT system. Ranging and positioning performance of the system is evaluated with experimental work and benchmarked against UHF and UWB technologies.

Finally, the summary of this work, global conclusion and perspectives are provided.

List of publications

International journal:

1. Vighnesh Gharat, Geneviève Baudoin, Elizabeth Colin, Damien Richard 2017. "Low Frequency RFID system for identification and localization in smart cities -

Comparison with UHF RFID", International Journal of RF Technologies : Research and Applications , vol. 8, no. 4, Feb 2018, pp. 191-211.

International conferences:

1. Vighnesh Gharat, Geneviève Baudoin, Elizabeth Colin, Damien Richard 2017. "Indoor Performance Analysis of LF-RFID based Positioning System : Comparison with UHF-RFID and UWB", 2017 International Conference on Indoor Positioning and Indoor Navigation (IPIN), Sapporo, 2017, pp. 1-8.

2. Vighnesh Gharat, Geneviève Baudoin, Elizabeth Colin, Damien Richard 2017. "Impact of ferromagnetic obstacles on LF-RFID based indoor positioning systems", 2017 IEEE International Conference on RFID Technology & Application (RFID-TA), Warsaw, 2017, pp. 284-289.

National conference:

1. Vighnesh Gharat, Elizabeth Colin, Geneviève Baudoin, Damien Richard 2017. "Étude des perturbations des systèmes de positionnement magnéto-inductifs en intérieur", 20èmes Journées Nationales Microondes 16-19 mai 2017 – Saint-Malo.

Submitted to a journal:

1. Vighnesh Gharat, Geneviève Baudoin, Elizabeth Colin, Faress Bekkouch 2020. "Extremely Loosely Coupled Near-Field Magneto-Inductive System for Ranging in Harsh Propagation Environments", IEEE Access Journal.

Chapter 1

Indoor Positioning and Related Applications

The DOT technology is mainly oriented towards ranging and positioning within indoor environments. This chapter intends to provide an overview of indoor positioning techniques and technologies. Wide range of existing and potential location-based applications of indoor positioning are discussed along with the criteria influencing the choice of indoor positioning techniques and technologies.

1.1 Indoor positioning

Outdoor positioning applications are common nowadays since the generalization of satellite-based navigation systems. Over past few years, satellite-based navigation systems have become integral part of location-based application scenarios and Location Based Services (LBS) in outdoor environments. Such application scenarios and services are easily implemented in open outdoor spaces, thanks to good signal reception from navigational satellites. However, Global Navigation Satellite System (GNSS) signals are strongly attenuated when penetrating through buildings where the multiple reflections at surfaces cause multipath fading which is the cause of uncontrollable localization errors[7]. Application scenarios and LBSs that are intended to work in closed environments (indoors) usually require better accuracy than that offered outdoors by GNSS based positioning (5-10 m). Thus, GNSS based localization solutions are not suitable for most indoor location-based applications [8, 9]. Additionally, factors such as cost and power consumption can restrict the use of GNSS based localization solutions in the case

of localization [10].

Positioning is very important aspect of operations within smart buildings and smart cities as location information is a useful attribute to drive many applications and services such as emergency services, asset management, environmental monitoring, industrial sensing and diagnosis, surveillance, context-aware computing, and more [11]. Many positioning-based applications are required to work indoors. Moreover, most of the asset and people tracking needs are in closed environments such as warehouses, factories, hospitals, airports, etc.

In order to solve the indoor positioning problem, over the years, much effort has been put into designing accurate local positioning systems based on different methodologies and technologies [7, 12, 13] which are discussed in the following sections.

1.2 Positioning Methods

This section aims to provide an overview of position estimation principles which make use of various observations such as proximity, distance, signal strength measurements, angular measurements, etc. These observations are made with respect to the target object and one or more reference points. The target object is the object whose position is to be found which can be either absolute or relative with respect to the known points of references of the positioning system.

1.2.1 Proximity Detection

Proximity based positioning methods [14] estimate the position of the target by determining whether the target object is in the proximity to the reference point or not. This is achieved with the help of some kind of sensing mechanism, placed either at the reference point or at the target, specifically aimed at detecting the presence. The proximity can either be detected within a limited range using a physical contact with capacitive sensors [15], pressure sensors [16], Passive Infrared (PIR) sensors [17] or by detecting an object in the coverage zone of remote identification systems such as Bluetooth [18] and RFID cards [19]. In the case of detection of presence by multiple nodes, the magnitude

of parameter used for proximity detection is considered for determining the position of the target. The accuracy of this method relates to the density of proximity detecting nodes and their operational range. Proximity detection is the simplest positioning method used for applications that do not require very high accuracy.

1.2.2 Centroid Determination

Position estimation using centroid determination method involves the calculation of the geometric center using the positions of multiple reference nodes within the detection range of the target node [20]. If the Cartesian coordinates of i^{th} reference node are (x_i, y_i) and if n is the total number of reference nodes in the detection range of the target node, the Cartesian coordinates (X_t, Y_t) of the target can be calculated as follows.

$$X_t = \frac{1}{n}\sum_{i=1}^{n} x_i, Y_t = \frac{1}{n}\sum_{i=1}^{n} y_i \tag{1.1}$$

This low complexity positioning method is easy to implement but it offers low accuracy as it only takes the proximity data into account and simply performs averaging of the coordinates in order to obtain the position of the target. Weighted Centroid Localization (WCL) is an improvement to the centroid determination method in which centroid calculation is influenced by weights that can be functions of signal strength [21] or distances [22] of each node. If w_i is the weight corresponding to the i^{th} reference node in the case discussed above, the Cartesian coordinates (X_t, Y_t) of the target can be calculated as follows.

$$X_t = \frac{\sum_{i=1}^{n}(w_i x_i)}{\sum_{i=1}^{n} w_i}, Y_t = \frac{\sum_{i=1}^{n}(w_i y_i)}{\sum_{i=1}^{n} w_i} \tag{1.2}$$

Weighting factors are calculated such that more weight is assigned to the nearest reference point. By dynamically adapting the weighting factors [23, 24], the accuracy and robustness of this method can be further improved.

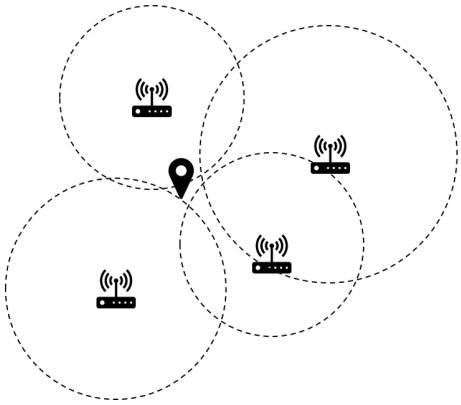

Figure 1.1: Lateration positioning method with four reference points.

1.2.3 Lateration

Lateration is a position determination method using simultaneous distance measurements of the target from three or more reference nodes with known positions [25]. Lateration based positioning method can utilize distance measurements from various ranging methods. After the distance measurements are available, the position of the target can be determined as the intersection of the circles or spheres formed with radii representing the respective distance measurement for each reference node and the geometric centers of the circles or spheres coinciding with the positions of reference nodes (Fig. 1.1).

The mathematical model for the lateration problem can be written as follows.

$$\begin{cases} d_i^2 = (x_t - x_i)^2 + (y_t - y_i)^2 + (z_t - z_i)^2 \\ i = 1, 2..., n \end{cases} \tag{1.3}$$

where (x_t, y_t, z_t) are the coordinates of the target and (x_i, y_i, z_i) are the known coordinates of i^{th} reference node out of n. A purely analytical solution for position of the target can be determined with a system of n equations with n unknowns. However, this method does not account for ranging errors as seen in Fig. 1.1, the circles do not intersect at a single point and errors in the position determination are introduced. Additionally, if any of the distance measurement is unavailable, the system becomes underdetermined and hence not solvable analytically. Also, there are certain constraints regarding the placement of the reference node e.g. reference nodes should not be collinear or coplanar

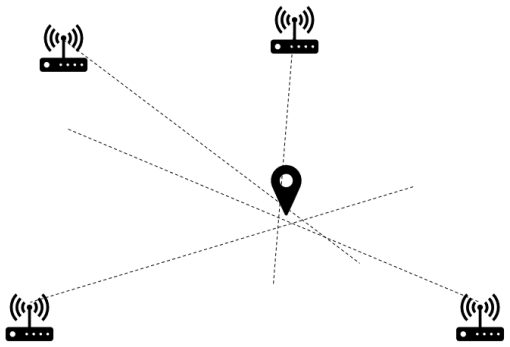

Figure 1.2: Angulation positioning method with four reference points.

[26]. When the number of reference points or the number of measurements is high, the system is overdetermined. Different approaches can be used to take into account measurement noise and solve the nonlinear set of equations. One of the simplest one is to linearize the system and use pseudo-inverse to solve the possibly overdetermined system. When the distance estimation is accurate, lateration offers very high positioning accuracy.

1.2.4 Angulation

Angulation is similar positioning method to lateration, except it determines the position of the target by using the angle measurements relative to multiple reference points (Fig. 1.2) instead of distance measurements. Phased array antennas [27] with direction detection capabilities are popular for angle measurements in the case of wireless signals. The position of the target is estimated at the intersection point of the lines formed using the angle measurements and passing through respective reference points (Fig. 1.2). Error in each angle measurement determines the error in positioning using this method as the lines formed using the angle measurements will not intersect at a single point (Fig. 1.2).

1.2.5 Fingerprinting

Fingerprinting is a scene analysis-based positioning method which relies on the fingerprints obtained by the environmental survey. Fingerprinting is most often performed using Received Signal Strength Indicator (RSSI) of Radio Frequency (RF) signals

[28], although audio signals [29], magnetic fields, visual information from images [30] and combination of multiple observations from surroundings [31] are also the quantities used for fingerprints. This method generally has two phases. First, is the calibration phase which is performed offline, meaning before deployment of the system. In this phase, a map is created using the measurements of the fingerprints over the operational area of the system. The second phase is online positioning phase. During this phase real time measurement of the fingerprint is compared with the offline measurements in order to predict the position of target. Buildings with an already existing infrastructure for technologies such as Wi-Fi and Bluetooth are examples where the fingerprint is interesting as a location method with low cost and low accuracy.

K-Nearest Neighbors (kNN) algorithm [32] is the most common way of position estimation using fingerprinting. Fingerprinting maps can be used as training data by machine learning approaches such as Support Vector Machines (SVM) [33] and Neural Networks (NN) [34] in order to improve the positioning accuracy.

1.2.6 Dead Reckoning

Dead reckoning [35] is the process of estimating position of the target with the help of previously known or estimated positions and known or estimated speeds and sometimes accelerations over the elapsed time. Inertial Measurement Units (IMU), with motion sensors and rotation sensors are generally used for dead reckoning. IMUs are capable of determining the position and speed of the target without external inputs. Inertial sensors can be designed in a Microelectromechanical Sensors (MEMS) technology and thus can be embedded in lightweight devices such as smartphones.

The inaccuracy of the dead reckoning process is cumulative [36], thus the estimated position drifts from the actual position with increasing deviation as the time increases. The term Pedestrian Dead Reckoning (PDR) is often used in the field of indoor applications to indicate that the accelerometers have been attached to the body of the user.

1.2.7 Kalman Filter

Unwanted noise in the measurements due to low Signal-to-Noise Ratio (SNR), severe multipath effects, reflection and link failure [37] is a main challenge faced by different positioning systems in most of the target environments. With the help of filters, the quality of the measurement data can be enhanced. Kalman filter [38] is the most widely used method for estimating processes that can be modelled using mathematical model. This is an ideal method to obtain better state estimates by combining multiple measurement sources. In the case of indoor positioning, this linear filtering model is particularly useful in predicting position of target in-between data samples and estimating path through noisy measurements [32]. Extended Kalman Filter (EKF) [39] is used in the case of nonlinear observation and state transition models. In this method, linearization of the nonlinear functions is carried out before filtering.

1.2.8 Map Matching

In the absence of positioning update due to reasons such as bad signal reception, the position estimated by an indoor navigation system, can be controlled, corrected or updated using a map database. To find a correct representation of target's position, certain elements of the map are associated with the characteristics of the target's trajectory, which is called as Map Matching (MM) [40]. MM algorithms [41] associate current positioning data with spatial map data to establish an accurate link between them, thereby improving positioning accuracy. Geometrical MM, topological MM, pattern recognition assisted MM, fuzzy logic based MM, etc. are some of the widely used MM techniques.

1.2.9 Combination of Positioning Methods

In the case of some positioning system architectures, more than one measuring principles or positioning techniques are used [42, 43, 44, 45]. For example, angulation can be used in combination with lateration in order to reduce the angle measurements required for estimating the position of the target or to improve the positioning accuracy [44]. In addition to angle and distance measurements, other information such as

proximity or various kinds of sensor data can be used to enhances the performance of a positioning system. Recently, positioning methods utilizing heterogeneous information [46, 47] and data fusion techniques [48] are focus of research in the field of indoor positioning.

1.3 Distances and Angles Estimations for Positioning Methods

Over the past years, various techniques have been developed for estimating distances or angles which make use of different basic measuring principles. This section describes commonly used basic measuring principles for indoor positioning.

1.3.1 Received Signal Strength (RSS)

RSS or RSSI is a measure of the received radio signal power. Distance estimation using this measurement principle requires prior knowledge of the path loss models (e.g. [49, 50, 51]) of RF transmitters obtained either empirically or statistically. Generally, propagation path loss increases with increase in distance and operating frequency as shown in (1.4), where P_l is the average propagation path loss, r is the distance between the transmitter and receiver, λ is the wavelength and n is the path loss exponent.

$$P_l = 10log\left(\frac{16\pi^2 r^n}{\lambda^2}\right) \tag{1.4}$$

The accuracy of distance estimation using this approach depends strongly on the accuracy of the path loss model used. RSS-based ranging and positioning techniques [52, 53, 54] are popular since they don't require high complexity hardware and are relatively cheaper and easier to implement [55]. However, RSS-based range estimation using RF signals is less accurate and less reliable in presence of obstacles. Multipath propagation and shadowing from obstacles cause challenges for RF wave propagation as RF electromagnetic waves are easily reflected and strongly attenuated by obstacles [37]. Also, significant deviation in RSS values of RF waves can be seen due to human presence [28],

as the direct Line-of-Sight (LOS) is blocked because of the absorption of electromagnetic waves in RF band by the human body [56].

1.3.2 Time of Arrival (TOA)

TOA measurement represents the exact time taken by the signal to travel from the transmitter to the receiver. In this case distance travelled by the signal can be calculated from TOA measurement and the propagation speed of signal (usually the speed of light). Most notable example of range estimation using TOA measurements is the GPS [57]. In general, direct TOA based positioning results in two problems. First, all transmitters and receivers in the system must be precisely synchronized. Second, a timestamp must be labeled in the transmitting signal for the measuring unit to discern the distance the signal has traveled. In order to have a good precision you need wide bandwidth signals such spread-spectrum signals or very short pulses. Also, noise, reflections, multipath, and scattering of the signal cause errors in ranging. In multipath situations, it is difficult to identify the first path of the signal in order to obtain accurate TOA measurement. TOA measurements with Two-Way Ranging (TWR) [58] does not require synchronization between transmitters and receivers as it considers bidirectional communication path of the signal and the Round-Trip Time (RTT) can be calculated using offset time between transmitter and receiver. Distance estimation using bidirectional communications without synchronous clocking was demonstrated in [59] where variety of TOA and phase-shift approaches that use bidirectional signaling are considered to bypass the need for accurate synchronous clocking.

1.3.3 TDOA

TDOA is a technique to determine relative position of the target transmitter based on the difference in time at which the signal arrives at multiple reference receivers instead of considering absolute arrival time used in TOA technique [60]. The position can be obtained as the intersection of several hyperbolas corresponding to each reference receiver. This technique requires highly precise synchronization between the reference receivers. Precision of TDOA based distance estimation depends on criterias such as the characteristics of the signal (signal modulation and bandwidth), SNR, environment

(multipath propagation and interference).

1.3.4 PDOA

PDOA method translates difference in phase of arrival measurements of the multi-frequency carrier signal into the distance between the transmitter and the receiver. This method is based on dual-frequency radar technique for range estimation [61]. In PDOA technique, two continuous wave signals of different frequencies with frequency difference Δf between them are transmitted. At the receiver, the phase difference $\Delta\phi$ is measured. The distance between the transmitter and the receiver is proportional to $\Delta\phi$ and inversely proportional to Δf [62]. Because of the presence of extremely small signal bandwidth phase estimation error can be very small. This method is limited because of the requirement of the complexity of the hardware for phase of arrival measurements and the need of multifrequency carrier signal. Another difficulty is the range ambiguity due to phase wrapping [63]. The maximum unambiguous range is equal to $C/(2\Delta f)$. Decreasing the frequency difference allows to increase this unambiguous range but it decreases the robustness to noise.

1.3.5 Angle of Arrival (AoA) and Angle of Departure (AoD)

AoA and AoD (Fig. 1.3) measurement principles rely of angle measurements in order to estimate the direction of RF transmitter and receiver respectively. As seen in Fig. 1.3 phased array of antennas is deployed at the receiver and the transmitter respectively for direction finding using AoA and AoD. The accuracy of angle measurements is limited by multipath reflections, shadowing and directivity of the antennas. In order to achieve good accuracy in direction finding, accurate orientation information of stationary locators is required in addition to complex hardware providing accurate angle measurements.

The Bluetooth core specification 5.1 provided by Bluetooth Special Interest Group (SIG) include a direction-finding feature that makes it possible to detect the direction of a Bluetooth signal [64]. With Bluetooth direction finding feature, either AoA or AoD method can be used for direction estimation with the help of phased array antennas.

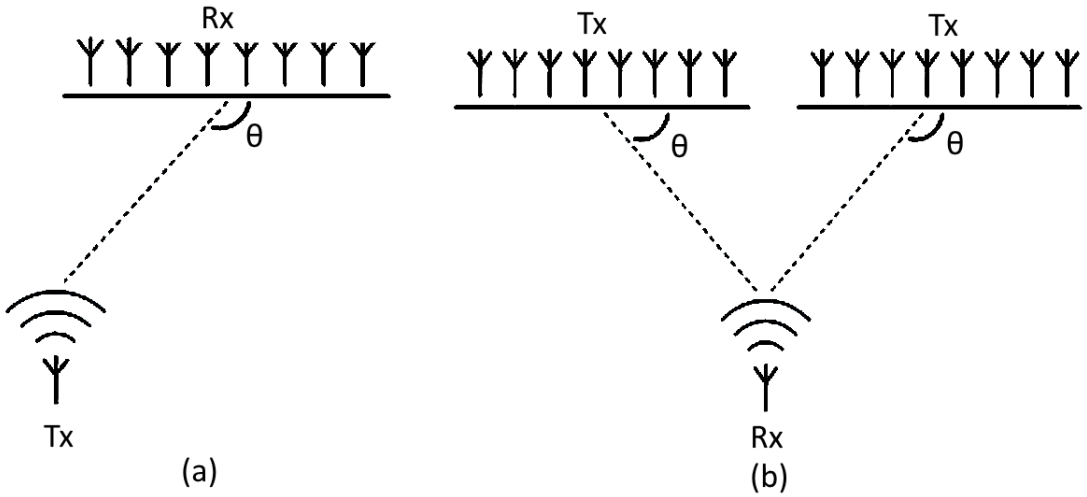

Figure 1.3: Direction finding schematic in the case of a) AoA and b) AoD

During the work of this thesis, an AoA based positioning system was tested for the positioning accuracy. Details of this work is included in annex B.

1.3.6 Channel State Information (CSI)

CSI [65] was introduced as an index to improve upon the limitations of the RSS. RSS provides only the information of strength of the signal, while the CSI provides more fine-grained physical layer information [66]. In addition to signal strength information, phase shift information of the individual signal components is provided by CSI. Thus, main path of received signal can be easily distinguished from the reflections of the signal. In the case of fingerprinting, CSI provides more information compared to RSS for fingerprinting thereby improving positioning accuracy [67]. CSI associated with different deep learning approaches allow to obtain more precise positioning results [68].

1.4 Positioning Technologies

Positioning technologies are the technologies used for sensors or communication in order to locate target objects using the positioning techniques discussed in previous section. In this section different positioning technologies are listed.

1.4.1 RF-based technologies

Technologies based on RF signal are the widely used technologies in indoor positioning. The most important characteristic of RF signal is that they can penetrate through most of the obstacles present indoors and are less vulnerable to indoor NLOS conditions which is a major issue faced by indoor positioning-based applications. Additionally, RF signals offer large coverage omnidirectionally. However, these signals are affected by interference and multipath. Also, availability of the required of infrastructure and complexity of implementation are the issues important while choosing the technology. The main functionality of these signals is to transfer information, the most popular technologies are discussed as follows:

1.4.1.1 Wi-Fi

Wi-Fi is a wireless communication technology, based on the protocols defined by the IEEE 802.11 standard, enabling wireless communications between Wi-Fi enabled devices and wireless internet access to these devices. It is a common platform providing wireless internet connectivity within the coverage area [69]. Wi-Fi typically operates at 2.4 GHz and 5 GHz ISM (Industrial, Scientific, and Medical) bands with narrow bandwidth channels (few megahertz) and with typical coverage of 50 to 100 m. IEEE 802.11 standards define RSSI of Wi-Fi signals, which is generally used for positioning of Wi-Fi compatible devices such as smartphones, laptops, tablet PCs, and others connected to Wi-Fi Access Points (AP). Positioning using Wi-Fi technology doesn't require additional infrastructure and positionin can be carried out within large coverage area. Disadvantages of this technology are limited localization accuracy (of the order of a few meters), channel interference and sensitivity to movable objects. Fingerprint techniques using RSSI measurements of Wi-Fi signal are usually considered in order to extract position information for devices compatible with Wi-Fi [70]. Recently RSS information of Wi-Fi signals is associated with CSI, sensor fusion and machine learning approaches [71, 72] in order to obtain much more precise positioning results.

1.4.1.2 ZigBee

ZigBee (based on IEEE 802.15.4 standard) is a communication standard intended for providing wireless Personal Area Network (PAN) with the focus on low data rate, low-power consumption and short-range applications. Indoor positioning system based on ZigBee technology usually use proximity detection [73] or lateration methods [74] for positioning. RSS is often used as measuring principle for range estimation. ZigBee based positioning systems require hardware with moderate to low cost and low energy consumption. However, utilization of this technology for positioning is limited because of band interference introduced due to other technologies in the proximity and the requirement of specific infra-structure which is not as widely available as other technologies.

1.4.1.3 Bluetooth

Bluetooth (IEEE 802.15.1) is wireless technology standard enabling short distance communication between mobile devices operating at short-wavelength UHF radio waves in the 2.4 GHz ISM band and it forms PAN for communication. Bluetooth devices hop over 79 RF channels with a bandwidth of 1 MHz. Bluetooth Low Energy (BLE) takes advantage of low power consumption and can therefore run on battery power for years at a cheaper cost. Similar to Wi-Fi, BLE is widely available thanks to its integration in most smartphones. BLE uses very small bandwidth compared to Wi-Fi and is designed for interconnection of electronic gadgets and sensors which usually have lower power consumption. Fingerprinting, lateration and Kalman Filtering methods based on RSSI and CSI are popular in the case of BLE based indoor positioning [75, 76]. In the new standard Bluetooth 5, in addition to RSS based approaches, AOA and AOD methods are foreseen for positioning [64]. Limiting factors for BLE based indoor positioning are, band interference due to other technologies operating at ISM band, requirement of large number of nodes to achieve acceptable accuracy, lower covering range and sensitivity to NLOS and multipath scenarios.

1.4.1.4 RFID

RFID technology is generally used to transmits the identity of an object or person wirelessly using RF waves. Using RFID technology, data is exchanged between RFID readers and RFID tags. RFID tags can be either passive, semi-active, or active [77, 78] depending on the method of powering the tags and can operate at LF, High Frequency (HF) or UHF frequency bands. Operational ranges of passive RFID tags are less compared to that of active RFID tags. In the case of positioning and tracking of RFID tags, active tags broadcast their own RF signal, thus existing positioning, and tracking methods such as lateration, angulation, fingerprinting can be applied [79, 80]. Among different wireless technologies, active RFID is a very interesting technology for indoor positioning because of its low operating cost and low power consumption. Active RFID systems operating at UHF face challenges such as multipath propagation and shadowing from obstacles affecting the wave propagation similar to other RF technologies.

1.4.1.5 UWB

UWB (IEEE 802.15.4, IEEE 802.15.4z-2020) is an emerging technology which as an RF signal occupies a portion of the frequency spectrum that is greater than 20% of the center carrier frequency or has a bandwidth greater than 500 MHz [81]. UWB systems operate in the band from 3.1 to 10.6 GHz with limited transmit power. This technology transmits information over a very wide portion of frequency spectrum with a very low power spectral density. UWB based positioning solutions are mainly based on lateration method and distance range estimation with measuring principles such as TOA and TDOA as precise time measurements are possible with this technology [82]. It acts based on transmission of narrow impulses in time domain which corresponds to wide bandwidth in frequency domain. This way, a good localization accuracy in the range of tenth of a meter can be achieved. UWB technology allows to achieve high positioning accuracy as a result of low sensitivity to multipath effect, low interference with other radio-based technologies, penetration capability through objects. Another advantage of UWB technology is its low power consumption. The limitations of the UWB technology are complexity of implementation, and higher cost of infrastructure [83]. AOA and RSS measurements based positioning approaches are also possible with

UWB technology. However, in these cases accuracy suffers due to multipath in NLOS conditions [82].

1.4.2 Pseudolites

Pseudolites or pseudo-satellites are means to generate signals equivalent to GNSS signals within indoor environments such as buildings, mines, tunnels and others where GNSS signals cannot penetrate [84]. Pseudolites allow GNSS receivers to function within indoor environments and improve the availability of navigation services by transmitting pseudo-range and carrier phase measurements signals over frequency band identical to that used by GNSSs [85]. Performance of pseudolites within indoor environments suffers from near-far problem [86], multipath, signal interference among pseudolites, weak time synchronization due to less precise clocks within pseudolites, and carrier phase ambiguities [87]. Use of pseudolites is limited due to requirement of a local infrastructure.

1.4.3 Magnetic Fields

AC (Alternating Current) based magnetic tracking systems are less affected by the Earth's magnetic field and artificial magnetic fields from electric devices. [88] classifies the magnetic-based solutions into those that use the natural Earth magnetic field, those that use DC (static) artificial magnetic fields, and those that use AC (time-varying) artificial magnetic fields. In the case of the ambient (Earth) magnetic field, such variations are usually caused by steel structures in the target indoor scenario, requiring the creation of a database with the recorded variations of the magnetic field strength.

1.4.4 Sound signals

Ultrasonic waves have higher frequencies (beyond 20 kHz) than the audible sound waves and are not detectable by humans. Audible sound signals when used for ranging can be annoying to nearby humans or cause sound pollution. But there are solutions like watermarking [89] to make it more acceptable to the human ear. As the sound velocity varies significantly with changes in humidity and temperature, these changes must be

taken into account in order to retain the accuracy [90].

Ranging based on sound signals mostly make use of the TOF measurements of ultrasound [91, 92] or acoustic signals [93]. As the speed of sound is much less compared to that of electromagnetic signals, cheaper and less complex hardware can be used to estimate the distance accurately based on this technology. Sound signal based ranging techniques are low cost, they offer centimeter level accuracy and not affected by radio interference. However, they suffer from distortions due to sound interferences and signal fading in NLOS conditions.

1.4.5 Inertial technologies

Inertial technologies are based on the measurement of motion in terms of parameters such as physical displacement, speed, acceleration or rotation [94]. These technologies are used as supportive technologies in other positioning system based on other technologies as they only provide relative position information of moving targets. Positioning using inertial technologies include step detection, characterization, inertial navigation, step-and-heading-based dead-reckoning and incorporation of building maps through particle filters [94].

1.4.6 Optical signals

Optical technologies such as visible light [95], IR [96, 97] and laser [98] are popular ranging and positioning techniques which are very accurate. Optical signals have similar characteristics as other radio waves, but they are less sensitive to radio noises. However, they suffer from LOS constraints. VLC (Visible Light Communication) is a technology which makes use of visible light mostly produced by LEDs for high-speed data transfer [95]. VLC based positioning techniques use light sensors to register the light pulses from the transmitter. To find the position of the VLC receiver, direction finding approach [95, 99], RSS based fingerprinting [100] or RSS based ranging [101] can be used. IR technology uses invisible light waves which have wavelengths longer than that of visible light to transfer information [102]. IR based systems suffer from issues such as security, privacy, interference, and failure due to NLOS conditions [7].

1.4.7 Magneto-Inductive Technology

MI technology utilizes coiled loops or solenoids in order to generate and receive quasi-static magnetic fields at VLF(3-30 kHz) and LF (30-300 kHz). At these frequencies, the magnetic field produced by the transmitter coil is quasi-static and inductive coupling occurs between transmitter and receiver coils. MI technology is the wireless communication technology which has the property of being able to penetrate most naturally found materials. Over the last few decades, MI technology has gained popularity in applications involving underground and underwater communications. MI signal suffers less attenuation through water, rock, or soil compared to that of RF communications [103, 104]. Additionally, MI signals have significantly greater wavelengths compared to the distance between the transmitter and receiver and thus are less affected by multipath compared to RF communications. Also, compared to conventional technologies such as RF, acoustic, and light-based communications, MI signals are much less affected by changes in the channel medium because MI communication depends primarily on the magnetic permeability of the channel medium. This makes MI a very good choice for communicating in harsh propagation environments where other wireless communication technologies would be unreliable.

Based on the application type and operational system parameters requirements, variety of MI systems of different sizes and different power levels exist. Due to its earth penetrating capability MI technology has been popular for underground communication. Around year 1900, Nikola Tesla first conducted MI resonant coupling experiment through air and through underground medium. After that, the MI technology has gained popularity in underground mine communication.

In [105] a VLF based audio communication system was proposed which could successfully transmit voice signals up to 100 m underground. An MI based multi-hop communication system was proposed in [106]. This system used three axis antennas at transmitter and receiver which have two main advantages in a communication system: firstly, orientation of the receiver antenna with respect to transmitter antenna is not a concern, and secondly, the tri-axial transmitters (consisting of three mutually orthogonal loops) can be used to generate 3D magnetic vector fields and by controlling the input of each transmitting coil, this enables increased data rates by three times without modifications

to power or bandwidth.

MI technology is popular in motion-tracking systems such as [107, 108]. Such systems are widely used to study human or non-human body movement (kinesiology). In this case, the LF electromagnetic field generated by the transmitter is measured in its vector form at the receivers and based on that 3D position and orientation (yaw, pitch, and roll) of the receiver sensor is calculated. MI technology is widely used in medical applications as it can provide very high precision in order to guide medical instruments inside the human body e.g. [109].

1.5 Applications of Indoor Positioning

Indoor positioning applications and services are traditionally associated with people positioning and tracking or asset tracking. These applications and services, in addition to several new application scenarios are constantly emerging in order to fulfill the location-based needs of modern indoor environments such as smart buildings and smart factories, etc.

In this section, existing and potential application scenarios of indoor positioning are discussed.

1.5.1 People Tracking and Navigation

Indoor environments such as airports, train stations, medical facilities, supermarkets, museums, can be huge, and crowdy. In this case wayfinding is a difficult task. In the case of visually impaired, systems specifically designed to aid the navigation and operate seamlessly in indoor and outdoor environments are required to assist walking in such environments. Indoor tracking and navigation systems which can guide users individually in navigation within such spaces are convenient and time saving for the users. People tracking is a very important aspect in the case of mining and tunneling. In these cases, dusty, dark, humid and space limited indoor environments pose challenges to the movement and safety of the workers and positioning capabilities are necessary for tracking and navigation of the workers. More generally, automatic safety systems benefit largely

thanks to the real-time positioning and tracking of workers.

1.5.2 Asset Tracking and Management

Asset tracking involves tracking the locations of assets such as portable electronic devices, IoT devices, portable industrial equipment, mobile medical appliances, etc. The amount of mobile assets that needs to be traced in the indoor environments such as factories, logistics centers, hospitals, is growing day-by-day and making organization of these assets very difficult. When these assets are needed of their intended operation, often it is difficult to correctly identify and quickly find them. Asset tracking allows to keep track of the location of assets during the various phases of asset handling, better inventory management and optimization of operations related to the assets. Indoor positioning information enables efficient and effective asset management services that are beneficial for improving traditional workflows within indoor spaces.

1.5.3 Context-aware Applications

In the case of context aware applications, context of the target object is determined with the help of location information. LBSs make use of the geographical position of objects or people in order to provide information based on the context. Examples include location-based marketing, location-based billing, proximity-based notification, automated authentication procedures, automated access, tour guidance, etc.

1.5.4 Safety, Surveillance and Security

Security conditions can be greatly improved with the help of positioning information. Possible security threats can be identified with the help of tracking information about user mobility, user's interaction with the environment, presence of dangerous objects, etc.

Law enforcement, rescue services, and fire services hugely benefit from indoor positioning as knowing the exact location of the target person, objects or sensors is essential in these cases. In the case of these applications, indoor positioning information is

also helpful for post-incident investigations, crime scene recovery, statistics and training, prevention of crime using geofencing, etc.

1.5.5 Environmental Monitoring

Environmental monitoring applications involve observing phenomenon such as heat, pressure, humidity, air pollution, deformation of objects and structures, with spatially distributed sensor nodes within a WSN. Linking the sensor information with location of the sensor node is important in the case of environmental monitoring.

1.5.6 Motion Tracking and Gesture Recognition

Motion tracking involves capturing movements of objects, people, or animals, so that these movements can be followed by other elements or another application can utilize this recorded motion data. Gesture Recognition means detection of physical gestures based on the tracking of body parts. Accurate positioning information with sufficient responsiveness is necessary in order to track the motion and position of people, animals, body parts, or robots. Motion Tracking and Gesture Recognition technologies find applications in gaming, animated films, and medical studies [110].

1.5.7 Augmented Reality (AR)

Augmented Reality (AR) refers to superimposing graphical or sound information onto a direct (photos or live camera images) or indirect (maps or diagrams) real-world view. With the rapid growth in usages of mobile devices, AR is an emerging and rapidly evolving consumer technology. Positioning information is fundamentally important for AR applications as the user perceives overlaid information which is spatially and semantically related to the target environment.

Technology	Positioning technique	Positioning accuracy	Operational range	Cost	Comments
Ultrasound	TOA/TDOA	Few centimeters	20-30 m	low	Complex hardware, Performance affected by NLOS, multipath
IR	TOA/TDOA	Few centimeters	20-30 m	high	Complex hardware, Performance affected by NLOS, multipath
UWB	TOA/TDOA	Few centimeters	25-30 m	high	Complex hardware, Performance affected by NLOS
Bluetooth	RSS	2-5 m	60 m	low	Performance considerably affected by NLOS, multipath
	AOA	Few centimeters	10-20 m	high	Complex hardware, Performance affected by NLOS, multipath
UHF-RFID	RSS	2-5 m	100 m	low	Performance considerably affected by NLOS, multipath
Wi-Fi	RSS	2-5 m	60 m	low	Performance considerably affected by NLOS, multipath
ZigBee	RSS	2-5 m	75 m	low	Performance considerably affected by NLOS, multipath
MI	Induced magnetic field intensity	Tens of Centimeters	5-10 m	low	Shorter operational range, Performance not affected by NLOS, multipath

Table 1.1: Comparison of positioning technologies.

1.6 Choice of positioning technology

The choice of certain positioning technology for a certain application scenario is mostly dependent on the factors such as cost, accuracy, range, scalability, availability, energy efficiency, latency and robustness [7, 13]. The accuracy requirement depends upon the use case e.g. an accuracy of a few meters would be enough to guide a patient in a hospital however, for a robot performing precise operations accuracy in centimeter level is necessary. Ease of installation, infrastructure requirement, operational coverage area of the system, are deciding factors in selection of suitable indoor positioning technology. Table 1.1 compares indoor positioning technologies.

Among different ranging technologies, MI is very interesting technology for indoor positioning because of its low operating cost and low power consumption. RF

signals of technologies such as UHF-RFID, Wi-Fi and Bluetooth are widely considered for RSS-based distance estimation and localization. However, RSS-based range estimation using RF signal is less accurate and less reliable in presence of obstacles. Multipath propagation and shadowing from obstacles cause challenges for UHF wave propagation [37] as RF electromagnetic waves are easily reflected and strongly attenuated by obstacles. Also, significant deviation in RSS values of RF waves can be seen due to human presence [28] , as the direct Line-of-Sight (LOS) is blocked [56] because of the absorption of electromagnetic waves in UHF band by the human body [111, 112].

On the other hand, MI signals at VLF and LF do not suffer from multipaths. VLF and LF magnetic fields can penetrate most obstacles with negligible attenuation. This makes magnetic field strength signal more reliable for range estimation and localization in presence of obstacles. With this in mind, ELA Innovation developed the DOT system.

1.6.1 Ranging and Positioning based Applications of MI Technology

Indoor environments within public buildings such as hospitals, airports, shopping malls, which have a large public presence, are very challenging for most of the RF signal strength based localization techniques as RF signals are highly attenuated by water (present inside the human body). On the other hand, MI signals at LF can be used in presence of human body as attenuation of LF signals due to water is negligible [111]. Thus, MI signals at LF can be used as accurate and reliable human tracking or keyless access technology within environments. Apart from public buildings, this technology can also be applied effectively within smart home infrastructures. Conclusively, the robustness of this technology will ensure improved security, guidance, and direct support services.

Another potential application field of this technology can be asset tracking within environments with higher metallic presence. In the industrial world, the use of the Internet of Things (IoT) is growing considerably for which identification and location information is very important. MI technology is reliable in terms of localization in the presences of metallic obstacles generally present within industrial environments. This

technology can be used for IT/data center asset tracking, tracking of machinery, tools and vehicles at manufacturing or construction sites, tracking of equipment in hospitals, etc. Accurate location information provided by MI signals at LF will help to achieve accurate real-time monitoring, increased efficiency for production and shipping as well as improved loss prevention of important assets. In addition to this, MI technology will also ensure added security by recording asset movements and creation of alarms and notifications when the asset moves from a controlled location or when it enters a prohibited area.

Passive Keyless Entry (PKE) systems based on near field bubble are widely used in automotive field. These systems allow users to automatically unlock or lock doors and start their vehicles while the user is in proximity to the vehicle. Using this system, the doors of the vehicle can be unlocked when the user approaches the vehicle or when the door handle is pulled. Similarly, the doors can be locked when the user leaves the proximity of the vehicle. Passive keyless entry start (PKES) offer additional passive start feature which allows keyless start of certain features inside the vehicle e.g. mirror and seat position, radio, engine, etc. PKE systems are also popular in building access and security applications. LF-RSSI based ranging system find application in keyless entry systems [113, 114]. The entry can be allowed from a certain range depending on the near field bubble size. Access control applications don't require large number of tags to be detected simultaneously.

The transmitter used to produce MI signal generate the magnetic field with nearly circular attenuation pattern. This phenomenon can be used to create accurate geofencing or the virtual zones representing boundaries. These boundaries enable the automatic triggering of a situation aware signal depending on whether the receiver is inside this boundary or not. This can be used to define hazardous zones which are much more reliable than other UHF based system in the industrial environment.

Situation awareness use cases combine people tracking with tracking moving objects, such as tracking forklifts in the industrial environments to prevent accidents with the pedestrians. Within the industrial environments, forklifts are widely used and are operational at any time during the working hours parallelly with the workers present in this environment. This causes a lot of accidents yearly. MI based real time tracking

system can be used to accurately detect the presence of the forklift or the pedestrian and both parties and be alarmed and accidents can be avoided.

1.7 Conclusion

In this chapter an overview of indoor positioning techniques and technologies is provided in order to get an introduction to the indoor positioning problem. Indoor positioning applications and the suitable criteria for these applications are discussed. MI technology, on which operation of DOT system is based, is discussed along with its applications. MI technology is compared with other technology in terms of different criteria important for selecting a positioning technology for indoor positioning applications. In the next chapter theoretical background of the MI technology, problem statement and physical modeling of MI component of the DOT system is presented.

Chapter 2

Theoretical Background of MI Technology and System Modeling

In this chapter, theoretical background of MI technology is presented. Existing approaches to ranging and positioning using MI technology are presented and the challenges faced by these approaches are discussed. Physical modeling of the part of the DOT system that is based on the MI technology is presented.

2.1 Definitions and Assumptions

Before going into the details of MI technology, some definitions and assumptions are discussed below.

2.1.1 Quasi-static Magnetic Field

For an MI based ranging or positioning system, the quantity that is of special interest is magnetic field B, since the estimation of distance is based on the measurement of this quantity. In general, B is coupled with the electric field E as described by Maxwell's equations. However, in the stationary case these fields are decoupled. If J is the current density, the magnetic field will be represented by magneto-static equations as follows

$$\nabla \times \vec{B} = \mu_0 \vec{J} \tag{2.1}$$

$$\nabla \cdot \vec{B} = 0 \tag{2.2}$$

From these equations, it is clear that the source of static magnetic field B is the current density J. For these magneto-static equations to be held true, the current density must not be time-dependent. However, magneto-static equations (2.1) and (2.2) still hold true when changes in current density are sufficiently small. In this case, the currents are quasi-stationary, that means they are slowly varying with time and the quasi-static approximation is applicable. When a quasi-static approximation is valid, the field patterns produced by quasi-stationary currents vary correspondingly with time but at any instant of time, these field patterns are similar to the static-field patterns. If the changes in current density are periodic with a frequency f_0 and if the maximum physical dimension of the system is represented by D, then the condition [115] for quasi-stationary approximation is given by,

$$D f_0 \ll c \tag{2.3}$$

where c is the velocity of light.

2.1.2 Electrically Small Antennas

An antenna whose maximum overall dimension (D) is less than about one-tenth of a wavelength ($D < \lambda/10$) is called an electrically small antenna. All electrically small antennas of different shapes (elliptical, rectangular, etc.) have a similar radiation pattern which resembles that of an infinitesimal dipole. An electrically small antenna has a doughnut-shaped radiation pattern with a null perpendicular to the plane of the loop and maximum along the plane of the loop. In such antennas, charges and currents in each sub-section of the antenna can be considered the same at any given time, as the dimensions of the antenna are small. Thus, quasi-static approximation can be applied to such antennas.

Electrically small loop antennas have small radiation resistances which are usually smaller than their loss resistances. Thus, they are rarely used as transmitting antennas in radio communication. However, they are usually used to produce and measure quasi-static magnetic fields.

Quasi-stationary approximation is true in the case of DOT system, as it uses electrically small transmitter loops and satisfies condition (2.3). Thus, the field patterns of

the transmitter antennas used in this system can be treated as static.

2.1.3 Near-field

The space surrounding an antenna is normally divided into three regions [116] reactive near field, radiating near field and far field as shown in Fig. 2.1.

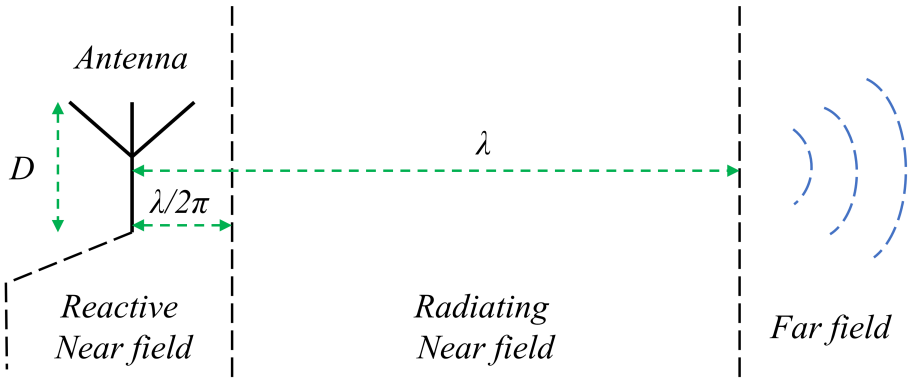

Figure 2.1: Near and Far fields of an electrically small antenna with transmission wavelength λ.

In the reactive near field region, which is immediately surrounding the antenna, field components, E (electric) and H (magnetic) are 90 degrees out of phase with each other and therefore reactive. Antenna gain is not a meaningful parameter in this region and the nature of the field around the antenna is affected. In this region the reactive component of the near field is held back and is stored very near the antenna surface and this affects the field generated by the antenna. A very simple example of this type of near-field electromagnetic interaction is magnetic induction as seen in a transformer. For electrically small antennas, the outer boundary of reactive near field exists at a distance $R = \lambda/2\pi$. At 125 kHz ($\lambda = 2398.34$ m), this boundary exists at about 381.71 m.

Radiating near field region is the region between the reactive near field region and the far field region where the field does not contain any reactive field components from the antenna and the energy is all radiant energy [117] although the relationship between field components E to H is still complex. In the far field region, the ratio of field components E to H has the constant value of 120π or $377\,\Omega$ which is equal to the wave impedance. In this region, the radiated power decreases as the inverse square of distance.

For all electrically small antennas near field boundary exists at the distance of approximately one transmission wavelength and unlike electrically large antenna this boundary does not depend on antenna dimensions. Near fields have characters of static fields and can be treated as quasi static fields [118].

2.2 MI Technology for Ranging and Positioning

MI technology and its application has been introduced in previous chapter. In this section theoretical background of MI technology and approaches to ranging and positioning using this technology are discussed.

2.2.1 Theoretical Background of MI Technology

An MI system typically consists of a transmitter driver, a transmitter source coil (transmitter antenna), a receiver coil and a receiver circuit. At VLF or LF, MI transmitter coil is an electrically small antenna and can be treated as a magnetic dipole loop antenna driven by the transmitter driver producing an Alternating Current (AC). As a result, the MI transmitter produces quasi static magnetic field in the near field region of the transmitter loop antenna.

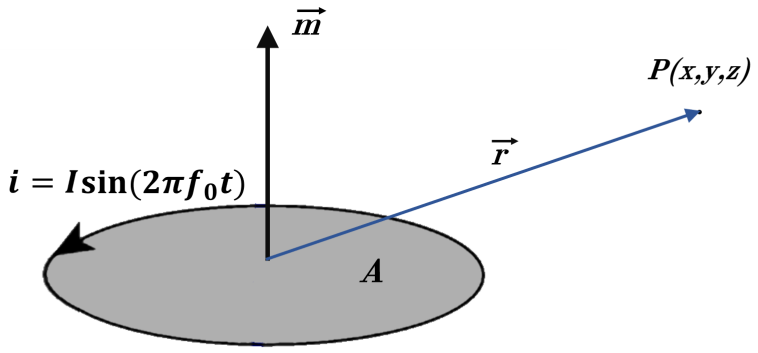

Figure 2.2: Magnetic moment of a planar circular current loop with area A and current i.

For a planar circular current loop (Fig. 2.2) of area A centered at origin, carrying sinusoidal current i with amplitude I and frequency f_0, the magnetic moment $\vec{m}$ (2.4) can be considered to be a vector quantity with direction perpendicular to the plane of

the loop in the right-hand-rule direction.

$$\vec{m} = iA\vec{n} \tag{2.4}$$

where $\vec{n}$ is the unit vector perpendicular to the plane of the loop.

For an electrically small loop antenna, magnetic vector potential $\vec{A}$ at point $P(x,y,z)$ in terms of magnetic moment [118] is given by (2.5) where $\vec{r}$ represents the distance of point P from the origin.

$$\vec{A} = \frac{\mu_0}{4\pi}\frac{\vec{m}\times\vec{r}}{|\vec{r}|^3} \tag{2.5}$$

From Maxwell's equations,

$$\vec{B} = \bigtriangledown \times \vec{A} \tag{2.6}$$

where $\vec{B}$ is the magnetic field strength due to the planar circular loop at point P and it can be expressed in terms of magnetic moment [118] as,

$$\vec{B} = \frac{\mu_0}{4\pi}\left[\frac{3\vec{r}\,(\vec{m}\cdot\vec{r})}{|\vec{r}|^5} - \frac{\vec{m}}{|\vec{r}|^3}\right] \tag{2.7}$$

If we consider a transmitter coil placed at origin with number of turns N_{tx} while a sinusoidal current i_{tx} is passing through transmitter coil in anticlockwise direction. If I_{tx} is the amplitude of the current and f_0 is the frequency transmission,

$$i_{tx} = I_{tx}\sin(2\pi f_0 t) \tag{2.8}$$

If A_{tx} is the cross-sectional area of the transmitter coil while the central axis of the coil is along Z-axis and if $\vec{k}$ is the unit vector along the Z-axis, then the magnetic moment $\vec{m}_{tx}$ of a coil is given by,

$$\vec{m}_{tx} = N_{tx} i_{tx} A_{tx}\vec{k} \tag{2.9}$$

The magnetic moment $\vec{m}_{tx}$ of transmitter antenna can be enhanced by using a fer-

romagnetic material as a core for the coil. This way the magnetic moment of the transmitter antenna can be increased by a factor μ_{e-tx} called as the effective relative permeability of the core which is function of the geometry of the coil and the core as well as the permeability of the material used as the core.

$$\vec{m}_{tx} = \mu_{e-tx} N_{tx} i_{tx} A_{tx} \vec{k} \tag{2.10}$$

From (2.7) and (2.10), the magnetic field strength $\vec{B}_{tx}$ at point P due to the circular transmitter loop placed at origin can be given by,

$$\vec{B}_{tx} = \frac{\mu_0 \mu_{e-tx} N_{tx} i_{tx} A_{tx}}{4\pi (x^2+y^2+z^2)^{\frac{5}{2}}} \begin{bmatrix} 3xz\vec{i} \\ 3yz\vec{j} \\ (-x^2-y^2+2z^2)\vec{k} \end{bmatrix} \tag{2.11}$$

Thus, magnetic field strength produced by the transmitter antenna is also enhanced by a factor μ_{e-tx} when a ferromagnetic material is used as a core for the coil. From (2.10), even though $\vec{m}_{tx}$ can be increased by increasing either N_{tx}, I_{tx}, A_{tx} or μ_{e-tx}, there are trade-offs. If N_{tx} is increased, coupling losses also increase and additionally coil becomes heavier due to increased mass. Increasing I_{tx} results in ohmic losses and core losses. As the value of $\vec{m}_{tx}$ is proportional to the square of coil diameter, increasing A_{tx} can be effective way to increase $\vec{m}_{tx}$, especially with air-cored coils. However, this makes the coil bulky and it may not be suitable for certain applications requiring compact transmitter design. A larger value of μ_{e-tx} can be achieved by modifying the coil geometry to increase m_{tx}. However, this again can lead to increase in bulkiness of the coil and the losses. All these issues cause practical limitations on design of MI transmitter coils [119] as the compact transmitter antennas are unable to achieve sufficient operational range and the bulkier transmitter designs are not practical for certain applications where there is lack of space to accommodate the antenna or the where the large form factor of the antenna makes it less portable.

MI transmitters can have modest power requirements and can be battery operated when efficient drive and modulation techniques are utilized. MI transmitter coils usually have high quality factor Q_{tx}. Various approaches (different types of amplifiers and oscillators) are taken in order to design a suitable transmitter driver circuit. The AC

magnetic field produced by an MI transmitter must be varied or modulated in some way to transmit the information using MI signal.

If a circular MI receiver coil is placed at point P in presence of magnetic field produced by the transmitter coil and if N_{rx} is the number of turns and A_{rx} is the cross sectional area of the MI receiver coil, according to Faraday's law, sinusoidal voltage v_{Lrx} (with amplitude V_{Lrx}) induced in the receiver coil,

$$v_{Lrx} = -N_{rx}\frac{d\Phi}{dt} \tag{2.12}$$

where Φ is the magnetic flux passing through the receiver coil.

$$\Phi = \int \vec{B}_{tx} \cdot \vec{d}s \tag{2.13}$$

The sensitivity of the magnetic field sensor present at the MI receiver determines the distance over which MI signal can be successfully received. At this distance, the magnetic field strength is close to the ambient noise level, so the noise starts to affect the ability of the receiver to successfully decode the signal. Similar to the MI transmitter antenna, a receiver antenna is normally treated as a magnetic dipole, therefore its sensitivity can be enhanced by increasing parameters from (2.10). Using ferromagnetic material as a core and modifying cross-sectional area, number of turns, and the coil geometry of the receiver antenna. the value of sensitivity and inductance of the receiver coil can be controlled. If where μ_{e-rx} is the effective permeability of the core used at the MI receiver, v_{Lrx} is enhanced by this factor. The sinusoidal output voltage v_{out} (with amplitude v_{out}) across the load resistor of the MI receiver sensor when it is used to measure an AC magnetic field produced by the MI transmitter is given by (2.14). If the receiver coil is tuned with the quality factor Q_{rx}, v_{Lrx} is transformed by the factor Q_{rx}.

$$v_{out} = Q_{rx}v_{Lrx} \tag{2.14}$$

The MI transmitter antenna coil is designed for maximum efficiency while the receiver antenna coil must be designed considering factors such as power transfer, noise figure and bandwidth [119, 120]. At lower frequencies (VLF and LF) external background noise is the main contributor to the noise figure of the system. External background noise

includes galactic noise, atmospheric noise, lightening, and man-made noise (e.g., noises from other radios, electrical equipment, motors, power supplies, improper grounding.) [121]. In addition, electronic circuits of the MI system introduce internal noise to the system. The SNR of the air cored coil is primarily dependent on the diameter of the coil [122] as the larger cross-sectional area intersects more flux lines. A material with high permeability as a core can be used to reduce the size of the receiver coil. The voltage output from the coil is related to the rate of change of the magnetic flux, so inherently has a frequency dependence. At VLF and LF, it is necessary to have higher number of turns in the receiver coil in order to compensate for the reduced induction and to achieve adequate sensitivity value. However, this can increase the parasitic capacitance of the receiver coil. The operational range of the MI system depends on the magnetic strength produced by the transmitter antenna and on the sensitivity of the receiver antenna. The constraints on the size and weight of the transmitter coil, and the power available at the transmitter are the limiting factors for the design of more powerful transmitter antennas. The medium of transmission also affects the operational range of MI system. However, the permeability for most non-ferromagnetic materials is close to that of the air or free space. For such mediums, MI magnetic field strength decreases as the inverse cube of the distance between the transmitter and receiver (2.7). Also, for the mediums with higher permeability values, even though the operational range is reduced, MI technology is the only viable approach as it is more reliable than other RF technologies.

The channel bandwidth depends on the frequency response of transmission medium and the quality factors of the resonant MI coils. Also, the SNR is dependent on the field strength and system noise which depend on the operational frequency of the MI system. Thus, the optimum choice of carrier frequency is determined by bandwidth requirements and the required transmission range in the targeted operating environment. The operational frequency providing higher SNR with sufficient bandwidth is mostly preferred for MI communication.

Conventional MI transmitters use a capacitor to form a resonant circuit with the transmitting coil. However, the resonant transmitter will have a finite bandwidth, producing limits on the maximum bit rate that can be transmitted. In addition to previously discussed constraints on the operational range, there are some limits set on the maximum allowable magnetic moment for the MI systems operating in VLF and LF bands. These

limits are in place for health and safety of humans and also for compliance to intrinsic safety standards and may limit the operational range of the MI system based on the frequency of operation. Limits for maximum H-field strength measured in dBμA/m at 10 m set by European Telecommunications Standards Institute (ETSI) are shown in Table 2.1 [123].

Frequency range (kHz)	H**-field strength limit (H_f) dBμA/m at 10 m**
9-90	72 descending 3 dB/oct above 30 kHz
90-119	42
119-135	66 descending 3 dB/oct above 119 kHz
135-140	42
140 - 148.5	37.5
148.5-300	-5

Table 2.1: H-field limits according to ETSI 300 330-1 standard at 10 m for frequencies in VLF and LF bands

MI based data communications can be achieved using various modulation schemes. An optimal modulation scheme can be selected based on the signal-to-noise ratio requirements.

2.2.2 Approaches to MI based Ranging and Positioning

As the magnetic field generated by MI transmitter is a vector quantity, by measuring the magnitude and orientation of this field at any point can provide the distance and orientation of the transmitter from that point. However, this approach requires multiple coils and complex measurement techniques. A position and orientation tracking system was presented in [124] which could use a single three-axes antenna to determine both the position and orientation of a three-axes receiver antenna, for the first time the MI signal was treated as a vector quantity with both magnitude and direction. The authors showed that the position and orientation of the receiver could be determined by treating the transmitter antenna as three orthogonal dipoles.

RFID systems using inductive electromagnetic coupling at LF or High Frequency (HF) do not suffer from multi-paths. LF or HF magnetic fields can penetrate most obstacles with negligible attenuation. This makes the magnetic field strength signal more reliable for localization in the presence of obstacles.

In [125] a distance estimation approach using HF RFID (13.56 MHz) technology was proposed. The assessment of the proposed system was done over a 0.5 m maximal range in LOS condition using a single coil antenna. In order to detect the orientation of the tag a tilt sensor was added to the tag.

In [126] a range estimation technique is proposed with a MI based system operating at 125 kHz. This system maks use of three receiver coils in orthogonal planes thus avoiding the use of a tilt sensor. The evaluation was done in an indoor environment without obstacle between reader and tag and for ranges up to 10 m.

Three-Dimensional (3D) underground tracking based on Magneto-Inductive (MI) localization at 125 kHz was proposed in [106], where larger transmitter antenna loops of dimensions 15 m x 2 m were used to track underground animals moving within 3 m from the transmitter loops, with accuracy below 0.5 m. In this case, the UHF transmissions on the tags were handled by a 2.4 GHz ZigBee module.

A positioning system based on the LF (24.4 kHz) Alternating Current (AC) magnetic fields was proposed in [127], where coverage of 12 m in cluttered indoor and accuracy of 0.3 m was achieved. In this case, the bigger receiver antenna is used along with an instrumentation amplifier having 12-bit resolution and a costly data acquisition system directly connected to the computer.

When instead of using 3D or vector magnetic field, the magnitude of the field strength is considered as a measuring principle, estimation of distance between MI transmitter and receiver becomes less complex. However, the magnitude of the field strength depends on the orientation of the receiver relative to the magnetic vector. Thus, the distance measurements using this approach are subject to significant errors when the orientation of the receiver is not ideal. This problem can be solved by using three-axes orthogonal antenna at either transmitter or receiver. This approach is presented in [128] where three orthogonal sensor coils are considered at the receiver. The DOT system makes use of similar approach for ranging.

MI based ranging and positioning systems can be analyzed and compared using criteria such as environment of operation, coil dimensions, operational range, accuracy, complexity of processing, electronics in the transmitter and receiver, number of antennas, 2D or 3D measurements. For the MI based ranging and positioning systems, the operational range determines the scalability and cost of the infrastructure. For such systems there is always a tradeoff between the coil sizes and the operational range.

2.3 Problem Statement

2.3.1 Problems faced by existing systems

Although MI signals are suitable for ranging and positioning in obstacle prone environments, it also presents some constraints such as low operational range, bulkiness of the system, complexity of the system, impact of ferromagnetic obstacles, etc. The main drawback faced by most of the MI based ranging and positioning systems is the balance between the sizes of the loop and the operational range of the system. Most of these systems are either bulky in order to achieve greater operational ranges or offer shorter operational ranges due to compact coil sizes. As seen in [129, 130, 131, 132], even though these systems achieve operational ranges of around 10-30 m, the large sizes of the loop make these systems difficult to deploy in day-to-day use cases.

Furthermore, some of the aforementioned systems which offer good ranging or localization accuracies [132, 133, 134, 135] use complex data acquisition and computational techniques, therefore are costlier to implement. Noise from Electromagnetic Interference (EMI) is another constraint of MI based positioning system which affects the operational range as well as the accuracy. As seen in [136] the operational range obtained by magnetic field simulations was 18 m compared to actual operational range of 10 m from the transmitter as it was affected by random noise from EMI. On the other hand, the positioning system presented in [133] was benefited from high resolution receiver and accuracy of few tens of centimeters was achieved. As seen in [137] sizes of the coils are one of the constraints on such system which affects its ability to be deployed easily. However, they have constraint on the operational range which is related on the loop sizes and the transmitter circuit.

Systems presented in [131, 138] make use of multiple receiver coils and vector magnetic field is used to estimate the position and orientation of transmitter coil in 3D with respect to multiple receiver coils. Such systems can achieve very high accuracy (few centimeters). However, they are complex and bulky.

2.3.2 Addressing the Issues faced by Different MI Ranging and Positioning Systems

This section discusses various aspects of our proposed MI based system in order to address the problems discussed in previous section.

2.3.2.1 Resonant Coupling

In the case of proposed system, tuning of the transmitter coil is done with high quality film capacitors in order to minimize the transmission losses. At the receiver, tuning is performed by the micro-controller with the precision of 1 pF in order to maximize the output voltage at the receiver. This helps to maximize the operational range. However due to precise tuning, bandwidth of the system is reduced, therefore user adjustable switches are provided at the transmitter in order to adjust the tuning when the system is deployed in close vicinity of ferromagnetic objects.

2.3.2.2 Ferrite cored coils

Use of ferrite material at transmitter coil helps to increase the strength of the magnetic field produced and at the receiver it helps to increase the sensitivity of the receiver. This helps to achieve larger operational range without increasing the sizes of the coils. The proposed system makes use of ferrite core transmitter and receiver coils in order to achieve large operational range with compact sizes.

2.3.2.3 Low Complexity Approach with 3-Axis Antenna

Usually multi-coil antenna increases complexity of the system. However, in proposed system instead of making use of all three output channels of the 3-axis antenna,

only coil with maximum induced voltage value at any measurement point is selected as an output channel. Even though this approach ignores the available data from two other channels and therefore is unable to provide the orientation data, it reduces complexity of calculations and cost of the receiver unit significantly. In 3.1.4 it will be shown that the highest channel output of a three-axis antenna for any given receiver orientation, provides a good approximation to the output produced by a dipole of the same parameters considering certain limits. Thus, this approach can provide the approximate ranging information for any given orientation of the receiver unit with acceptable accuracy and with less computational complexity as well as low cost receiver unit.

2.3.3 Need for System Modeling

DOT system tries to achieve high operational range while keeping the size of the transmitter and receiver coils small compared to existing systems. Our system intends to tackle the problems faced by MI based ranging and positioning systems and offer a ranging and localization solution with greater operational range, good accuracy while keeping its complexity and cost low. It achieves a good trade-off between coil sizes and operational range. This trade-off was obtained thanks to an optimization of parameters based on a modeling of the system.

Problem of low operational range is faced by many MI based system with compact sizes. With system modeling, we can quantify the effects of resonant coupling and ferrite. Existing systems offering high ranging and localization accuracies are usually complex in terms of number and sizes of coils or in terms of complex and costly measurement equipment and methods. The DOT system offers comparable accuracy with low complexity and cost and it achieves balance between accuracy and complexity. This system is easily deployable and moderately scalable. Another important point that the DOT system addresses is directionality which is solved with the use of multi-axis coils. Often, complexity of the system is increased when multi-axis coils are involved in order to address the problem of directionality. However, this system offers a low complexity approach for the compact multi-axis coils used at the receiver. Mathematical modeling of the system helps to validate this low complexity approach in order to achieve acceptable ranging accuracy.

Modeling the physical features of the system helps to define the optimum parameters for the transmitter coil. Length of ferrite rod, length of winding, inductance of winding are some parameters which affect the mutual inductance between the transmitter and receiver coil and eventually the operational range. Thus, these parameters are important in optimization of the system for compact size and high operational range. In addition to this, some parameters must be chosen by taking into consideration the market availability of ferrite rods of standard dimension and the availability of tuning capacitors as only standard values are available which can introduce design constraints. Modeling of the system depending on the coil sizes, ferrite sizes, quality factor, transmitter current allows to optimize the system for operational range and compactness.

2.4 Modeling

This section presents a mathematical model for this system and analyze it in order to optimize the system for larger operational range using compact coils. The modeling is performed considering the specific aspects of the system which may vary from other MI based systems. The system in consideration operates on very low amount of coupling compared to usual MI based systems. Based on the amount of coupling between transmitter and receiver coils, this system is categorized as extremely loosely coupled system. The coupling coefficient usually varies from about 10^{-5} to about 10^{-10} from the operational distance of 1 m to the distances beyond 5 m between the transmitter and the receiver. Modeling of extremely loosely coupled MI systems using mutually coupled coils and equivalent resonant circuit analysis has been performed in the field of Wireless Power Transfer (WPT) [139] in order to improve the power transfer efficiency (PTE). However, the coil sizes considered in this type of system are around 5 m in dimension. Also, the main focus of WPT is to improve the efficiency of power transfer rather than maximizing the operational range with compact coil sizes. System modeling in the case of a MI based ranging systems was performed in [140]. However, the important requirement for the presented ranging system is that it should be compact and easy to deploy. As the transmitter and receiver circuit of our system is already built for compactness, it is necessary to optimize the coils for long operational range and compactness. In this section we present the developed model and supporting simulations and measurements.

2.4.1 Helical transmitter coil

As the DOT system makes use of helical transmitter coil, we will consider a helical coil centered at origin as shown in Fig. 2.3 producing LF magnetic field and a receiver coil at distance r from the center of the transmitter coil. The transmitter coil with turns N_{tx}, radius a_{tx} is assumed to be placed at the origin as shown in Fig. 2.3 where l_c is the length of the coil. The transmitter carries a sinusoidal current i_{tx} given by (2.8).

We consider a single turn receiver coil of radius a_{rx} placed at point $P(x,y,z)$ and distance r from the origin. The unit normal vector to the loop surface is noted by $\vec{n}$ and it is defined by angles θ and ϕ where θ is the inclination angle with respect to Z-axis and ϕ is the azimuthal angle with respect to X-axis as shown in Fig. 2.3. A_{tx} and A_{rx} are the cross-sectional areas of transmitter and receiver coils respectively.

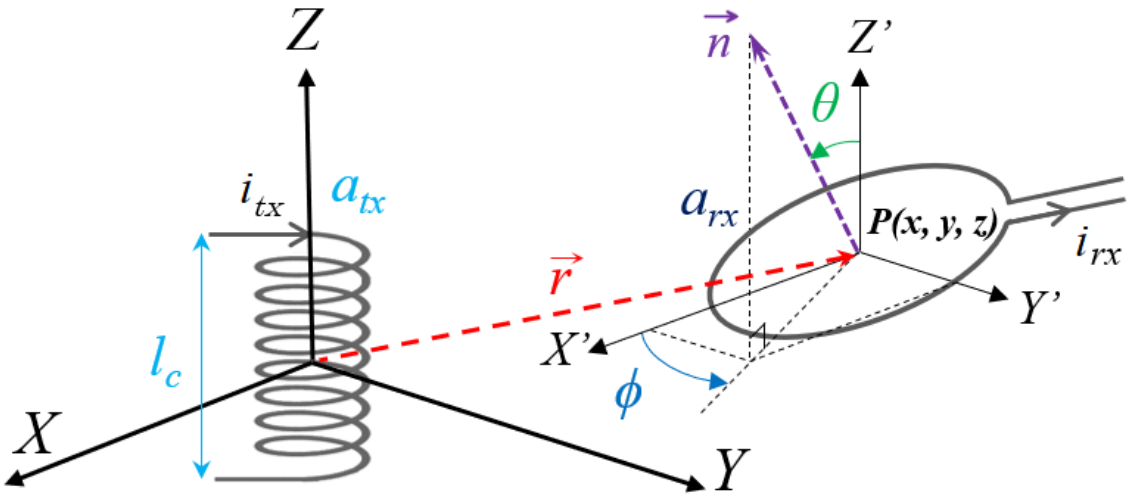

Figure 2.3: Helical transmitter coil of radius a_{tx} at the origin and single turn receiver coil of radius a_{rx} at point P with its normal making inclination angle θ with respect to Z-axis and azimuthal angle ϕ with respect to X-axis.

2.4.1.1 Off-Axis Magnetic Field due to Current Carrying Helical Coil

When the helical coil is centered at origin while keeping its axis orthogonal to $X-Y$ plane as shown in Fig. 2.4, we can derive the expression for the magnetic field at a point $P(x,y,z)$ when current i_{tx} is passed through the transmitter coil. The unit vectors along X, Y and Z axes are represented by $\vec{i}$, $\vec{j}$ and $\vec{k}$ respectively. If we consider an

infinitesimal element of the coil with height dr_z its magnetic moment can be expressed as,

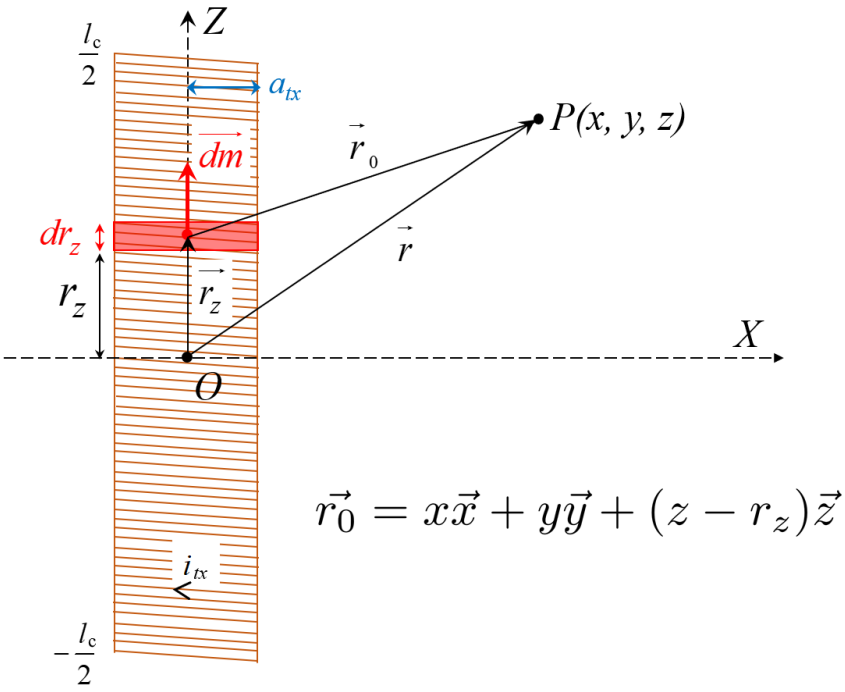

Figure 2.4: Solenoid of length l_c placed at origin with number of turns N_{tx}, radius a_{tx} and carrying current i_{tx}.

$$\vec{dm} = \left(\frac{N_{tx}}{l_c} dr_z\right) i_{tx} A_{tx} \vec{k} \tag{2.15}$$

Magnetic field at P(x,y,z) due to infinitesimal element dr_z when the distance between the center of this element and point P is r_0,

$$\vec{dB} = \frac{\mu_0}{4\pi}\left[\frac{3\vec{r}_0(\vec{dm}\cdot\vec{r}_0)}{{r_0}^5} - \frac{\vec{dm}}{{r_0}^3}\right] \tag{2.16}$$

Vector magnetic field due to entire helical coil can be obtained by integrating $\vec{dB}$ over the length of the coil,

$$\vec{B}_{tx} = \frac{\mu_0 N_{tx} A_{tx} i_{tx}}{4\pi l_c} \int_{-\frac{l_c}{2}}^{\frac{l_c}{2}} \begin{bmatrix} \frac{3x(z-r_z)}{\{x^2+y^2+(z-r_z)^2\}^{\frac{5}{2}}}\vec{i} \\ \frac{3y(z-r_z)}{\{x^2+y^2+(z-r_z)^2\}^{\frac{5}{2}}}\vec{j} \\ \frac{2(z-r_z)^2-x^2-y^2}{\{x^2+y^2+(z-r_z)^2\}^{\frac{5}{2}}}\vec{k} \end{bmatrix} dr_z \tag{2.17}$$

The expression for magnetic field at the center of the receiver coil placed at point P due to the helical transmitter coil is given by (2.18).

$$\vec{B}_{tx} = \frac{\mu_0 N_{tx} A_{tx} i_{tx}}{4\pi l_c} \begin{bmatrix} \left(\frac{1}{q^3} - \frac{1}{p^3}\right) x\vec{i} \\ \left(\frac{1}{q^3} - \frac{1}{p^3}\right) y\vec{j} \\ \left(\frac{z+\frac{l_c}{2}}{p^3} - \frac{z-\frac{l_c}{2}}{q^3}\right)\vec{k} \end{bmatrix} \tag{2.18}$$

where,

$$p = \sqrt{x^2 + y^2 + (z + l_c/2)^2}$$

$$q = \sqrt{x^2 + y^2 + (z - l_c/2)^2}$$

If the receiver coil is centered at point P, the voltage induced across it according to Faraday's law can be obtained using (2.12) and (2.13). Assuming the magnetic field inside the receiver coil to be uniform, if $\vec{n}$ is the unit vector along the area vector, the area vector $\vec{ds}$ can be expressed as,

$$\vec{ds} = \left|\vec{ds}\right| \cdot \vec{n} = ds \cdot (\sin\theta\cos\phi\vec{i} + \sin\theta\sin\phi\vec{j} + \cos\theta\vec{k}) \tag{2.19}$$

Equation (2.20) which gives the amplitude V_{Lrx} of the sinusoidal induced voltage v_{Lrx} across the receiver coil due to helical transmitter can be obtained from (2.18), (2.12) and (2.19).

$$V_{Lrx} = \frac{\mu_0 N_{tx} N_{rx} A_{tx} A_{rx} I_{tx} f_0}{2l_c} \begin{bmatrix} \left(\frac{1}{q^3} - \frac{1}{p^3}\right) x\vec{i} \\ \left(\frac{1}{q^3} - \frac{1}{p^3}\right) y\vec{j} \\ \left(\frac{z+l_c/2}{p^3} - \frac{z-l_c/2}{q^3}\right)\vec{k} \end{bmatrix} \cdot \begin{bmatrix} \sin\theta\cos\phi\vec{i} \\ \sin\theta\sin\phi\vec{j} \\ \cos\theta\vec{k} \end{bmatrix} \tag{2.20}$$

$$V_{Lrx} = \frac{\mu_0 N_{tx} N_{rx} A_{tx} A_{rx} I_{tx} f_0}{4l_c} \left[\frac{2\left(p^3 - q^3\right)(x\sin\theta\cos\phi + y\sin\theta\sin\phi - z\cos\theta) + l_c(p^3 + q^3)\cos\theta}{p^3 q^3}\right] \tag{2.21}$$

If the number of turns of the receiver coil is N_{rx} then the amplitude V_{Lrx} of the induced voltage across the receiver coil in open circuit is given by (2.20), where μ_0 is per-

meability of free space, A_{tx} and A_{rx} are the areas of transmitter and receiver respectively and f_0 is the operating frequency of the transmitter. If the receiver coil having number of turns N_{rx} is placed in $X-Y$ plane ($z=0$), then the amplitude V_{Lrx} of the induced voltage across the receiver coil in open circuit can be simplified to (2.22),

$$V_{Lrx} = \frac{\mu_0 N_{tx} N_{rx} A_{tx} A_{rx} I_{tx} f_0 \cos\theta}{2\left[r^2 + \frac{l_c^2}{4}\right]^{\frac{3}{2}}} \tag{2.22}$$

If the receiver coil having number of turns N_{rx} is placed in $X-Y$ plane ($z=0$) with $\theta = 0$, then the amplitude V_{Lrx} of the induced voltage across the receiver coil in open circuit can be simplified to (2.23),

$$V_{Lrx} = \frac{\mu_0 N_{tx} N_{rx} A_{tx} A_{rx} I_{tx} f_0}{2\left[r^2 + \frac{l_c^2}{4}\right]^{\frac{3}{2}}} \tag{2.23}$$

2.4.2 Impact of Ferrite Core

As the DOT system uses ferrite core antennas at both transmitter and receiver, it is important to study the impact individually. Ferrite is ferromagnetic material with high magnetic permeability and a low electrical conductivity and has many applications in electromagnetics. In MI systems ferrite is used in order to increase the magnetic coupling between coupled coils [141]. In the presented extremely loosely coupled system, use of ferrite is very important as it increases mutual inductance between transmitter coils and helps to increase the operational range for very small coupling factor. When a cylindrical ferrite rod is placed inside a helical coil, self-inductance of the coil is increased by a factor μ_{rod-tx} [142] .

This factor is called as the effective relative permeability of that particular rod. This factor depends on the length of the ferrite rod used, the dimensions of the coil and position of winding relative to the rod. Similar effect is observed after introduction of cylindrical ferrite rod at the receiver coil and its self-inductance is increased by factor μ_{rod-rx}. With the help of (2.24), if the ferrite rod is used at both transmitter and receiver the mutual inductance between them is increased by $\sqrt{\mu_{rod-tx}\mu_{rod-rx}}$, and for, $z=0$

and $\theta = 0$,

$$V_{Lrx} = \frac{\mu_0 \sqrt{\mu_{rod-tx}\mu_{rod-rx}} \cdot N_{tx}A_{tx}N_{rx}A_{rx}f_0 I_{tx}}{2\left[r^2 + \frac{l_c^2}{4}\right]^{\frac{3}{2}}} \tag{2.24}$$

2.4.3 Electrical Equivalent Circuit

In the previous part, the voltage induced across the receiver antenna of the system is obtained. However, it is not the same as the output of the receiver circuit. The tuning circuit used at the receiver has influence on the output of the receiver and in order to model this influence the equivalent circuit analysis of the system is performed.

2.4.3.1 Full Bridge Inverter

In order to drive AC magnetic field, as a driver for the transmitter antenna, a full bridge inverter is used in the DOT system. In comparison with commercial amplifiers, full bridge inverters with built-in protections against damage from mismatched loads are more convenient to supply high current output with adjustable frequencies. Full-bridge inverter is widely used in DC-to-AC conversion applications, due to the following features:

- High DC voltage utilization to support wide input voltage range
- More control variations for different application conditions
- Unipolar fixed-frequency Pulse Width Modulation (PWM) control that reduces switching losses and generates less EMI
- Phase-shifted control strategy for possible soft switching operation to improve system efficiency
- Small power component stresses for medium/high power applications

The current output of the full-bridge inverter depends on its load i.e. the transmitter antenna in this case. In order to validate the modeling, measured and spice simulated values of I_{tx} are considered.

2.4.3.2 Resonant Circuit

In loosely coupled MI systems, there are considerable losses due to flux leakage. To combat these losses, loosely coupled inductors are designed to resonate at the same frequency as one another. The reason for having parallel tuning of the secondary circuit is to increase the load voltage v_{out} because the induced voltage is quite small for this extremely loosely coupled case and it must be substantially amplified by resonance.

Fig. 2.5 shows the equivalent circuit for the MI based component of the DOT system. M is the mutual inductance between the transmitter and the receiver coils. i_{tx} and i_{rx} are the sinusoidal currents passing through transmitter and receiver coils respectively. I_{tx} and I_{rx} are the amplitudes of these currents respectively. R_{tx} and R_{rx} are the internal resistances of transmitter and receiver coils respectively. Transmitter coil is tuned with a series capacitor C_{tx} and the receiver coil is tuned using a parallel capacitor C_{rx}. In order to obtain the relationship between the voltage V_{out} across the load resistor R_{out} at the receiver and its distance from the transmitter, (2.23) is used in this circuit analysis.

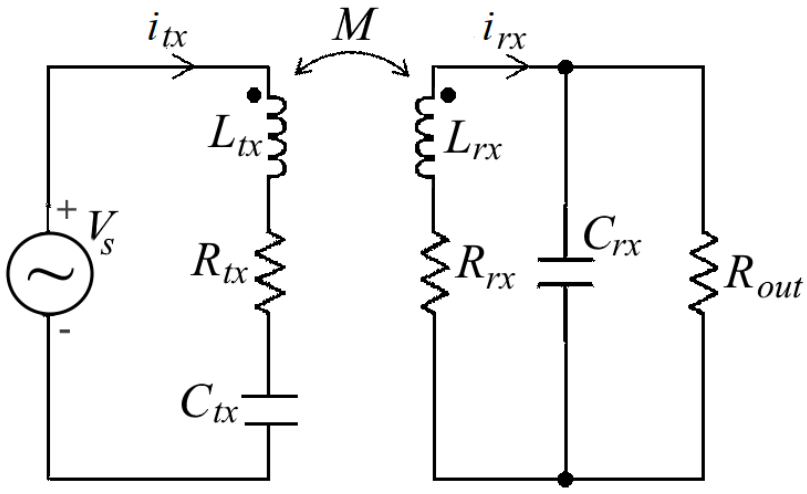

Figure 2.5: Equivalent circuit for extremely loosely coupled inductive coils.

If we consider an open circuit receiving loop ($R_{out} \rightarrow \infty$), using the mutual inductance approach, the sinusoidal voltage u_{Lrx} induced across the receiver loop is given by (2.25).

$$u_{Lrx} = j\omega M i_{tx} \tag{2.25}$$

In this case, the voltage induced in the receiver depending on the position and the

orientation of the receiver coil with respect to the transmitter coil can also be obtained using (2.20).

In the case of closed-circuit receiver in addition to R_{out}, R_{rx} and C_{rx} affect current in the circuit. In this case, the sinusoidal voltage v_{Lrx} induced across the receiver can be replaced by u_{Lrx} and its amplitude V_{Lrx} is given by,

$$V_{Lrx} = \omega M I_{tx} \tag{2.26}$$

The amplitude V_{out} of the voltage across the load resistor can be given by (2.27).

$$V_{out} = V_{Lrx} |H(\omega)| \tag{2.27}$$

In this case, $H(\omega)$ can be treated as the influence of the circuit elements R_{rx}, R_{out} and L_{rx} on voltage V_{out}.

$$|H(\omega)| = \frac{1}{\sqrt{\left(1-\omega^2 L_{rx} C_{rx} + \frac{R_{rx}}{R_{out}}\right)^2 + \left(\frac{\omega L_{rx}}{R_{out}} + \omega R_{rx} C_{rx}\right)^2}} \tag{2.28}$$

In the case of the resonant circuit, the quality factor Q_{rx} of the receiver is a measure of the step-up in the current and voltage at its resonant frequency f_0 ($\omega_0 = 2\pi f_0 = [143]$ and it is given by,

$$Q_{rx} = \frac{1}{\frac{R_{Lrx}}{\omega_0 L_{rx}} + \frac{\omega_0 L_{rx}}{R_{out}}} \tag{2.29}$$

The expression for the amplitude V_{out} of the voltage across the load resistor can also be written as,

$$V_{out} = V_{Lrx} Q_{rx} \tag{2.30}$$

The mutual inductance between transmitter and receiver coil M can be related to self-inductances of coupled coils by (6), where k is coupling coefficient ($0 \leq k \leq 1$).

$$M = k\sqrt{L_{tx} \cdot L_{rx}} \tag{2.31}$$

The value of coupling coefficient is calculated as seen in [143]. Value of k depends

on the dimensions of Tx and Rx coils. Coupling coefficient as a function of the distance r between Tx and Rx can be calculated using (2.32). When the coupling between the transmitter and receiver coil is very strong, classical transformer equations can be used to represent the inductive coupling [144].

$$k(r) = \frac{{a_{tx}}^{\frac{3}{2}} {a_{rx}}^{\frac{3}{2}}}{\left(\sqrt{r^2 + {a_{rx}}^2}\right)^3} \tag{2.32}$$

2.4.3.3 Comparison between Physical and Electrical Model

Physical modeling equation (2.24) gives us the value of V_{Lrx} considering the impact of ferrite cores. However, as there is no general agreement on calculation of values of effective relative permeability of the ferrite coil, this approach is not used for modeling the behavior of the system.

The electrical model ((2.26), (6), and (2.32)) using the mutual inductance approach, takes into account the impact of ferrite core as the contribution of the ferrite coil is represented by the inductance values of the coils and the mutual inductance between the two. V_{Lrx} can be obtained using both the approaches and we can compare the two expressions and can observe the resemblance.

$$V_{Lrx} = \frac{2\pi f_0 {a_{tx}}^{\frac{3}{2}} {a_{rx}}^{\frac{3}{2}} \sqrt{L_{tx} \cdot L_{rx}} I_{tx}}{\left[r^2 + {a_{rx}}^2\right]^{\frac{3}{2}}} = \frac{\mu_0 \sqrt{\mu_{rod-tx} \mu_{rod-rx}} \cdot N_{tx} A_{tx} N_{rx} A_{rx} f_0 I_{tx}}{2\left[r^2 + \frac{{l_c}^2}{4}\right]^{\frac{3}{2}}} \tag{2.33}$$

Self-inductance L of an air cored solenoid with N turns, length l, and radius a with a current I flowing through each turn is independent of the current I and depends only on the geometrical factors (N, R and l)

$$L = \frac{\mu_0 N^2 \pi a^2}{l} \tag{2.34}$$

In the case of ferrite cored solenoid, value of self-inductance is affected by physical characteristics of the ferrite and its relative placement with respect to the coil. Thus, the

expression for mutual inductance (6) takes into account the impact due to the ferrite. Using the quality factor Q_{rx} of the receiver, the value of the amplitude V_{out} (2.30) of the output voltage of the receiver can be obtained.

2.5 Conclusion

Theoretical aspects of MI technology along with the required definitions and assumptions are discussed in this chapter. The problem statement for this work is presented. Bulkiness of the transmitter coils and shorter operational range are the main issues usually faced by similar MI systems. In order to tackle these issues physical modeling approach is explored. The physical modeling for the MI based component of DOT system which is designed is presented.

In the next chapter characterization of NFMI signal of the DOT system and validation of system model will be presented.

Chapter 3

Characterization of NFMI Signal and Validation of System Model by LF-FSI Measurements and Simulation

It is important to characterize the behavior of the NFMI signals and their attenuation model in different environments and in the presence of different obstacles in order to use it for ranging based applications. This study enables us to determine the operational range of this system in different environmental conditions and the factors which has impact on it. Distortion in the attenuation model is also an important point to study as it will affect the ranging accuracy of the system. In addition to the operational range it is important to have omnidirectional attenuation model for a ranging system. In this chapter, the term LF-FSI which represents the strength of the NFMI signal of DOT system is explained. Measurements of LF-FSI values of DOT system in the case of different transmitter antenna configurations, different measurement setups and different environmental conditions are recorded in order to characterize the NFMI signal of the system. System model developed in the previous chapter is validated with the help of LF-FSI measurements and simulations for different transmitter and receiver antenna configurations.

The high-penetration properties of the magnetic field within the near-field region imply the robustness of the DOT system to multipath and reflections compared to the conventional RF systems. Thus, field strength measurements of the DOT system are expected to be more consistent with what predicted by the physical model.

System architecture is shown in Fig. 3.1. The LF-activator generates a quasi-static

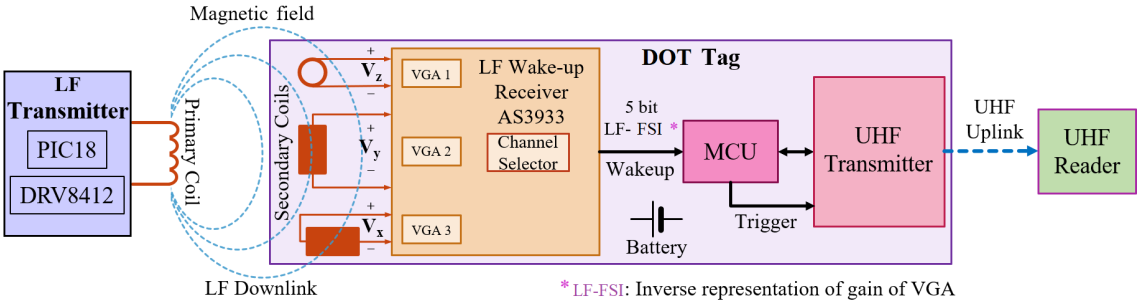

Figure 3.1: Architecture of the DOT system.

magnetic field which is amplitude modulated using Amplitude Shift Keying (ASK). This ASK pattern is transmitted periodically by the activator (LF downlink). A DOT tag has three receiver coils in orthogonal planes attached to an LF wake-up receiver which is in active state all the time. The three-coil receiver antenna, also called 3-axes antenna, allows the DOT tag to be used quasi-omnidirectionally. The resonant inductive coupling between transmitter and receiver coils induces electric voltages across the tag's receiver coils. Whenever the LF wake-up receiver detects strong enough voltage (greater than its sensitivity) across the receiver coils, the tag is activated (wake-up). On activation, tag calculates LF-FSI value (expressed in dB) which is inverse representation of the gain of the Variable Gain Amplifier (VGA) present at the receiver on the tag. After this step, UHF transmitter transmits the identity of the tag to the UHF reader along with the 5-bit LF-FSI and the identity of the activator by which it has been activated. ASK is used to avoid false activation of the tag. This architecture greatly reduces power consumption as the wake-up receiver requires a very low amount of energy to remain operational all the time and the UHF radio is only functional whenever there is an activation by an LF transmitter.

3.1 LF-FSI

The LF-FSI value measured by DOT tag corresponds to the output voltage of the receiver loop antenna, which corresponds to the strength of the magnetic field produced by the transmitter antenna and the distance between the transmitter and the receiver loops. On the LF wake-up receiver, AS3933, each of the three channels corresponding to the three coils of the 3-axes receiver antenna has a VGA with Automatic Gain Control (AGC). The voltage induced in each of the receiver coil, due to the magnetic field

generated by the transmitter, is applied to VGA. Strength of these input signals applied to VGAs of each receiver channel define the value of LF-FSI for respective channel. The receiver evaluates which channel has the highest induced voltage and generates 5-bit LF-FSI value (0 to 31) using (3.1). This LF-FSI value is proportional to the inverse gain of the VGA of the selected channel on the tag and it is expressed in dB. The AGC of each channel vary its gain depending up on the value of the input signal to the VGA. The reduction gain corresponds to a larger LF-FSI value and vice versa. The gain in the VGA is set to maximum at the beginning and then reduced by the AGC according to the strength of the input (received signal of the channel) level. Maximum 35 carrier periods are needed in order to get a stable LF-FSI value.

When the DOT system is used for real-time distance estimation, the user doesn't have access to the value of the voltage generated at the receiver, which is modeled in the previous chapter. In this case, the user has access only to the LF-FSI value generated and sent by the tag to the reader. Different target environments for the deployment of DOT system may affect the signal differently. As this aspect is not covered by the system modeling, it is important to study the behavior of LF-FSI in different environmental conditions.

If V_{out} is the amplitude of the output voltage of the selected coil of the 3-axes receiver on the DOT tag, and V_{ref} is the sensitivity of receiver AS3933 which is 0.226μVpp [145], the LF-FSI value FSI_{LF} can be calculated using (3.1). In this case the V_{out} is considered as the input to the selected channel of the receiver AS3933.

$$FSI_{LF} = 10log\left(\frac{V_{out}}{V_{ref}}\right) \tag{3.1}$$

Using (2.33), absolute value of FSI_{LF} can be modeled as,

$$FSI_{LF} = 10log\left(\frac{2\pi f_0 {a_{tx}}^{\frac{3}{2}} {a_{rx}}^{\frac{3}{2}} \sqrt{L_{tx} \cdot L_{rx}} I_{tx} Q_{rx}}{V_{ref}\left[r^2 + {a_{rx}}^2\right]^{\frac{3}{2}}}\right) \tag{3.2}$$

In the case of DOT tag, a_{rx} is less than 0.008 m which is negligible compared to the distance between the LF transmitter and receiver during real-time distance estimation scenarios of the DOT system. Thus, (3.2) can be simplified as follows.

$$FSI_{LF} = 10log\left(\frac{2\pi f_0 {a_{tx}}^{\frac{3}{2}} {a_{rx}}^{\frac{3}{2}} \sqrt{L_{tx} \cdot L_{rx}} I_{tx} Q_{rx}}{V_{ref} r^3}\right) \tag{3.3}$$

However, as LF-FSI value generated by the DOT tag is an integer between 0 and 31 (5-bit), quantization errors are introduced in LF-FSI measurements using DOT tag. From (3.1), LF-FSI value of 0 dB corresponds to $V_{out} = 113$ μV and LF-FSI value of 31 dB corresponds to $V_{out} = 142.25$ mV.

3.1.1 Measurement of LF-FSI

Fig. 3.3 shows a general setup considered for LF-FSI measurements. In order to observe the LF-FSI attenuation model of the LF transmitter with different transmitter antenna configurations (Fig. 3.2), LF-FSI values are measured on a straight line at measurement points separated by 0.5 m in open outdoor environment without any obstacles as shown in 3.3.

In this chapter, three different antennas (Fig. 3.2) are tested for the transmitter, the default activator antenna, the prototype ferrite antenna and the panel antenna are referred as antenna A, B and C respectively. Three different sets of measurements are carried out for the three transmitter antennas. LF activator and DOT tag are both placed at a height of 1.5 m from the ground with the help of tripods. Distance r between the transmitter and the receiver is kept 0.5 m for the first measurement of each set and then increased by 0.5 m each time the next measurement is recorded until the tag is no longer activated. An UHF reader attached to a computer is used to capture the data from the tag.

Fig. H compares the measured LF-FSI value for the three transmitter antennas when the measurements are performed in an outdoor environment with LOS conditions to the analytical LF-FSI values obtained using (3.3). In the proximity of the LF activator, the LF-FSI value measured is 31 dB and it decreases logarithmically as the distance between the tag and the activator is increased. Antenna A, B and C offer operational range of 5.7 m, 8.5 m and 16 m respectively in an open outdoor environment.

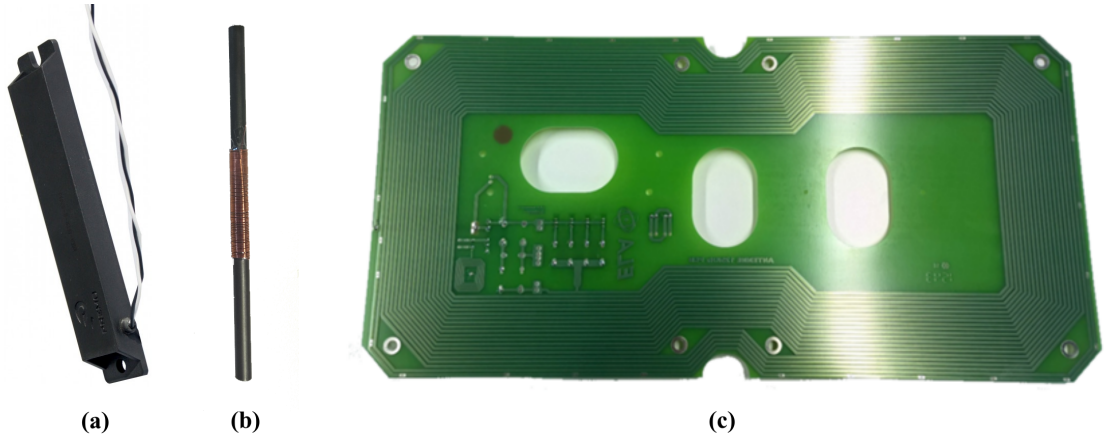

Figure 3.2: LF transmitter antennas : (a) default antenna (b) prototype ferrite antenna (c) panel loop antenna.

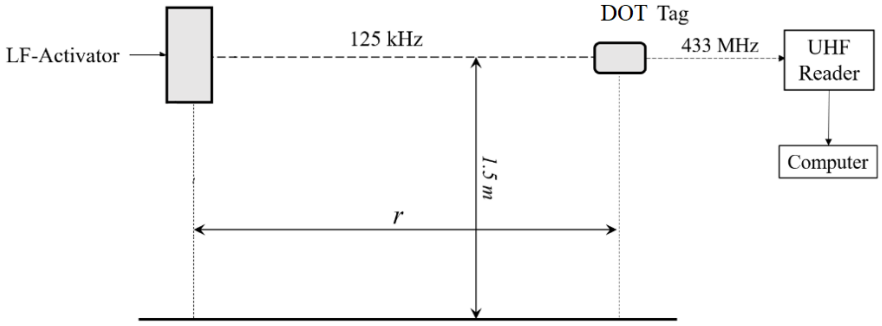

Figure 3.3: Setup for LF-FSI measurements

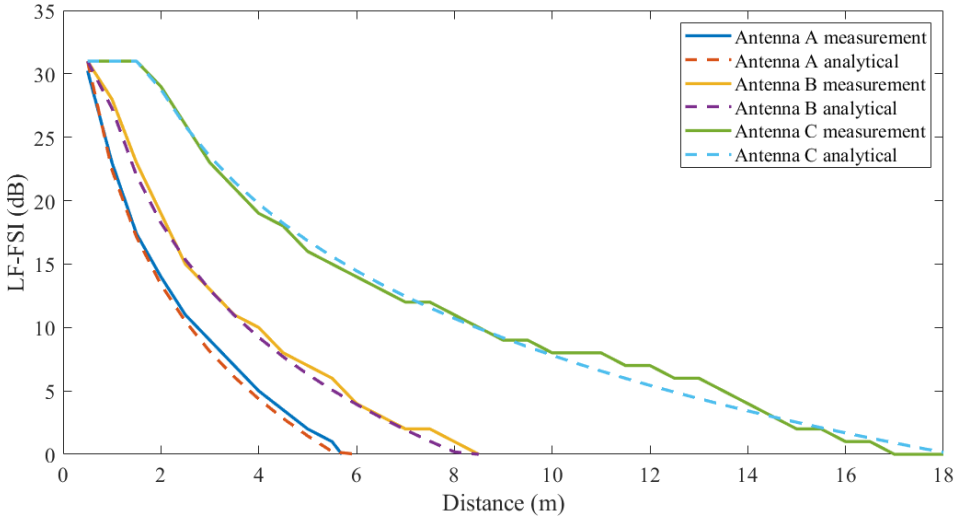

Figure 3.4: LF-FSI attenuation model for transmitter antennas A, B and C.

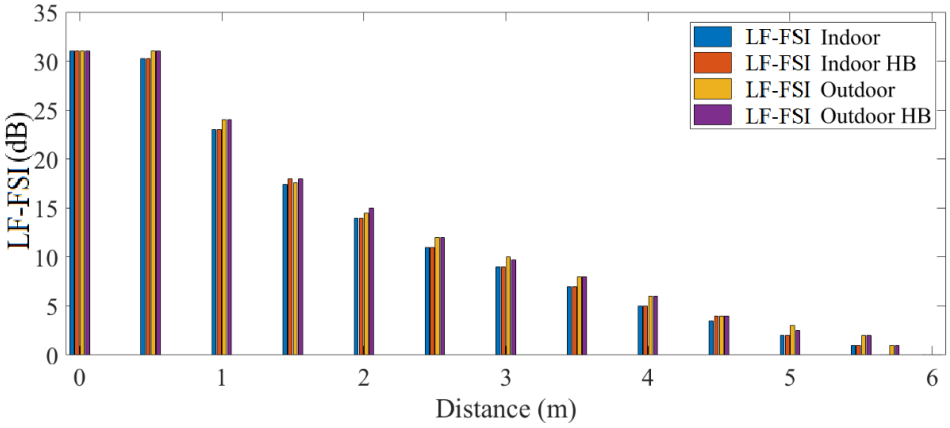

Figure 3.5: Comparison of LF-FSI versus distance in outdoor environment, and indoor environment for antenna A. 'Outdoor/Indoor HB' indicates that the tag is mounted on human body.

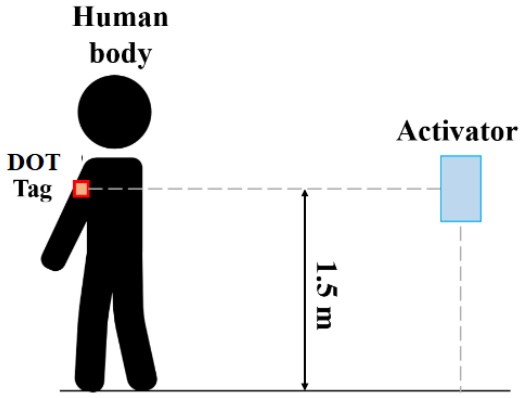

Figure 3.6: Setup for LF-FSI measurement when the tag is mounted on human body.

3.1.2 Impact of NLOS conditions

Fig. 3.5 compares the LF-FSI measurements in outdoor field and indoor NLOS field as well as the effect of the human body on LF-FSI in both kinds of environments in the case of antenna A. In order to observe the effect of human body, the DOT tag is mounted on the human body as shown in Fig. 3.6.

Similar measurements are recorded in the case of the transmitter antenna C and the results can be seen in Fig. 3.7.

The LF-FSI value measured in outdoor LOS conditions doesn't differ drastically with the measurements recorded in indoor NLOS conditions. Also, the impact of the presence of the human body in both environments is very low on LF-FSI as the LF-FSI value is differed only by 1 dB at few measurement points.

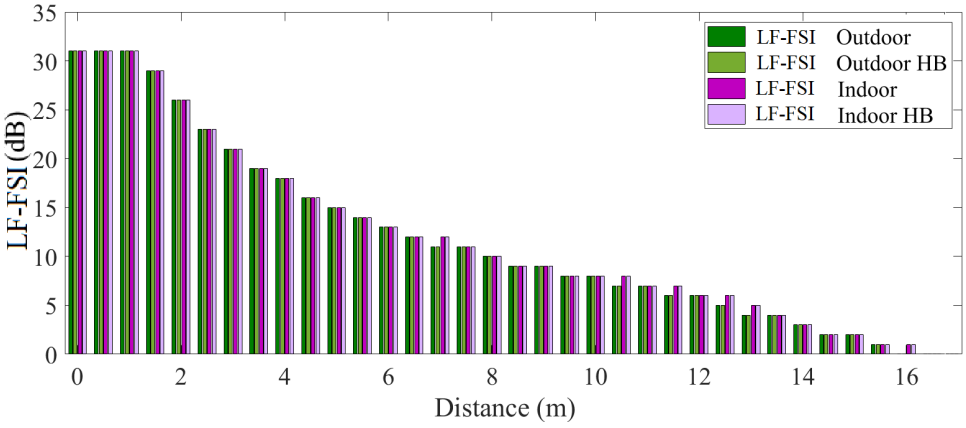

Figure 3.7: Comparison of LF-FSI versus distance in outdoor environment, and indoor environment for antenna C. 'Outdoor/Indoor HB' indicates that the tag is mounted on human body.

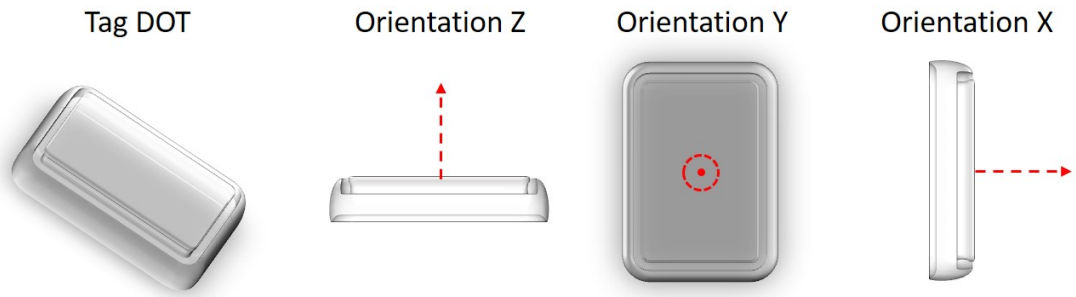

Figure 3.8: Different orientations of tag DOT at the measurement point.

3.1.3 Impact of tag orientation

As discussed in section 2.3.2.3, in order to avoid any impact of tag orientation observed in the case of single loop DOT tags, a 3-axes antenna is used. The effectiveness of this antenna is tested by placing the tag at the measurement positions in three different orientations as shown in Fig. 3.8. The measurements are recorded for these three orientations while antenna A is used as the transmitter. In this case only three orientations of the tags are compared.

It can be seen in Fig. 3.9 that tag orientation has negligible impact on the LF-FSI where the worst-case scenario is considered. The 3-axes antenna on the tag produced identical LF-FSI values in different orientations tested and worked as intended.

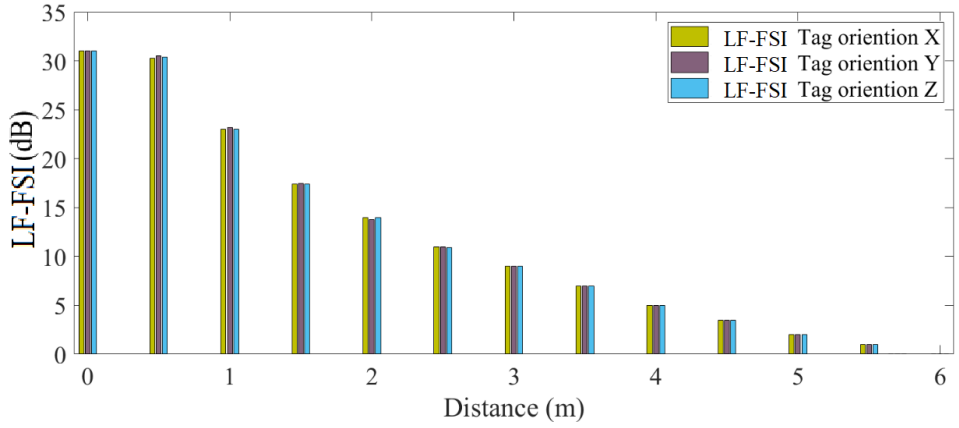

Figure 3.9: Comparison between the LF-FSI values measured for different tag orientations in the case of transmitter antenna A

3.1.4 Output Voltage of Three-axes orthogonal receiver antenna with low complexity approach

From (2.20), the amount of magnetic coupling depends on the distance and the orientation of the receiver coil with respect to the transmitter coil. When the receiver coil is orthogonal to the transmitter coil and when $z = 0$, the voltage induced at the receiver is zero. Thus, using a single receiver coil introduces limitations on the orientation of the receiver in a ranging system. To deal with this problem three-axes orthogonal antenna is used at the receiver in the presented system. Three-axes orthogonal antennas are studied in [129]. When the orthogonal coils are concentric, they don't affect the induced voltage in the other coils of the three-axes antenna [146]. Even though three concentric and orthogonal coils are used and three different LF-FSI values are available for processing, the receiver of the DOT system is unable to processes individual channel voltage, instead it selects the channel with highest value of induced voltage. This way the complexity of the system is significantly reduced. However, for good accuracy it is important to understand the impact of this limitation on the range estimation accuracy when the orientation of the tag is unknown.

In order to get good idea about the output voltage of the three-axes reveiver antenna of the DOT system, simulations based on (2.18) are performed. For this purpose, an imaginary helical transmitter ($a_{tx} = 0.01$ m, $I_{tx} = 1$ A, $N_{tx} = 100$, $l_c = 0.1$ m) placed at origin is considered. A 3-axes receiver antenna ($a_{rx} = 0.01$ m, $N_{rx} = 1000$, $Q_{rx} = 30$,

for all three orthogonal coils) placed at point $P(x,y,z)$ is used for simulations. The dimensions of the transmitter and receiver coils are comparable to the sizes of the coils used in the DOT system. In order to refer to the individual coils of the 3-axes antenna, let us call the coils along X-Y, Y-Z and Z-X planes as Coil-X, Coil-Y and Coil-Z respectively. In this case, θ is the inclination angle of Coil-X with respect to Z-axis and ϕ is the azimuthal angle of Coil-X with respect to X-axis as shown in Fig. 2.3. Inclination angles and azimuthal angles of other two orthogonal coils (Coil-Y and Coil-Z) vary accordingly as θ and ϕ are varied.

Fig. 3.10 (a) shows the induced voltages of all 3 coils (Coil-X, Coil-Y and Coil-Z) of 3-axes receiver antenna, when the transmitter and receiver are placed in X-Y plane ($z = 0$) and separated by distance $r = 1$ m and their maximum value. The orientation of each coil is varied by varying inclination angle θ from 0 to 180^o while ϕ is kept at 0^o. The curves in the case of Coil Y and coil Z are the same because of the loop circular symmetry. The maximum value for all three coils, which corresponds to the LF-FSI value produced by the LF receiver present in our system, is highlighted in the figure. Similarly, Fig. 3.10 (b) and (c) show the induced voltages for $r = 2$ m when $z = 0$ m and $z = 1$ m respectively. By considering the maximum value of the induced voltage among all three coils, it is ensured that the impact on the receiver antenna output due to variation in θ is minimized.

Fig. 3.11 (a), (b) and (c) show the LF-FSI values corresponding to Fig. 3.10 (a), (b) and (c) respectively. In this case, LF-FSI values are calculated using (2.14) and (3.1) and digitized to a 5-bit LF-FSI. When $r = 1$ m ($x = 1$ m $z = 0$ m) and $\phi = 0^o$, the LF-FSI value varies between 22 and 23 for different values of θ. When $r = 2$ m ($x = 2$ m $z = 0$ m) and $\phi = 0^o$, the LF-FSI value varies between 13 and 14 and when $r = 2.24$ m ($x = 2$ m, $z = 1$ m) and $\phi = 0^o$, the LF-FSI value varies between 12 and 14 for different values of θ. This shows that the variation of θ causes large variations in LF-FSI values corresponding to the individual coils of the 3-axes receiver antenna of the DOT system. The LF-FSI value measured using the low-complexity approach followed by the receiver minimizes the large variations in the LF-FSI measurements. However, this approach introduces small variation in ranging results which are based on the LF-FSI measurements. It should be noted that, when $z = 0$ m, the output voltages of the receiver coils do not vary with variation in ϕ.

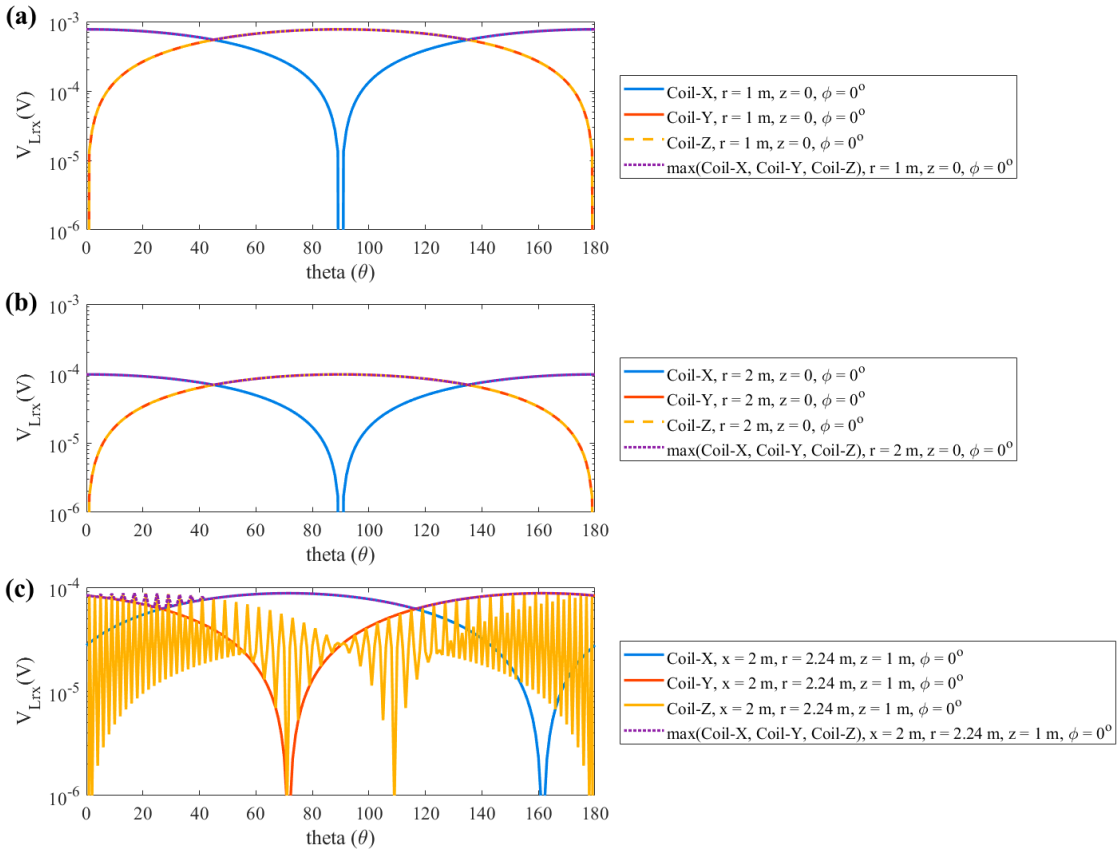

Figure 3.10: Voltage induced, obtained from (2.20), in individual coils of 3-axes receiver antenna due to field created by helical coil. Curves labeled as 'max(Coil-X, Coil-Y and Coil-Z)' represent the maximum induced voltage among three orthogonal coils of 3-Axes antenna.

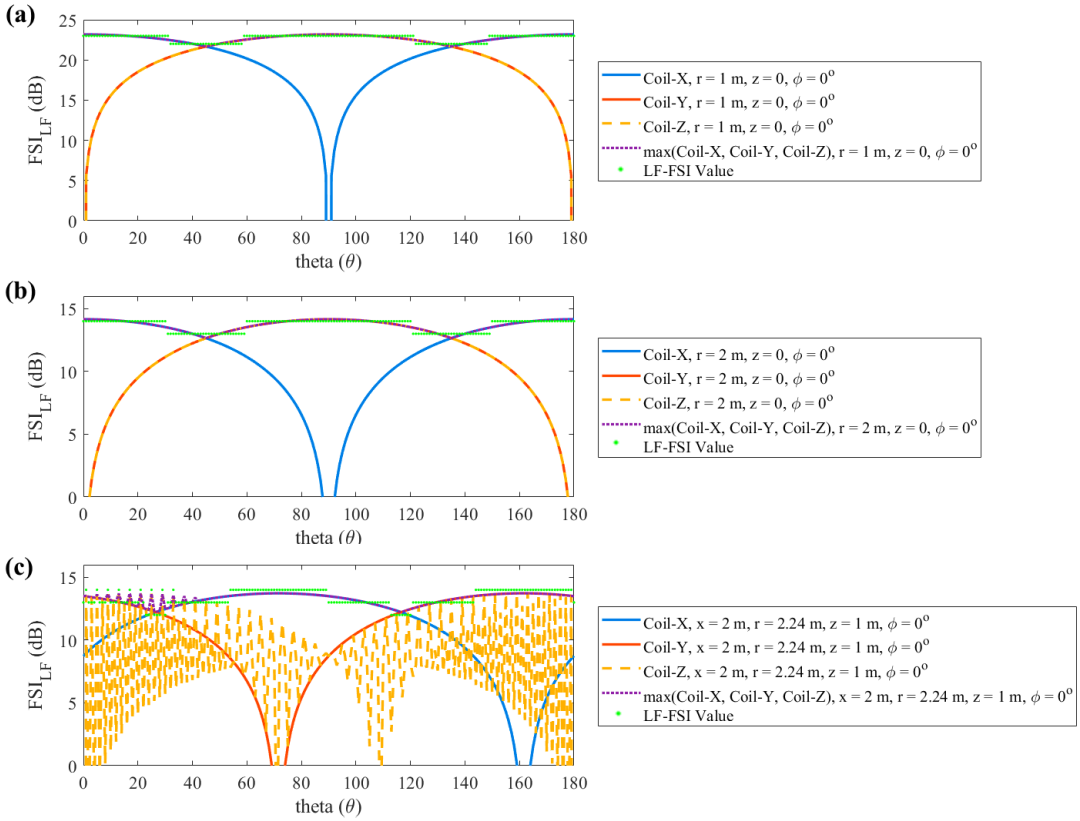

Figure 3.11: LF-FSI values generated by individual coils of 3-axes receiver antenna due to field created by helical coil.

In order to simulate the impact of variation in ϕ on the output of the receiver coils, two different scenarios are considered. In the first scenario, value of r is kept at 1.41 m ($x = 1$ m, $z = 1$ m). Fig. 3.12 shows the variation of maximum value of induced voltage among all three coils of the 3-axes receiver antenna due to field created by helical coil and variation of LF-FSI value for $\phi = 0^o, 30^o$ and 45^o when $r = 1.41$ m. The blue curve is included in order to compare these simulations with the case where $r = 1.41$ m ($x = 1.41$ m, $z = 0$ m) and $\phi = 0^o$. Similarly, in the second scenario, r is kept at 2.24 m ($x = 2$ m, $z = 1$ m) and Fig. 3.13 represents the simulation results.

As seen in Fig. 3.12 (a) and Fig. 3.13 (a), for $\phi = 45^o$ the output of the 3-axes antenna is the lowest. In this case, all three receiver coils are in symmetry with the center of the transmitter coil. Fig. 3.12 (a) shows that the LF-FSI value varies between 17 to 21 depending on variation in ϕ, x and z when r is kept at 1.41 m. When r is kept at 2.24 m the LF-FSI value varies between 11 to 14. This shows that, significant LF-FSI variation can be observed when the 3-axes receiver is not placed in the $X-Y$ plane with respect to the helical transmitter depending on the variation in ϕ.

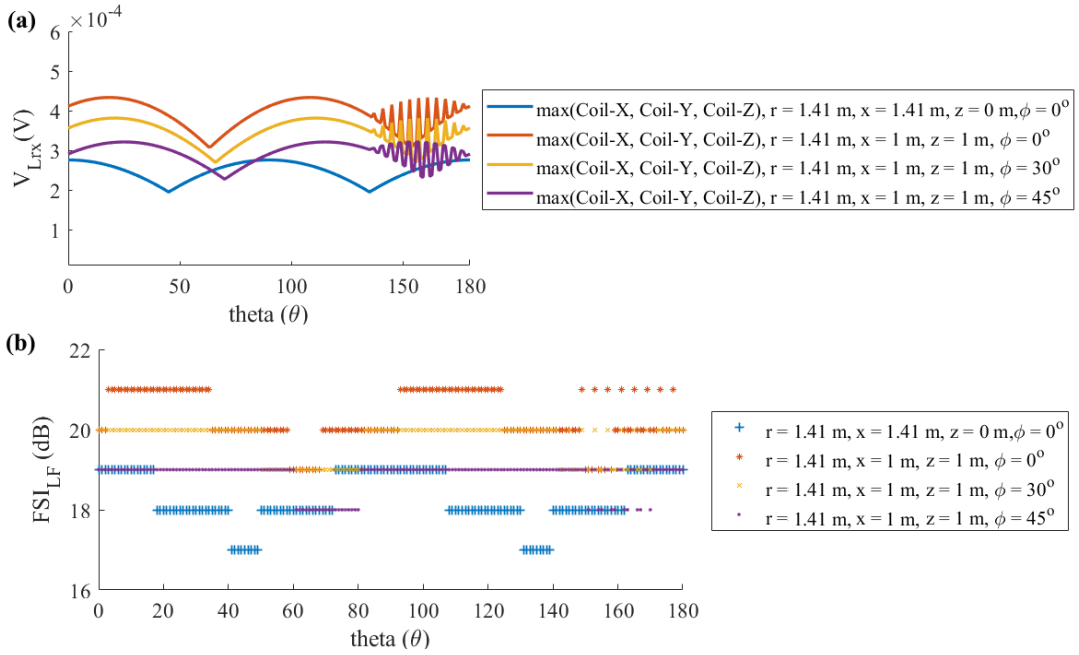

Figure 3.12: (a) Maximum value of induced voltage among all three coils of the 3-axes receiver antenna due to field created by helical coil for different values of ϕ when $r =$ 1.41 m (b) LF-FSI values for different values of ϕ when $r = 1.41$ m

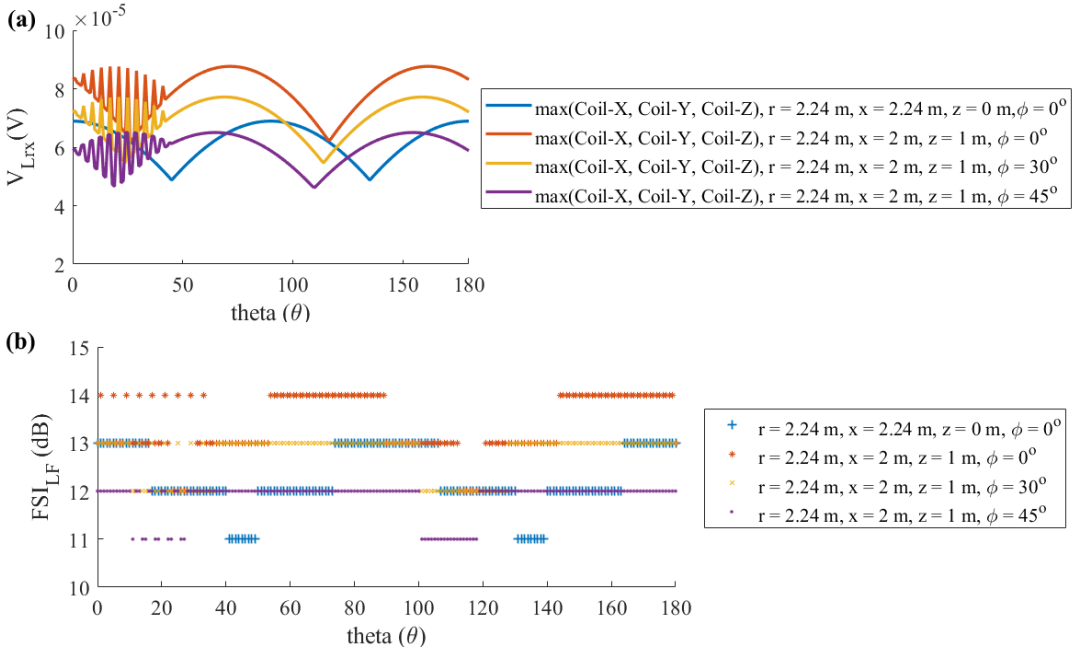

Figure 3.13: (a) Maximum value of induced voltage among all three coils of the 3-axes receiver antenna due to field created by helical coil for different values of ϕ when $r =$ 2.24 m (b) LF-FSI values for different values of ϕ when $r = 2.24$ m

The impact of variation in z on the output of the 3-axes receiver antenna is simulated and Fig. 3.14 shows the maximum induced voltage curve of the 3-axes antenna for different values of x and z when r is kept at 4 m and $\phi = 45^o$. The blue curve is included in order to compare these simulations with the case where $r = 4$ m ($x = 4$ m, $z = 0$ m) and $\phi = 0^o$.

As seen in Fig. 3.14 (a), the variation is maximum induced voltage curve in not very significant when the value of z is up to 2 m, which can also be seen in Fig. 3.14 (b) as the LF-FSI value varies between 4 and 5 for most of the time. As the receiver approaches the axis of the helical coil (x approaches to 0 and z approaches r), the drop in the output of the 3-axes receiver is slightly higher as seen in Fig. 3.14 (a) and (b). This shows that, the changes in value of z does not affect the LF-FSI value significantly if the value of r is kept constant. However, in the case of 2D ranging, if value of z is not taken into consideration, significant ranging error can be observed.

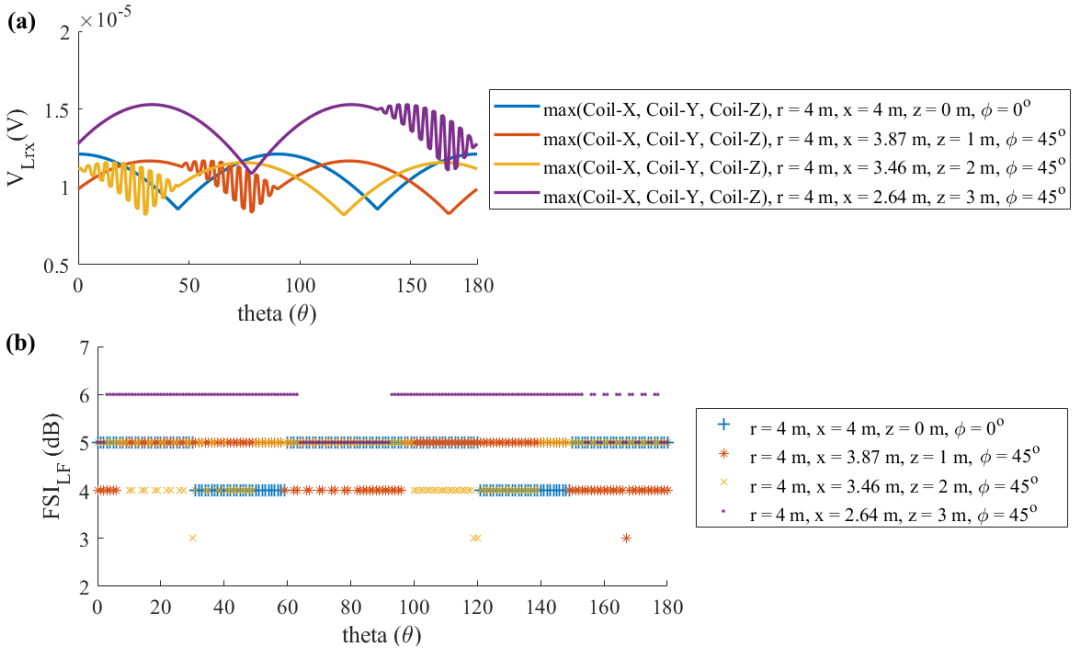

Figure 3.14: (a) Maximum value of induced voltage among all three coils of the 3-axes receiver antenna due to field created by helical coil for different values of x and z when $r = 4$ m (b) LF-FSI values for different values of x and z when $r = 4$ m

From these simulations regarding 3-axes orthogonal receiver, (2.23) can be used within some limits to model the DOT system without sacrificing range estimation accuracy when the orientation of the tag is unknown. Based on these results, we will

consider the Coil-X of the 3-axes receiver on the tag for measurements and simulations. The other solution to tackle the problem of orientation is to use three orthogonal coils at the transmitter as seen in [106]. However, it increases the bulkiness of the transmitter.

3.1.5 Impact of ferromagnetic obstacles

As the NFMI communication is based on the mutual inductive coupling between the transmitter coil and the receiver coil, the amount of mutual coupling depends on the magnetic flux passing through the receiver coil with respect to the total magnetic flux being generated at the transmit coil. Thus, any distortion in magnetic field changes the amount of mutual coupling between the transmitter coil and the receiver coil and affects the NFMI communication.

In the close proximity of ferromagnetic objects, the spatial distribution of the magnetic field is altered [104]. Therefore, in the close vicinity of ferromagnetic objects, the free space model for MI communication is invalid. Due to the magnetic field generated by the LF transmitter, eddy currents are induced in the ferromagnetic objects, which are responsible for a secondary field near the object. This secondary field causes deformation in distribution of effective magnetic field around that object [147]. This impact on the magnetic field distribution affects the mutual coupling between the LF transmitter and receiver coils. This affects the magnitude of voltage induced across the receiver coil and thus affects the LF-FSI recorded by the DOT tag. The amount of impact depends on three aspects: 1) relative magnetic permeability of obstacles 2) distance and relative position of transmitter or receiver from the obstacles and 3) size of ferromagnetic obstacles.

In order to observe this impact test #1, test #2 and test #3 are carried out using the transmitter antenna A of the activator. Usually, the most common ferromagnetic material found in indoor environment is steel, so as a ferromagnetic obstacle, a steel sheet of 0.5 m $\times$ 0.5 m with thickness of 0.004 m is used for test #1 and #3 which are carried out in an open outdoor environment to eliminate the effect of any obstacle other than steel sheet. For these two tests the activator, tag and the steel sheet are placed 0.5 m above from the ground using cardboard boxes as shown in Fig. 3.15 and 3.17.

The objective of test #1 is to observe the impact of the steel sheet when it is in the

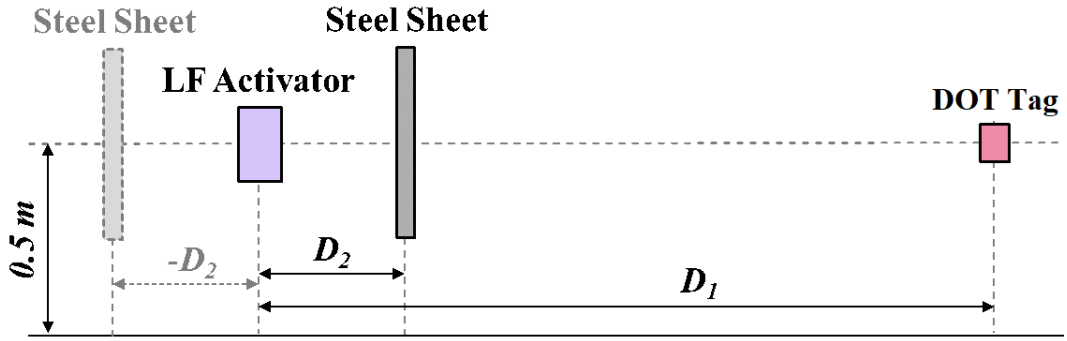

Figure 3.15: Setup for test #1 to observe the impact when the steel sheet is in the vicinity of the LF transmitter.

vicinity of the LF transmitter. As shown in Fig. 3.15, D_1 represents the distance between the activator and tag, while D_2 represents the distance between the activator and the steel sheet. During the test, position of the steel sheet is fixed at one of the predefined values of D_2 and the LF-FSI values are recorded by placing the tag at different values of D_1. The distance D_1 is increased until the tag is no longer activated. This procedure is repeated for different values of D_2 equal to 0.25 m, 0.1 m, 0.05 m and 0.01 m on either side of the activator on the line are joining the tag and the activator. Positive value of D_2 represents that the steel sheet is placed inside the segment formed by the activator and the tag as shown in Fig. 3.15, while negative value of D_2 represents that the tag is placed outside the segment formed by the activator and the tag.

The results for test #1 can be seen in Fig. 3.16. When the steel sheet is positioned closer to the LF transmitter, the LF-FSI value recorded by DOT tag is lower compared to the value recorded when the steel sheet is absent. The magnitude of LF-FSI at distance D_1 from the activator decreases as the distance between the activator and steel sheet, D_2, is decreased, regardless of the relative position of the sheet with respect to the tag and the activator. Tag detection range is also decreased as D_2 decreases. When steel sheet is absent, the tag detection range is around 5.5 m. Equivalent tag detection range is observed when the steel sheet is ±0.25 m away from the transmitter, also the LF-FSI values recorded are exactly same as the LF-FSI recorded in the absence of the steel sheet at different values of D_1. Thus, no impact on LF-FSI is observed when the distance of the steel sheet is 0.25 m or more. Tag detection range is around 5 m when D_2 is 0.1 m and around 5.5 m when D_2 is -0.1 m. When D_2 is reduced to ±0.05 m, tag detection range reduces to around 4.5 m. When D_2 is further decreased to ±0.01 m, tag detection

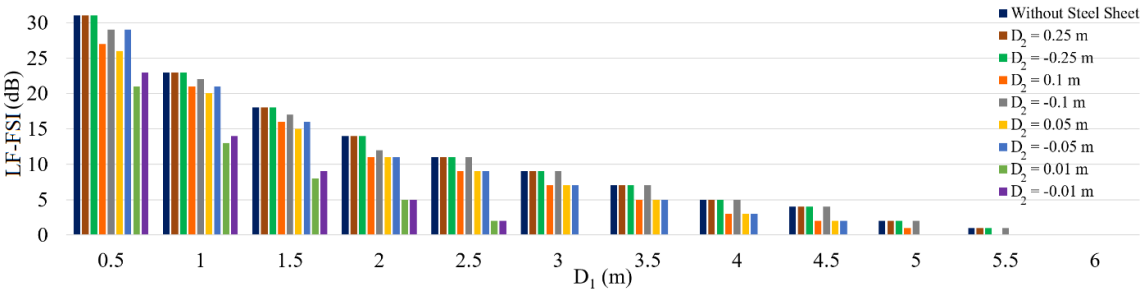

Figure 3.16: Results for test #1: LF-FSI at different values of D_1 for different values of D_2.

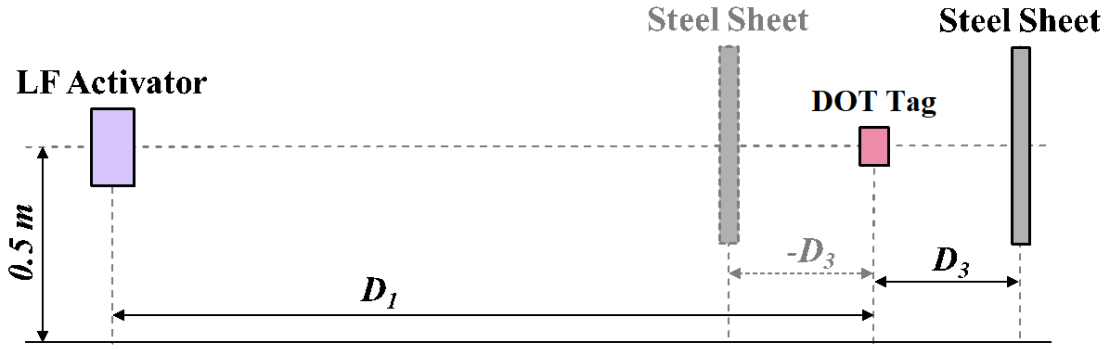

Figure 3.17: Setup for test #2 to observe the impact when the steel sheet is in the vicinity of the DOT tag.

range reduces to around 2.5 m. When the steel sheet is in-between the activator and tag, LF-FSI recorded is slightly less compared to LF-FSI recorded when the steel sheet and the tag are on the opposite sides of the activator.

Test #2 is performed to observe the impact when the tag is in the close proximity of the steel sheet. As shown in Fig. 3.17, D_3 represents the distance between the tag and the sheet, while D_1 represents the distance between the activator and tag. For different values of D_3, LF-FSI measurements, similar to the test #1, are carried out while increasing the distance D_1 by steps of 0.5 m. The distance D_3 is set to 0.25 m, 0.1 m, 0.05 m and 0.01 m on either side of the tag on the line joining the tag and the activator. Positive value of D_3 represents that the steel sheet is placed outside the segment formed by the activator and the tag as shown in 3.17, while negative value of D_3 represents that the steel sheet is placed inside the segment formed by the activator and the tag.

Fig. 3.18 shows the results for test #2. When the distance between the tag and steel sheet, D_3 , is ±0.25 m, no impact is observed on LF-FSI compared to the case when the steel sheet is absent. Also, no change in LF-FSI is observed when D_3 is -0.1 m and -0.05 m.

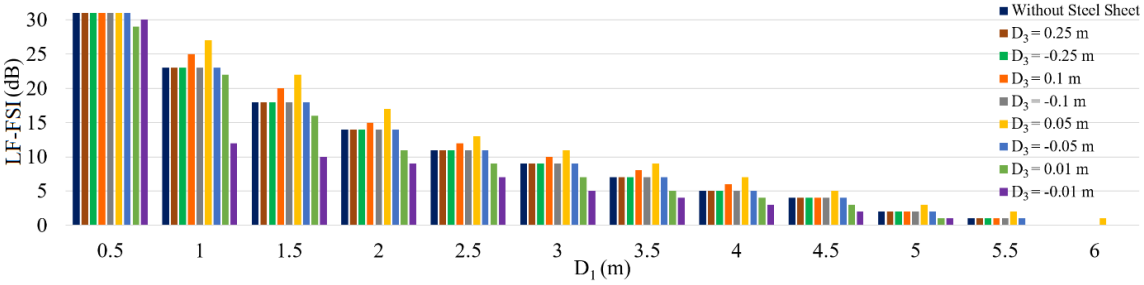

Figure 3.18: Results for test #2: LF-FSI at different values of D_1 for different values of D_3.

The tag detection range in all these cases is around 5.5 m. When D_3 is $\pm$0.01 m, reduction in LF-FSI is observed and the tag detection range also reduces to around 5 m. When D_3 is 0.1 m and 0.05 m increase in LF-FSI compared to the normal value is observed and When D_3 is 0.05 m tag detection range increases to 6 m.

When the ferromagnetic object is very close to the transmitter, the overall field generated by the transmitter around it is affected. This impact reduces as the distance between the transmitter and the ferromagnetic object is increased. After a certain distance from the transmitter, the deformation in the magnetic field distribution is only observed in the proximity of the ferromagnetic object and at any other point the magnetic field distribution is unaffected. In this case if the receiver is placed very close to the ferromagnetic object, the voltage induced in the receiver coil is affected. As the distance between the receiver coil and the ferromagnetic object increases, impact on the induced voltage across the receiver coil reduces.

Test #3 is performed in an office environment of dimensions 15 m $\times$ 21 m, to observe the impact of large walls containing mesh of steel bars inside them. The activator is fixed in the corner of two walls at approximately 0.1 m from the steel bars inside the walls. The LF-FSI value is recorded by placing the DOT tag at each position separated by 1 m in the office environment and at approximately 0.25 m from each wall as shown in Fig. 3.19. The height of the activator and the tag from the floor is set to 1.5 m.

Fig. 3.20 shows the map of the LF-FSI values recorded at each measurement position in test #3. The normal tag detection range for the activator used in test #3 is around 5.5 m beyond which the LF-FSI value is zero. Extended tag detection distance is observed closer to the walls, far beyond 5.5 m from the activator. This is caused by the mesh of steel bars inside the walls. The magnetic field propagates farther than the

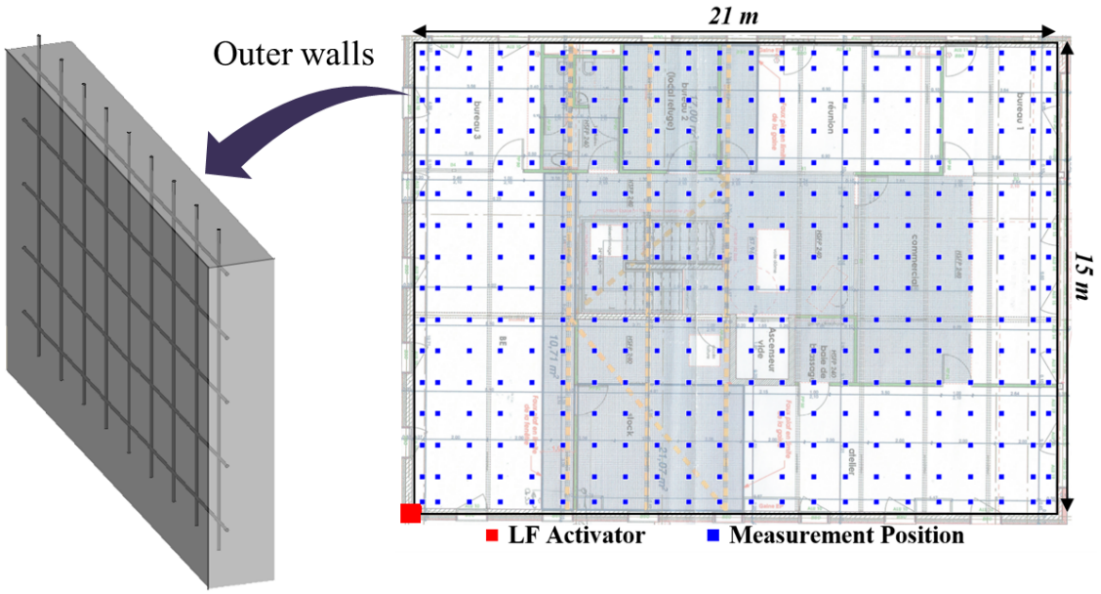

Figure 3.19: Setup for test #3 to observe the impact when the LF transmitter is installed on a wall containing mesh of steel rods.

expected distance due to the coupling between the steel bars, this effect is used as an extension technique for the MI waveguides [148]. Also, close to the walls, slight increase in LF-FSI values is observed when compared to the LF-FSI distribution elsewhere. Because of this effect the accuracy of range estimation, based on LF-FSI to distance relationship, is affected near such walls.

In order to simulate the behavior of the LF magnetic field near ferromagnetic materials, we used the software: EMCoS Antenna VLab [149]. This software performs EM simulation based on the Method of Moments (MOM) [150]. A transmitter coil with ferrite core is designed to generate magnetic field distribution at 125 kHz. The dimensions of the ferrite core designed are exactly same as those of actual ferrite core inside the activator. To simulate the effect of steel sheet, an obstacle is designed, and appropriate simulation parameters are defined. The simulations are performed in two different sets. Magnetic field distribution in the horizontal plane is observed in both simulation sets. The objective of the first set of simulations (Fig. 3.21) is to simulate the impact of the distance and the relative position of the steel sheet with respect to the transmitter. The obstacle of size 0.5 m $\times$ 0.5 m with a thickness of 0.004 m is placed near the transmitter coil. The distance between the transmitter coil and the obstacle is set as 0.01 m, 0.05 m, 0.1 m and 1 m.

The second set of simulations (Fig. 3.22), simulates the impact of different sizes

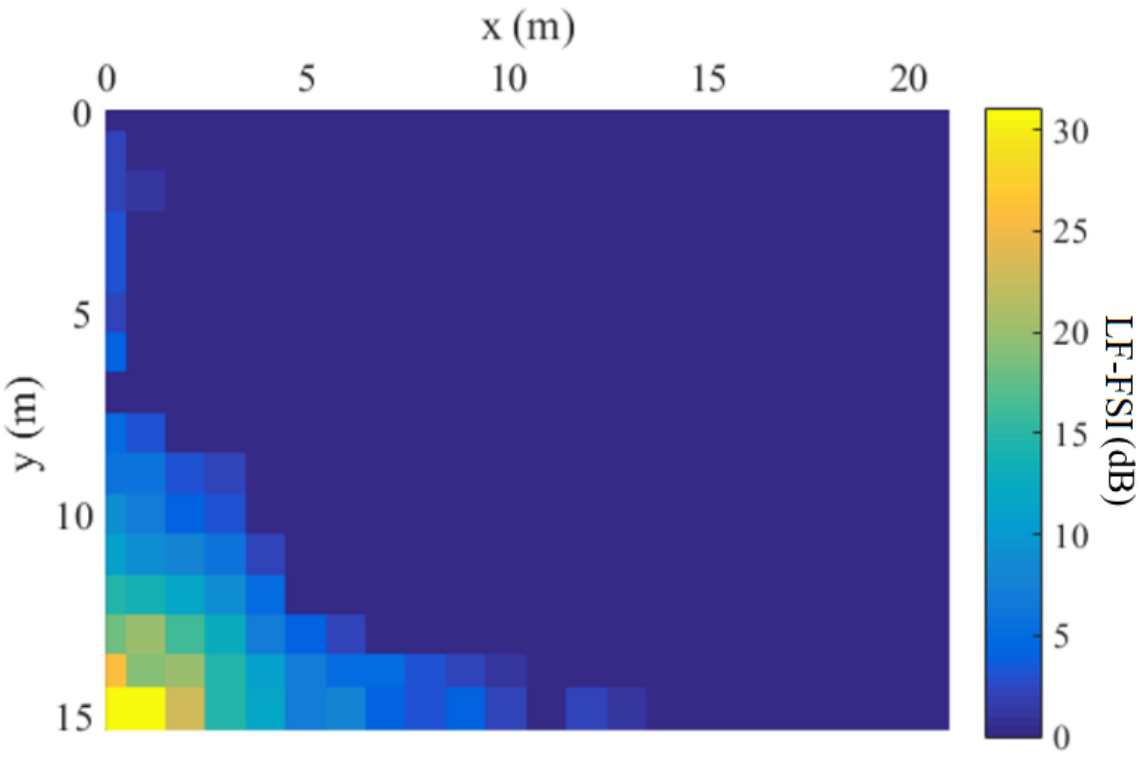

Figure 3.20: LF-FSI distribution map in the office environment (test #3)

of the steel sheet. The distance between the transmitter coil and the obstacle is set to 0.1 m. The size of the steel sheet is varied from 0.25 m × 0.25 m × 0.004 to 1 m × 1 m × 0.01 m. The impact of the large bars of steel bars is also simulated using steel rods of diameter 0.01 m. In this case, a mesh is created by separating each rod by 0.5 m and arranging them vertically and horizontally. This mesh is similar to the meshes used inside the walls. Simulation set 1 (Fig. 3.21) helps to understand the observations from test #1 and 2.

In Fig. 3.21, magnetic field distribution maps in the second row are zoomed versions of the maps in the first row. Fig. 3.21 (a) shows the magnetic field distribution around the transmitter when the steel obstacle is absent. Fig. 3.21 (b) shows the magnetic field distribution when the steel obstacle is placed 0.01 m from the transmitter. As the distance between the transmitter and the obstacle is increased for next two simulation scenarios, it can be observed that the impact on the field distribution is reduced. The magnetic field strength decreases more rapidly as the steel obstacle gets closer to the transmitter; this explains the reduction in tag detection range observed in test #1. Also, the difference in field distribution on either side of steel sheet can be seen. In Fig. 3.21 (e), where the obstacle is at 1 m from the transmitter, increase in magnetic field strength

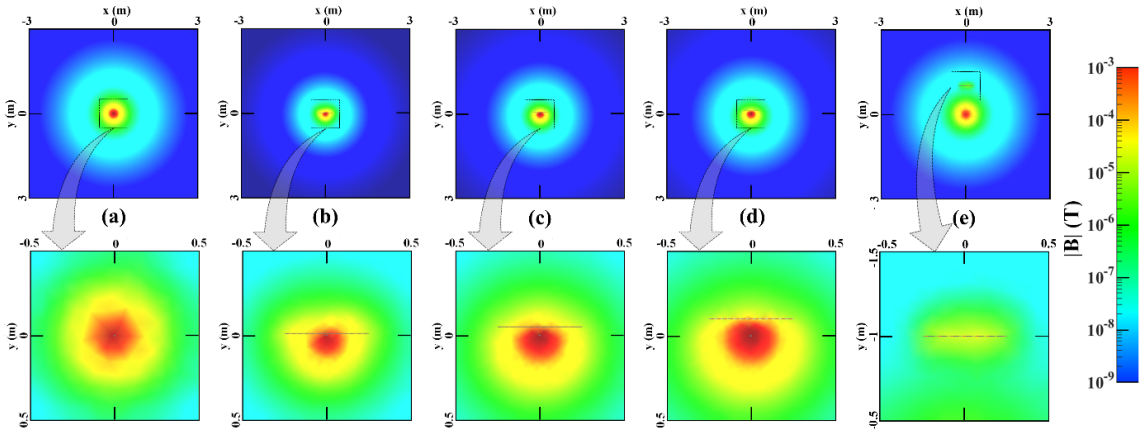

Figure 3.21: Simulation set 1: Magnetic field distribution around the transmitter (a): without any obstacle in the vicinity; (b): obstacle at 0.01 m from the transmitter; (c): obstacle at 0.05 m from the transmitter; (d): obstacle at 0.1 m from the transmitter; (e): obstacle at 1 m from the transmitter.

can be seen in the proximity of the obstacle and the field distribution is unaltered everywhere else.

From Simulation set 2 (Fig. 3.22) it can be seen that large ferromagnetic obstacles have a greater impact on the magnetic field distribution. Fig. 3.22 (c) shows the effect similar to that observed in test #3 where the increase in magnetic field strength is observed near the mesh. Based on all the above observations, the impact on LF-FSI caused by ferromagnetic materials is considerably larger when the LF transmitter is installed within approximately 0.2 m from the ferromagnetic objects compared to the case where the DOT tag is in the close proximity of these objects. As the range estimation using DOT system is based on the mathematical relationship between LF-FSI and distance, impact on LF-FSI due to ferromagnetic obstacles leads to errors in range estimation.

3.2 Experimental Verification of the System Model

3.2.1 Experimental Setup

In order to validate the system modeling equations in the case of differed types of loops, three sets of measurements with three types of transmitter antennas: 1) air core loops, 2) ferrite loops and 3) tuned loops are performed. The measurement system consists of LF transmitter and receiver units. The measurements are transferred to a com-

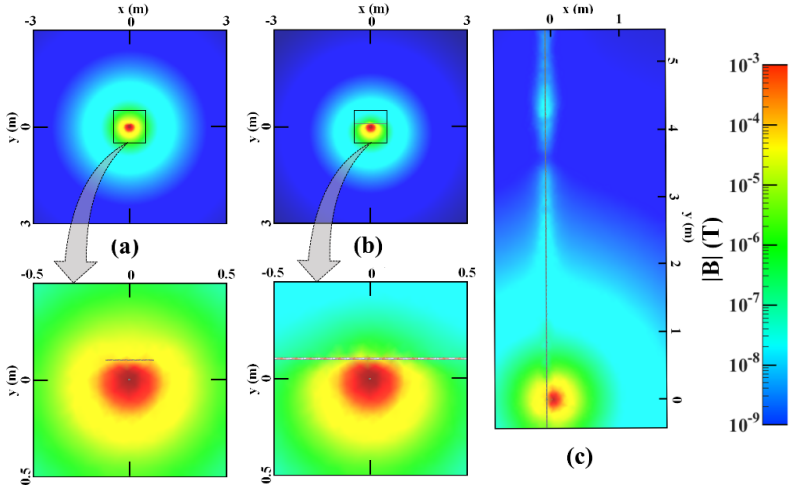

Figure 3.22: Simulation set 2: Magnetic field distribution around the transmitter with (a): obstacle size 0.25 m × 0.25 m × 0.004 m; (b): obstacle size 1 m × 1 m × 0.01 m. (c): mesh of steel bars of diameter 0.01 m.

puter for storage using a 433 MHz link between a UHF transmitter on LF Receiver unit and an UHF reader attached to the computer. Both LF transmitter and receiver units are held by tripods keeping the same height from ground. Three sets of experiments were performed in order to observe the impact on induced voltage at the receiver, due to different factors such as size of the receiver coil and use of ferrite at the transmitter and receiver. Fig. 3.23 shows the general setup of the experiments where different sets of transmitter and receiver antennas were used for each individual experiment.

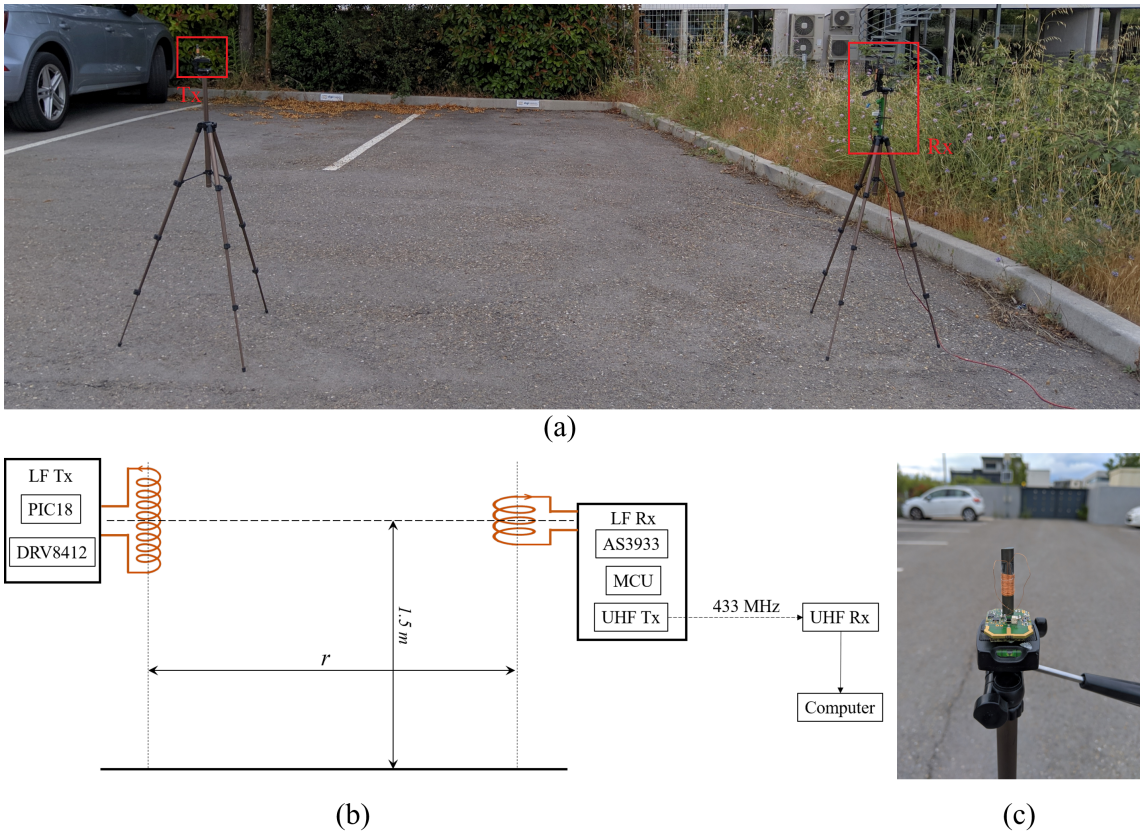

Figure 3.23: (a) Surrounding environment and placement of Tx and Rx for LF-FSI measurements. (b) Setup of LF-FSI measurement system (c) LF receiver with coil Rx4.

3.2.2 Transmitter Structure

The transmitter system shown in Fig. 3.23 was composed of an emitting loop, and the transmitter circuit board of dimensions 0.14 m x 0.05 m which contains a micro-controller, a full bridge inverter as the current driver and a power supply unit. The micro-controller was used to generate a 125 kHz square wave signal of length 4 ms after each 200 ms. Different emitting loops were tested during the experiments. The transmitter unit was powered by a 12 V power supply. Enameled copper wire of diameter 0.00032 m was used for all transmitter loop designs. The diameter of all transmitter loops was 0.00816 m.

3.2.3 Receiver Structure

Film capacitors with voltage rating of 2 kV are used for tuning the transmitter loops at 125kHz, as the voltages across the transmitter loops can be very high. 50V ceramic capacitors were used for tuning the receiver loops. An UHF (433 MHz) transmitter unit was used to transfer the LF-FSI measurements wirelessly to a UHF receiver attached a computer. The LF-FSI measurement from the receiver system are converted to the output voltage V_{out} of the three-axes receiver antenna or the input to the LF receiver AS3933 using (3.4) [151] where FSI_{LF} is the LF-FSI value measured by the receiver and V_{ref} is the sensitivity of the LF receiver which is 0.226 mVpp.

$$V_{out} = 10^{\left(\frac{RSSI_{LF}}{10}\right)} V_{ref} \tag{3.4}$$

3.2.4 Measurement coil parameters

DC values inductance and resistance of each coil is measured using a bench-top LCR meter at a test frequency of 125 kHz. During each measurement configuration, the current I_{tx} passing through transmitter coil is measured using a 15 A AC/DC current probe.

3.2.5 Simulation of Coil Parameters

3.2.5.1 3D Quasi-static Simulation

Simulations for inductance and resistance values of the coils is performed using the software ANSYS Q3D Extractor [152], which is specifically designed for carrying out 3D and 2D quasi-static electromagnetic field simulations. It employs MOM [150, 153] technique accelerated by Fast Multipole Method (FMM) [150] in order to perform 3D quasi-static electromagnetic field analysis. The MOM technique is a numerical computational method of solving linear partial differential equations which have been formulated as integral equations. It is a technique used to solve electromagnetic surface or volume integral equations in the frequency domain. Q3D Extractor easily and quickly provides 3D extraction of resistance (R), partial inductance (L), capacitance (C) and conductance

(G). The simulation results include proximity and skin effect, dielectric and ohmic loss, and frequency dependencies. The version of the software used for the simulations is 18.0.0. The data collected from the simulations is in the form of scattering parameters (also known as S–parameters), which can be transformed into a number of different electrical parameters such as inductance, resistance and Q–factor. Fig. 3.24 and 3.25 show the models used for Q3D simulations of transmitter and receiver coils respectively. The coils are set up in the 3D space using the helix geometry feature of the software. Instead of a wire of circular cross section, a wire of equivalent rectangular cross-section is considered which is a good approximation and helps to significantly reduces simulation time. Cylindrical ferrite rods are modeled using polyhedron geometry feature of the software. Source and sink for the current are assigned to the terminals of each coil. The simulation is performed at the solution frequency of 125 kHz and DC values of resistances and inductances are simulated.

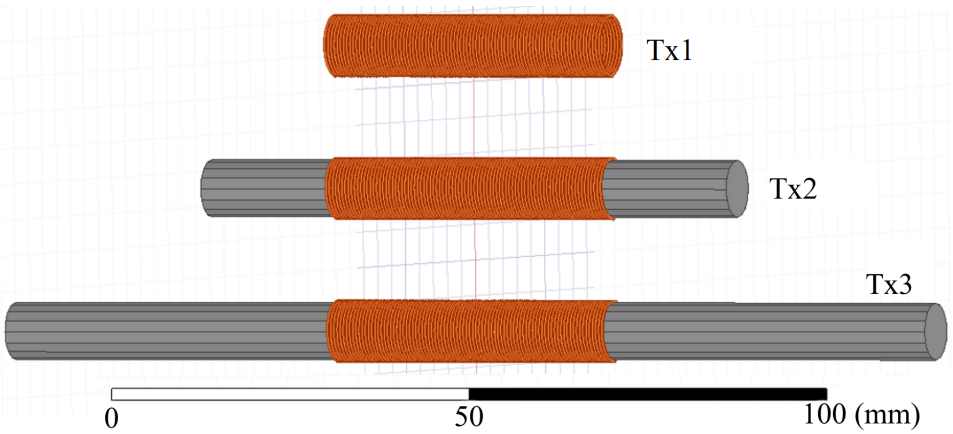

Figure 3.24: 3D models of different transmitter coils used during experimental work used for ANSYS Q3D simulation.

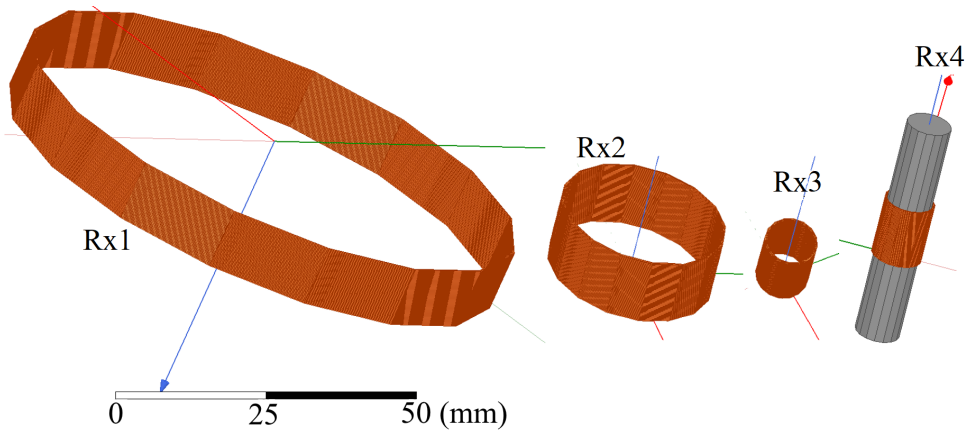

Figure 3.25: 3D models of different receiver coils used during experimental work used for ANSYS Q3D simulation.

3.2.5.2 Spice Simulation

LTspice [154] is a high-performance SPICE simulation software, schematic capture and waveform viewer with enhancements and models for easing the simulation of analog circuits. This software is used to simulate the transmitter and receiver equivalent circuits. Fig. 3.26 shows the equivalent circuits used in LTSpice for transmitter and receiver of the presented system.

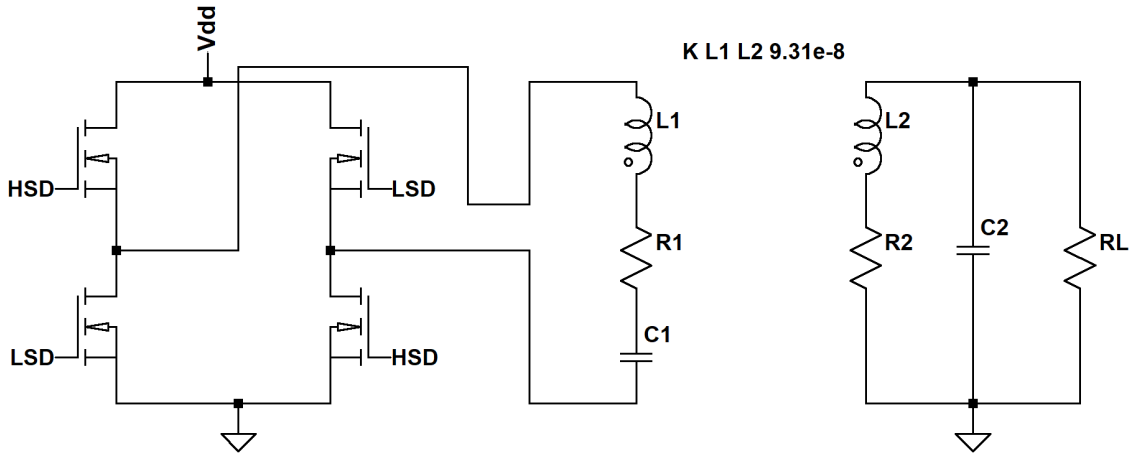

Figure 3.26: Spice simulation for the transmitter and receiver circuits of the presented system. K represents the coupling coefficient between the transmitter and receiver coil.

The full-bridge inverter which is used as a transmitter driver circuit was simulated along with equivalent resonant coupling circuit and the receiver load, using LTspice.

Inductance and resistance values from Q3D simulations are used for the coils. The coupling factor calculations are made using (3.4). This simulation is performed in order to obtain the value of current passing through the transmitter coil and the voltage V_{out} across R_{out} for each measurement configuration.

3.2.6 Comparison of Simulation and Measurement Results

Table 3.1 and 3.2 present the configurations of transmitter and receiver coils respectively.

Tx Coil	**Tx1**	**Tx2**	**Tx3**
Inductance measured (μH)	12.5	470	738
Coil diameter (mm)	8.16	8.16	8.16
Winding length l_c (mm)	40	40	40
DC resistance (Ω)	0.5	0.5	0.5
Length of ferrite (mm)	-	80	140
Inductance Q3D (μH)	11.65	480.34	766.4
Resistance Q3D (Ω)	0.5	0.5	0.5

Table 3.1: Specifications of Transmitter Coils used for Experimental work.

Rx Coil	**Rx1**	**Rx2**	**Rx3**	**Rx4**
Inductance measured (μH)	1821	360	32.6	430
Coil diameter (mm)	87.5	27.5	8.16	8.16
Winding length l_c (mm)	10	10	10	10
DC resistance (Ω)	22.75	7.2	2.1	2.1
Length of ferrite (mm)	-	-	-	40
Inductance Q3D (μH)	1667.5	341	38.7	475
Resistance Q3D (Ω)	23.5	7.43	2.21	2.21
$\|H(\omega)\|$	60.17	39.07	11.64	149.63
Quality Factor	60.16	39.05	11.64	149.63

Table 3.2: Specifications of Receiver Coils used for Experimental work.

Table 3.3 shows the measured and simulated values of current passing through the transmitter for various combinations of transmitters and receivers used during the experiments.

Tx Coil	**Rx Coil**	Itx **Simulated (A)**	Itx **Measured (A)**
Tx1	Rx1	17.6	17.2
Tx1	Rx2	17.4	17.3
Tx2	Rx1	8.5	8.3
Tx2	Rx2	9.3	9.2
Tx2	Rx3	7.4	7.3
Tx2	Rx4	9.1	9.1
Tx3	Rx4	7.6	7.5
Tx3	RX5	6.2	6.3

Table 3.3: Simulated and Measured Current I_{tx} through Transmitter Coil

During experiment set 1, value of induced voltage is measured using Rx1 at the receiver and Tx1 and Tx2 at the Transmitter. Similarly, during measurements set 2, Rx2 is used at the receiver and Tx1, Tx2 are used at the transmitter. These two sets of experiments were performed in order to observe the difference in induced voltage due to the use of ferrite at the transmitter and different receiver sizes. Aim of the third set of experiments was to compare the difference in induced voltage when coils Rx3 (without ferrite) and Rx4 (with ferrite) are used at the receiver while Tx2 was used at the transmitter. Receiver Rx5 refers to the 3-axes antenna on the DOT tag.

3.2.7 Results and analysis

As seen in Fig. 3.27, Operational range of 14 m is observed during experiment set 1, for combination of Tx1 and Rx1. When Tx2 is used at the transmitter overall gain in the measured voltage across the load resister is seen and operational range increases to 18 m.

Similar results are observed for Rx2 as seen in Fig 3.28 for experiment set 2. The operational range increases from 5 m to 7 m. These two cases observe the increase in operational rang due to the use of ferrite rod at the transmitter. Decrease in operational range is seen when the radius of receiver coil is reduced. Analytically calculated values of the V_{out} can be compared in the figures.

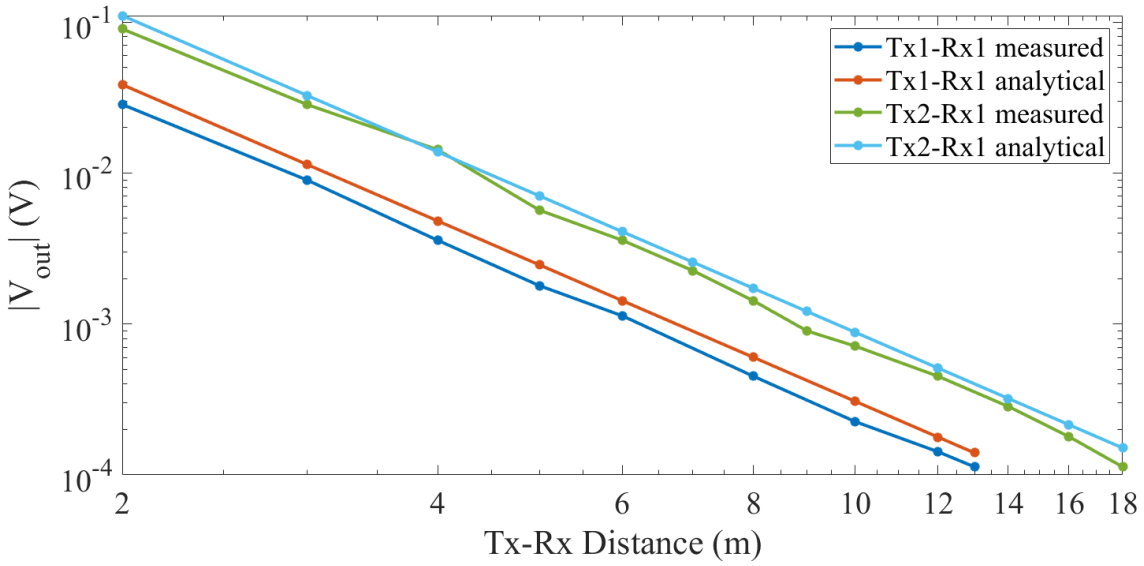

Figure 3.27: Measured and analytical values of V_{out} across load resistor for different distances between transmitter and receiver receiver in case of experiment set 1.

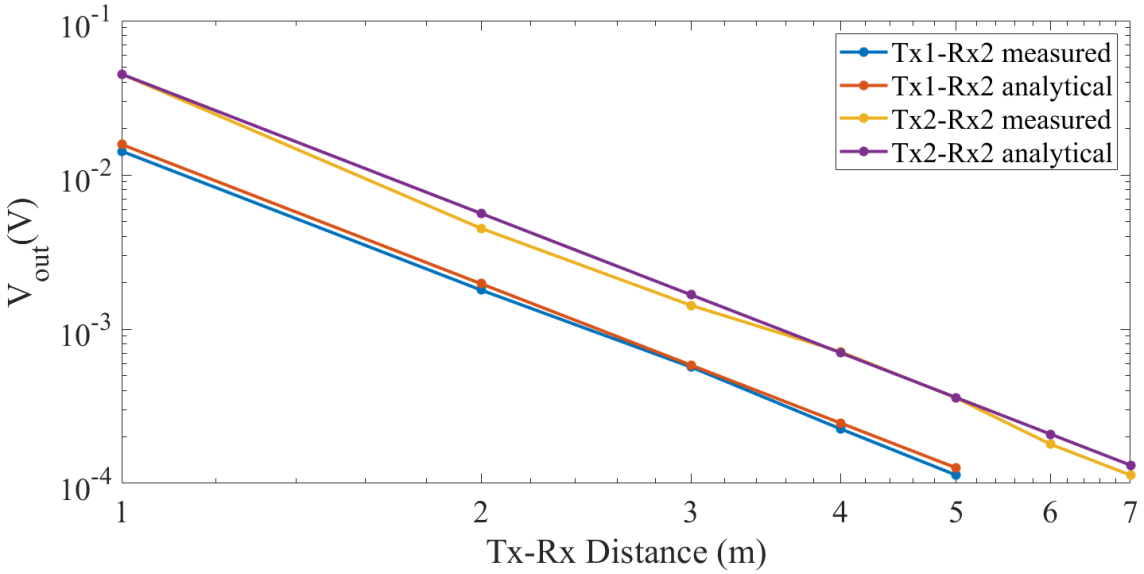

Figure 3.28: Measured and analytical values of V_{out} across load resistor for different distances between transmitter and receiver receiver in case of experiment set 2.

For the third set of experiment the dimensions of receiver coil is further reduced. Here the impact of use of ferrite at the receiver is observed. For Rx3 as the dimensions of the coil are very small operational range of only 1.8 m is observed while it is increased to 7 m as result of ferrite (Fig. 3.29). Measurement data from all sets of experiment are in agreement with analytical calculations obtained from the proposed model.

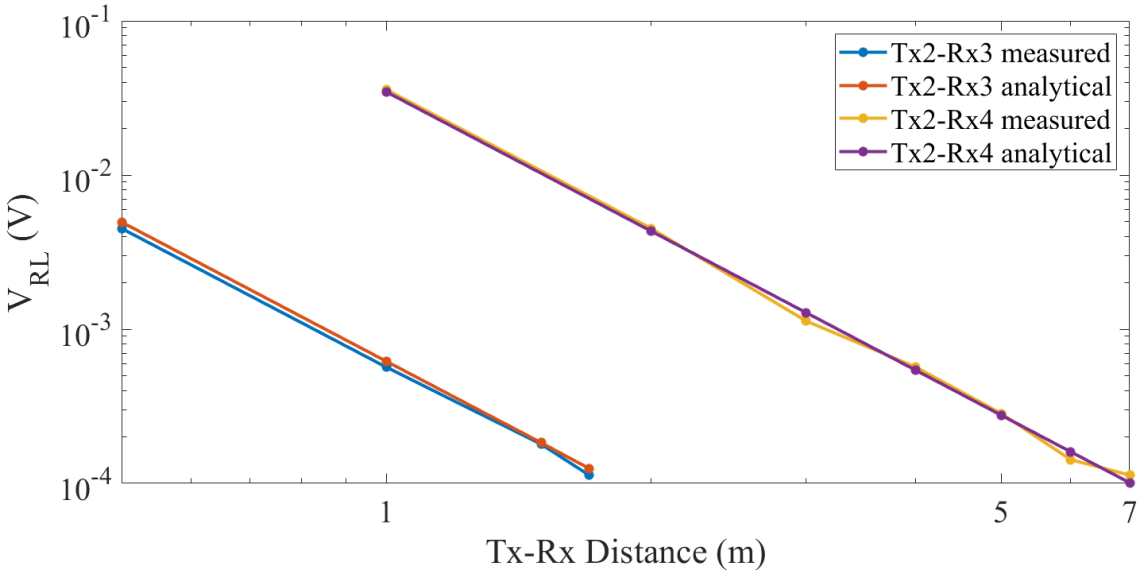

Figure 3.29: Measured and analytical values of V_{out} across load resistor for different distances between transmitter and receiver in case of experiment set 3.

3.3 Optimization

After validation of the proposed model, it can be used to design and optimize the actual system. In order to match the size of the transmitter circuit board (0.145 m x 0.05 m) a prototype transmitter loop Tx3 with a ferrite rod of length 0.14 m was designed while keeping the other parameters same as Tx1. Tx3 has measured inductance value of 0.74 mH and an off the shelf film capacitor of 3.3 nF is used for tuning this antenna at 125 kHz. Induced voltage measurements were performed using the COTS receiver antenna 3DC15-720J described in chapter 1. An operational range of 8.5 m was achieved with this combination. Tx3 provides 3 m increase in the operational range of which more than 50% increase to 5.5 m operational range obtained using the COTS transmitter antenna at the transmitter. Tx3 is designed considering the dimensions of the transmitter circuit board, availability of ferrite rod, capacitor value available in the market. Fig. 3.30 shows measurements and analytical results for Tx3. This study can be used to build and optimize a transmitter antenna with different configuration to achieve required size and operational range.

3.3.1 Design and Optimization Guidelines

Although close to 10 m coverage is obtained using the compact 3-axes receiver, the coverage can be increased substantially using different designs of the receiver loop. For example, the combination of Tx3 and Rx1 results in the coverage of more than 25 m. In this case a single loop is used instead of 3-axes antenna so they cannot be used omnidirectionally. However, in use cases where the tag always remains in the same plane e.g. tag installed on the vehicles; such design can be beneficial.

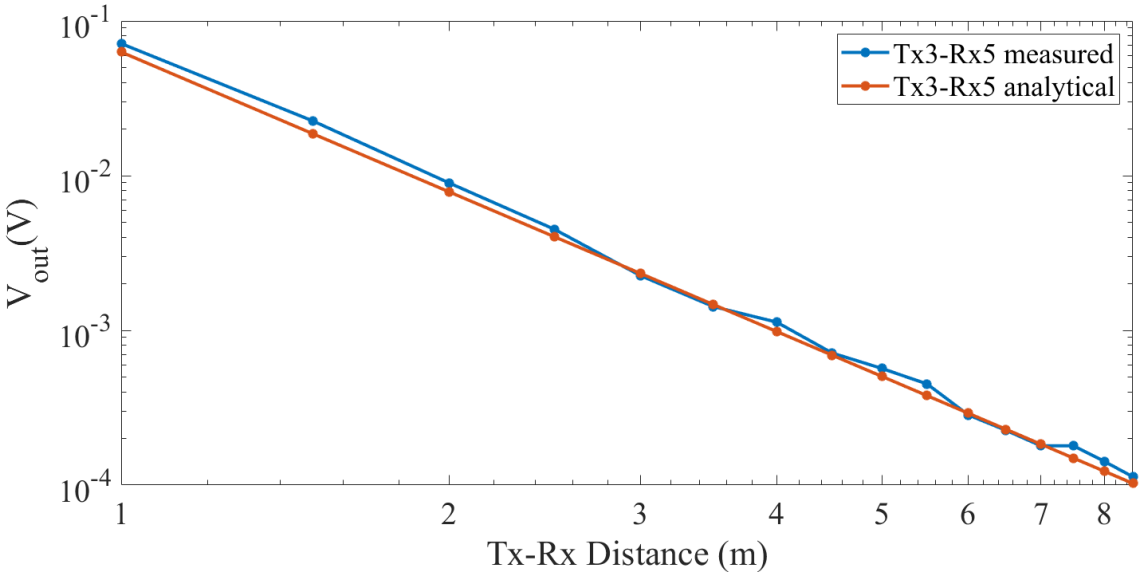

Figure 3.30: Measured and analytical values of V_{out} across load resistor for Tx3. Value of V_{out} is measured using 3-axes receiver antenna 3DC15-720J at the tag.

3.4 Conclusion

In this chapter characteristics of NFMI signal are observed with the help of LF-FSI measurements in different environmental and NLOS conditions. Various experiments are performed in order to validate the performance and limitations of LF-FSI in different environmental conditions. The strength of LF signals produced by DOT system can be varied by changing the configuration of the transmitter antenna as other parameters of the system are fixed. The operational range offered by our system is around 5-10 m, which is comparatively less against many other ranging and localization system. However, LF-FSI offer better performance in presence of obstacles and human body

(Fig. 3.5). Disturbances caused by ferromagnetic objects transmitter or DOT tag from these objects. Ferromagnetic objects, when placed very close to LF transmitter, affect the tag detection range and LF-FSI captured anywhere inside the tag detection range. This impact reduces as the distance between the transmitter and the ferromagnetic object is increased. After a certain distance from the transmitter, impact on LF-FSI is only observed when the DOT tag is in close proximity of the ferromagnetic object. In this case, if the tag is inside the segment formed by the transmitter and ferromagnetic object, increase in LF-FSI is observed and if it is outside this segment, decrease in LF-FSI is observed. Extension in tag detection range near the walls containing mesh of steel bars is observed when the LF transmitter is very close to such walls.

Chapter 4

Performance Evaluation of DOT system and its Use Cases

This chapter concerns the ranging and positioning performance evaluation of DOT system, which is physically modeled in chapter 2 and the use case analysis of this system. Range estimation methodology used by the DOT system is described and the experimental work evaluating the ranging performance of the system is presented. One of the important application scenario of the system i.e. real-time indoor positioning, is discussed along with the positioning methodologies used by the system. Positioning experiments showcasing the positioning capabilities of this system based on NFMI technology are presented and its 2D positioning performance is benchmarked with that of other positioning technologies i.e. active UHF-RFID and UWB, within similar environmental conditions. All these experiments were performed in different environments which are described in this section. Use cases of the DOT system for which testing, and demonstrations were performed are presented in this chapter.

4.1 Experimentation with DOT system and comparison with UHF-RFID and UWB systems

This section presents the methodology used to perform ranging and positioning based on LF-FSI based DOT system. To evaluate the ranging and 2D positioning capabilities of the system in terms of complexity of the methodology and accuracy, experimental work is carried out. The results of the experimentation are analyzed in the

context of potential application scenarios. In order to benchmark the ranging and 2D positioning performance of the DOT system, similar experimental work is carried out with active UHF-RFID and UWB technologies. This benchmarking helps to compare the suitability of DOT system for the ranging and positioning based applications in terms of accuracy in addition to other metrics such as cost, latency, ease of deployment, scalability, complexity, etc.

4.1.1 Ranging methodologies

RSSI-based distance estimation is usually based on propagation channel modeling [155, 156]. If we consider a wireless network composed of transmitting nodes and receiver nodes, the position of a receiver node can be calculated using the propagation channel model-based approach. After a receiver node measures the RSS of the signal from the transmitting nodes a channel model is used to estimate the distances between the transmitting node and the receiver node from the RSS measurements.

In the case of far field RF signals various propagation channel models [156] can be used for this purpose. Models for free space attenuation include free-space path loss model, dipole field strength in free space model and Friis transmission equation. Models for indoor attenuation include ITU model for indoor attenuation and Log-distance path loss model [155]. However, the received RSSI is highly influenced by various factors such as multipath propagation, signal reflection, signal scattering and noise. Therefore, it is necessary to adjust the channel model parameters according to the environmental influences. In such cases propagation channel model is obtained using calibration. In this case several RSSI measurements are pre-recorded and processed in order to obtain an attenuation model for the signal in that environmental conditions.

In the case of NFMI signal based ranging system capable of producing LF-FSI as the signal strength indicator, in addition to calibration approach, signal attenuation model can also be obtained using physical modeling equations. This physical modeling-based approach can neglect the impact of factors such as multipath propagation, signal reflection, signal scattering, as NFMI signal in LF is very less affected by these factors.

In the case of DOT system, we have used both ranging approaches i.e. calibration-based attenuation model and physical modeling-based attenuation model for distance

estimation.

4.1.1.1 Calibrated attenuation model based ranging approach

When calibration based attenuation model approach is considered, during the calibration phase, a set of LF-FSI values are pre-recorded for the target environment type and LF-FSI attenuation model equation is obtained for the DOT system with the help of least squares curve fitting technique. Least square fitting technique [157] is a mathematical procedure in order to determine the best-fitting curve to a given set of points by minimizing the sum of the squares of the offsets of the points from the curve. If DF is the deviation function for n data points, which is the sum of the square of the deviations between the curve-fit and actual data points, in this ranging approach, $F(FSI_i)$ is the curve-fit function, which may involve any number of unknown coefficients $(a_0, a_1, a_2, \ldots a_n)$. This function is an approximation of distance r between transmitter and receiver. D_i is the i^{th} data point representing i^{th} pre-recorded measurement of distance r for corresponding LF-FSI value FSI_{LF}.

$$DF = \sum_{i=1}^{n} (F(FSI_i) - D_i)^2 \tag{4.1}$$

In this ranging approach, the method of least squares curve fitting determines the coefficients of the mathematical function representing the relation between the distance and LF-FSI. In this case we kept this mathematical function to a third order polynomial and we can represent it as shown in (4.2) where $\hat{r}$ is approximation of the distance between transmitter and receiver and FSI_{LF} is the LF-FSI value measured by the receiver.

$$\hat{r} = F(FSI_i) = a_3 FSI_{LF}^3 + a_2 FSI_{LF}^2 + a_1 FSI_{LF}^1 + a_0 \tag{4.2}$$

During the ranging phase, real-time LF-FSI value is measured by the DOT tag. This value is used to estimate the distance between the activator and the tag with the help of the calibration-based attenuation model. This technique of relating LF-FSI to the distance requires significantly lesser memory and training time as compared to fingerprinting in the case of far field RF signals. This is because fewer calibration points are sufficient in order to obtain a fairly accurate attenuation model as the NFMI signal

characteristics don't change much at the different places of the environment.

4.1.1.2 Physical system modeling based ranging approach

The physical system modeling equations from chapter 2 are used for the second ranging approach to estimate the distance between LF transmitter and receiver when the physical parameters such as coil dimensions, current, self-inductances, are known in addition to the LF-FSI value generated by the DOT tag. As LF-FSI is not significantly affected by multipath and shadow fading, this approach can be used for ranging irrespective of the environment. From (3.3) we can obtain (4.3) for estimating the distance $\hat{r}$ which is the approximation of the actual distance between the transmitter and receiver from the LF-FSI value FSI_{LF} recorded in real-time by the DOT tag. In this case, the parameters of the coils are either taken from the datasheets if available or measured.

$$\hat{r} = \sqrt[3]{\frac{2\pi f_0 {a_{tx}}^{\frac{3}{2}} {a_{rx}}^{\frac{3}{2}} \sqrt{L_{tx} \cdot L_{rx}} I_{tx} Q_{rx}}{V_{ref} 10^{\frac{FSI_{LF}}{10}}}} \tag{4.3}$$

In the case of active UHF RFID technology UHF-RSSI calibration based propagation model approach is considered. TOF based TWR approach is used for the distance estimation using UWB technology.

4.1.2 Ranging experiment with DOT system in warehouse environment

This experiment is carried out in order to demonstrate the ranging capability of proposed approaches for DOT system in harsh propagation environment and to evaluate ranging accuracy which will help to determine the usability of this system for the application scenarios intended for the similar environment types i.e. manufacturing plants, warehouses, etc. A ranging experiment is performed in an indoor storage facility. This storage facility (Fig. 4.1(a)) of 8 m x 6 m contains metallic racks, stock of electronic devices and raw materials. A transmitter with prototype ferrite antenna is installed at a height of 1.5 m from the floor as shown in Fig. 4.1(b) in the storage facility.

In this experiment the physical system modeling equations are used to perform range estimation and the performance of this approach was compared with the MI magnetic field attenuation model-based approach using calibration. Range estimations are performed at the points shown in Fig. 4.1(c), based on LF-FSI captured at individual test points.

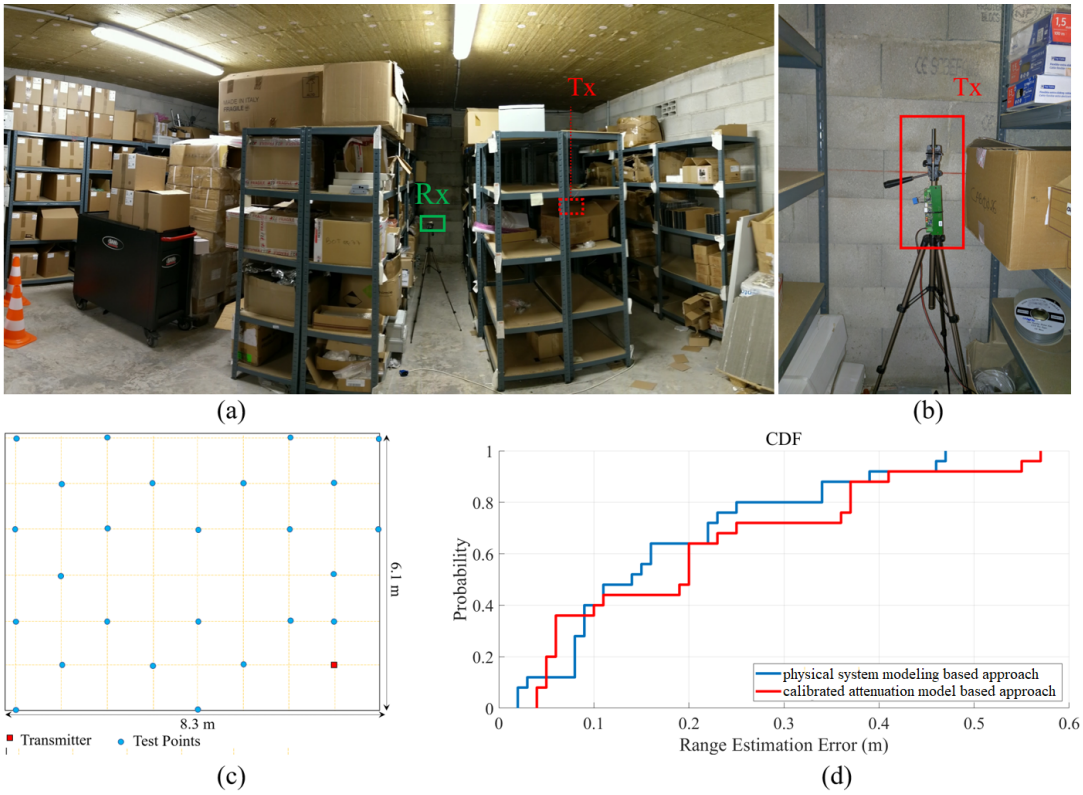

Figure 4.1: (a) Environment where ranging experiment is performed (b) LF transmitter with coil Tx3 (c) Setup for range estimation experiment. (d) Cumulative distribution function for range estimation errors.

Fig. 4.1(d) shows the comparison between overall range estimation performance of the system using calibration based and modeling based ranging methods. For 25 range estimations, mean range estimation error of 0.21±0.16 m was obtained with ranging method based on attenuation model obtained using calibration. With the help of system modeling equations ranging accuracy improved to 0.18±0.13 m. Range estimation error is below 0.41 m for 90% of estimations for method based on attenuation model obtained using calibration and below 0.37 m for the ranging method using physical system modeling equations.

4.1.3 Positioning methodologies

In the case of DOT system, during distance estimation stage, distances between the DOT tag and the LF activator devices are obtained. These distances are then used to calculate the position of the tag with the help of ranging-based positioning techniques. Two such techniques i.e. WCL and trilateration are discussed below.

4.1.3.1 Weighted centroid positioning

WCL approach is an improvement to the classic CL technique which uses a Link Quality Indicator (LQI) to get a more precise location information [22]. WCL is very efficient and low-complexity positioning technique which is less sensitive to errors in range estimation compared to triangulation techniques [158]. The steps involved in WCL calculations are shown in Fig. 4.2. In order to localize the j^{th} tag T_j (Fig. 4.3), range information from several activators are used. Estimated distance d_{ij} between the i^{th} activator A_i (Fig. 4.3) and the tag T_j is used to form weight w_i which determines the impact of that activator on final estimated position. The weight w_i for the i^{th} activator can be calculated using 4.4, where g is weighting degree. The degree g determines the influence of each activator in the positioning calculation in non-linear fashion. The optimal value of g depends on the arrangement of the activators. Weighting degree greater than one assigns greater weights to the activators which are closer to the tag. Determination of degree g is done using the measurements from the calibration phase. The attenuation models obtained after calibration are used to perform positioning simulation of each calibration point for different values of g. The value of g for which the mean positioning error is the minimum, is chosen as the optimum weighting degree which is used in the positioning phase.

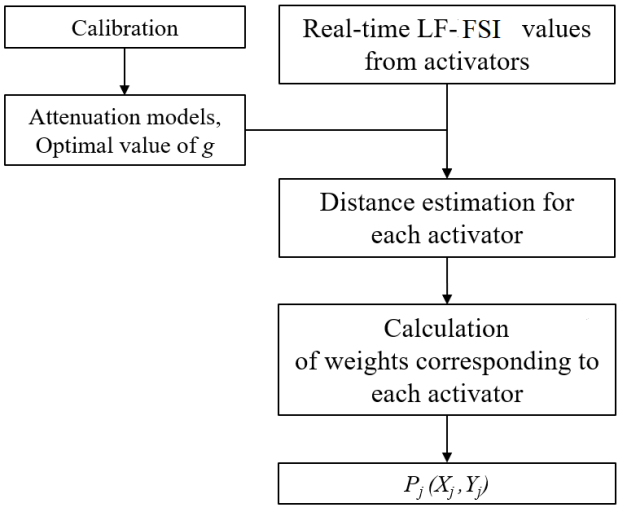

Figure 4.2: Steps involved in WCL algorithm for DOT system.

$$w_{ij} = \frac{1}{d_{ij}{}^{g}} \tag{4.4}$$

In 2D Cartesian coordinate system, let the location of the i^{th} activator be denoted by (x_i, y_i) and the number of activators contributing to positioning be n, then the estimated position (X_j, Y_j) of j^{th} tag T_j, using this algorithm is given by (4.5).

$$X_j = \frac{\sum_{i=1}^{n}(w_{ij}x_i)}{\sum_{i=1}^{n} w_{ij}}, Y_j = \frac{\sum_{i=1}^{n}(w_{ij}y_i)}{\sum_{i=1}^{n} w_{ij}} \tag{4.5}$$

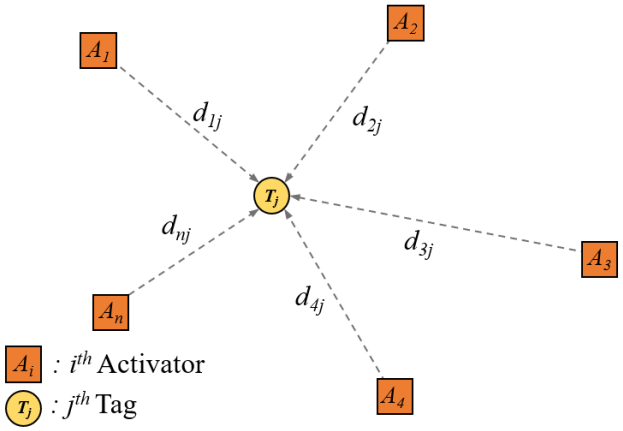

Figure 4.3: Schematics of WCL algorithm.

4.1.3.2 Trilateration Algorithm

In positioning stage with trilateration technique, the position of the tag is estimated using the steps shown in Fig. 4.4. Distances estimated between all detected activators and the tag are used to perform trilateration. Trilateration is performed on three distances at a time for all possible combinations of base stations. The combinations, resulting in the estimated positions which are outside of the experimental area by more than 5 m, are discarded. The final estimated position is obtained by averaging all position estimations from valid combinations of base stations. This technique is used to minimize the impact of distance estimation errors. Another possible approach with the trilateration technique is pseudo inverse approach [159]. However, this approach was not considered as it is more affected by the ranging error.

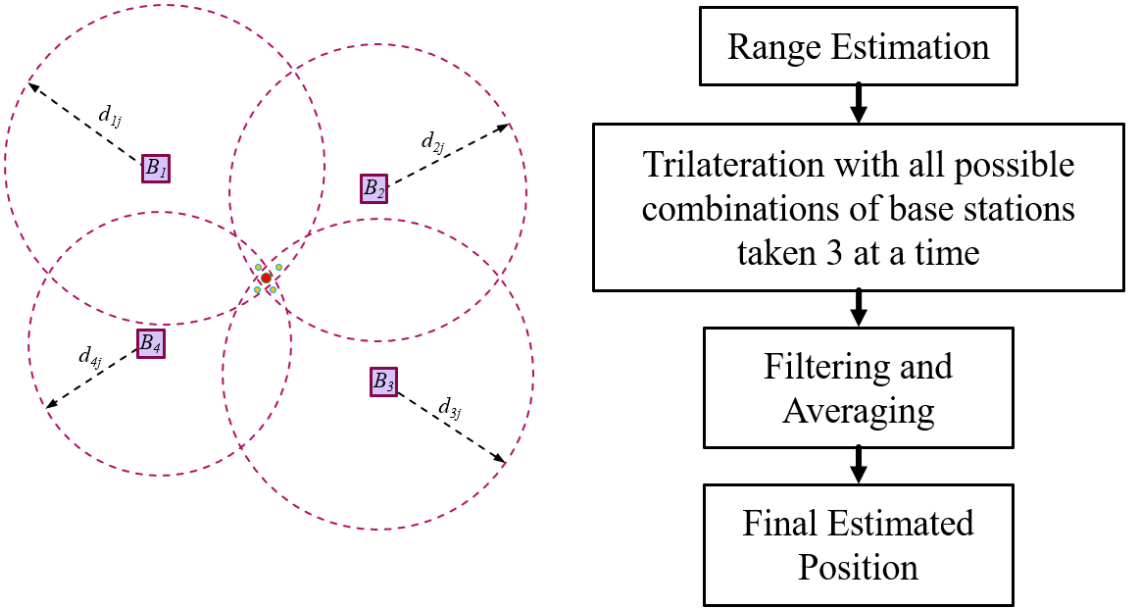

Figure 4.4: Schematics of trilateration algorithm and steps involved in 2D positioning using trilateration.

4.1.4 Positioning experiment inside a building with DOT system

The aim this experiment is to evaluate the 2D positioning performance of DOT system in an indoor environment with strong NLOS, multipath conditions, human presence, and multiple metallic and non-metallic obstacles. Entire first floor of the ELA Innovation building with a total surface area of around 315 square meters is used as the test

environment. This environment consists of multiple rooms separated by inner walls, metal window frames, outer walls containing steel bars and heavy metallic rods present inside the floor as well as the ceiling. Depending on the usage, this environment can be divided into different environment types such as office environment, storeroom and workshop as shown in Fig. 4.5. Within the area referred as office environment 1, there is less density of humans, computers, electrical equipment, and other metallic objects. In office environment 2, there are computers, screens, and other electronic equipment along with the humans in higher density. In this part of the environment, the number of metal objects is more than that observed in a typical office environment. In case of the storeroom with a surface area of around 25 square meters, there are several metallic racks used to keep inventory including electronic raw materials and different RFID products such as tags, readers, antennas etc. The density of metal present is very high in this part. In the workshop environments, there are metallic machines and tools present.

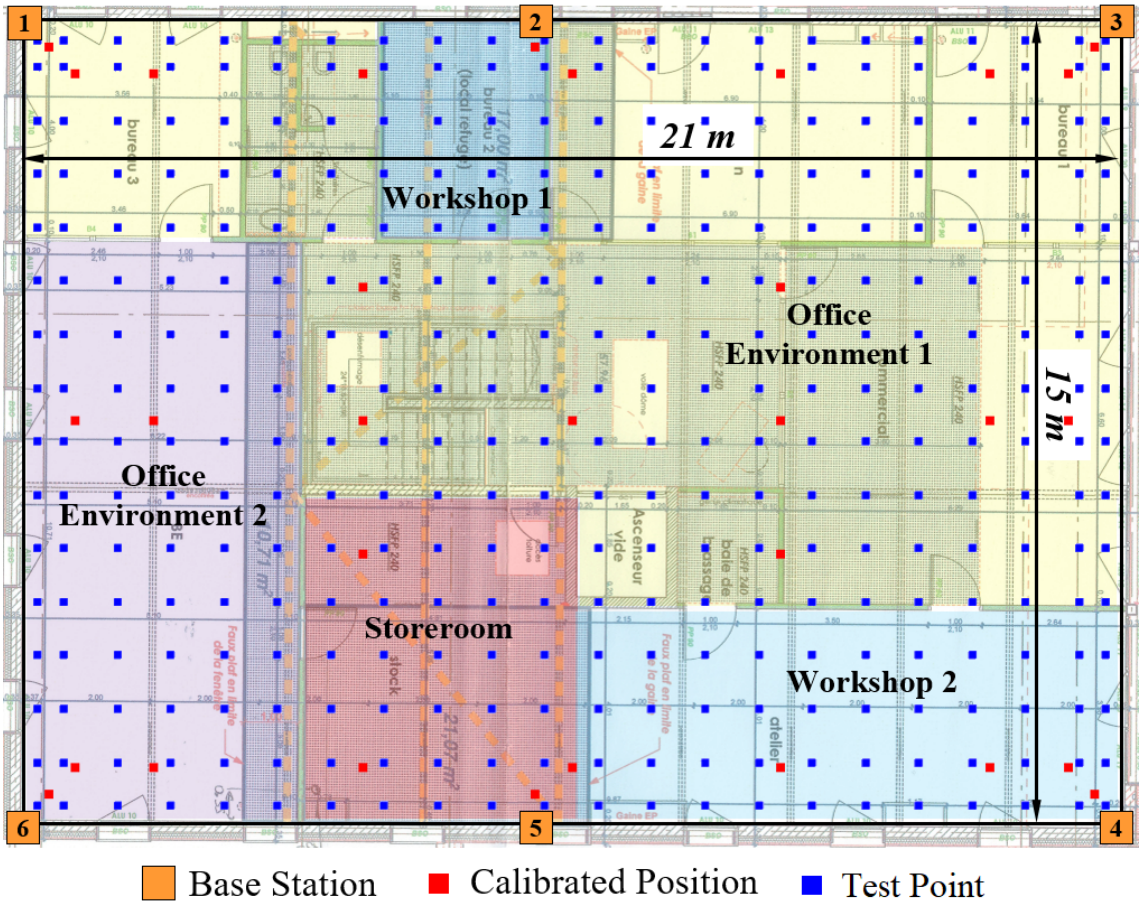

Figure 4.5: Experimental area showing different environments and positions of base stations for positioning experiment inside a building with DOT system.

The equipment used for this is made available by ELA Innovation. Six LF-activators, each consisting of a printed panel loop antenna of size 25 cm x 55 cm (Fig. 3.2), are used to generate quasi-static magnetic field at 125 kHz in the case of this experiment. Whenever the DOT tag is activated by the activator, it transmits the LF-FSI, the identity of that activator and its own identity to the UHF-RFID reader over 433 MHz frequency band.

The setup for DOT positioning system consists of six activators with their LF transmitter antennas installed on the wall with metal construction. The positions of the activators are at the orange markers shown in Fig. 4.5 and they are given the numbers as shown in the figure. Height of the antennas from the floor is kept 1.5 m so that the antennas are equidistant from the floor and the ceiling. The installation of the activators in the case of this experiment is made while keeping in mind the tag-activation range of the activators which is approximately 16 m. With the arrangement of the activators, it is ensured that the tag will always be within the tag-activation range of at least 4 activators, which is sufficient for positioning calculations. During this experiment all six activators are turned on simultaneously. Each activator is set to transmit the LF pattern at every 200 milliseconds. LF-FSI measurements during the calibration phase are recorded.

During the calibration phase, LF-FSI measurements are recorded at 31 calibration points (Fig. 4.5) while the DOT tag is placed 1.5 m above from the floor with the help of a cardboard stand. Based on these measurements, a mathematical expression for the attenuation model of each activator is obtained. Fig. 4.6 shows the calculated attenuation model for activator 5.

The measurements recorded during the calibration phase are also used to calculate the optimum weighting degree used in the weighted centroid algorithm. Fig. 4.7 shows the simulation results of positioning of all calibration points. In this figure mean positioning error is compared for different values of g varying from 1 to 5 by steps of 0.1. For DOT system the mean positioning error (for calibration points) is the minimum when the value of g is 2.2, which is used as the optimum weighting degree in the positioning phase of DOT system experiment.

Activator Number	Mean Error in Distance Estimation (m)	Standard Deviation (m)	CDF at 90 %
1	1.65	1.41	3.47
2	1.04	0.77	2.12
3	1.55	1.08	3.13
4	1.50	1.19	3.15
5	1.08	0.92	2.44
6	1.51	1.25	3.38

Table 4.1: Distance estimation performance of LF tag-activators in DOT system experiment

During the positioning phase, 2D real-time positioning tests are performed at 352 different test points within the experimental area as shown in Fig. 4.5 while the DOT tag is placed 1.5 m above from the floor with the help of a cardboard stand, at each test point. The positioning calculations are based on the real-time LF-FSI values (without any averaging) captured by the DOT tag.

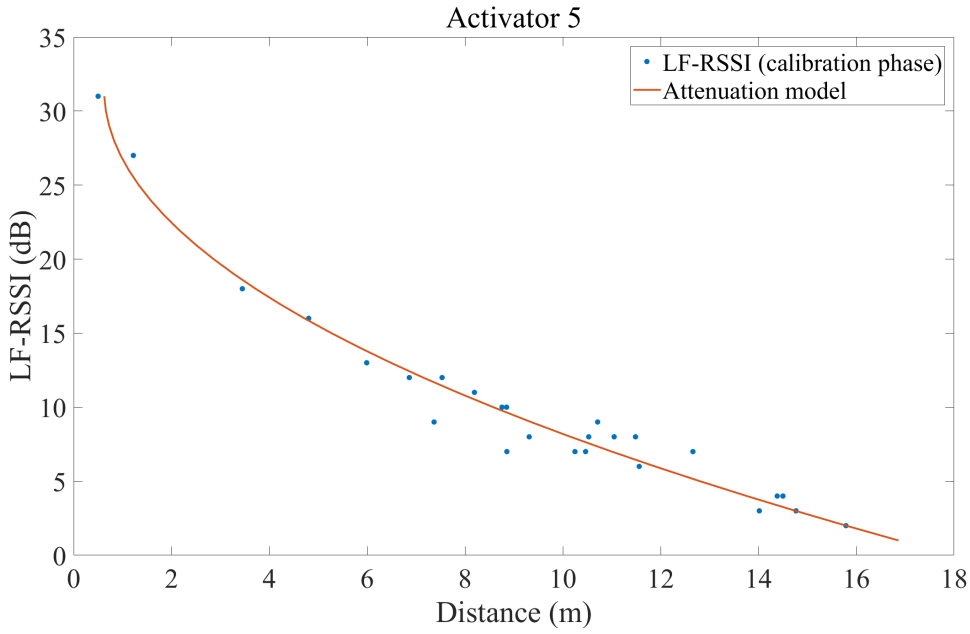

Figure 4.6: LF-FSI values measured during calibration phase for activator 5 and attenuation model obtained by least-squares fitting technique.

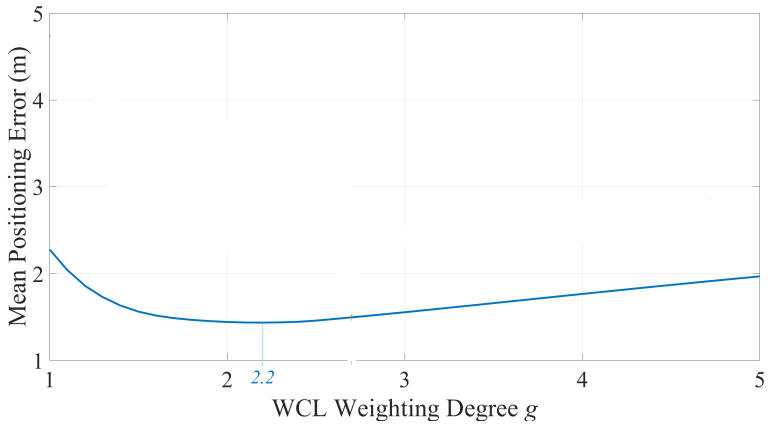

Figure 4.7: Optimal value of weighing degree g for DOT system for the building environment

Fig. 4.8 shows the distribution maps of the LF-FSI values captured by the DOT tag over the entire experimental area during this experiment for each activator. The magnitude of LF-FSI value at each test point is displayed as recorded. Different attenuation patterns are observed for the activators based on their placement in the experimental area. LF-FSI decreases more rapidly for the activators installed in the corners compared to activator 2 and activator 5 which are installed on the flat walls. As the outer walls contain steel, which is ferromagnetic, the tag activation range of the activators installed in the corners may be affected by the impact on resonant coupling. Table 4.1 provides the details about the distance estimation performances of all six activators in the DOT system. The performances of activator 2 and activator 5 are considerably better compared to the activators installed in the corners.

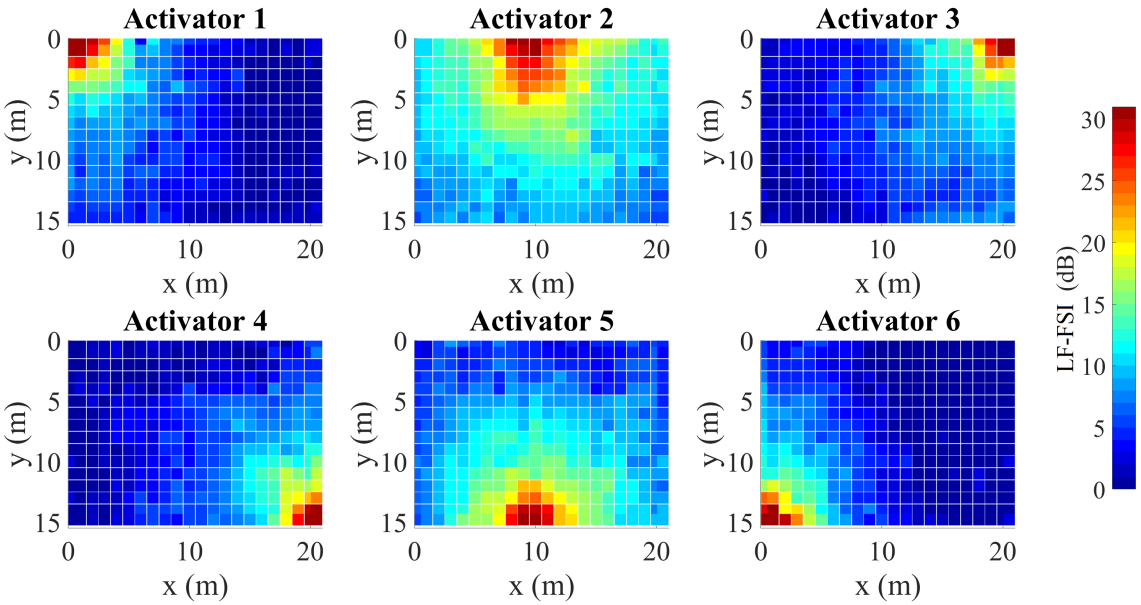

Figure 4.8: LF-FSI distribution maps for activators used in positioning experiment with placement of the activators is as shown in Fig. 4.5.

-	WCL	Trilateration
Mean error (m)	1.58	1.53
Standard deviation (m)	0.76	0.91
CDF at 50% (m)	1.54	1.41
CDF at 90% (m)	2.62	2.82
Maximum error (m)	3.75	4.81

Table 4.2: Comparison of 2D positioning error performance of DOT system using WCL and trilateration.

Comparison of WCL and trilateration techniques based on 2D positioning performance of DOT system is shown in table 4.2. Even though mean error using trilateration technique superior compared to that using WCL, overall performance with WCL technique is preferable as for 90% of the location estimations have error less than 2.62 m compared to 2.82 m in the case of trilateration.

The presented DOT system consists of COTS components, e.g. tag, activators, UHF-reader. These devices are also designed using electronic components available in

the market and they are not specifically designed for positioning applications. Thus, there are some limitations to the system because of these components.

In order to minimize the impact on positioning performance, WCL algorithm is used as it is less sensitive to distance estimation errors compared to triangulation techniques. Better LF-FSI resolution will improve the distance estimation accuracy, more importantly, it will reduce the large quantization errors introduced for longer distance estimations.

4.1.5 Positioning experiment in a small office with DOT system

This experiment is carried out to evaluate 2D positioning performance of DOT system inside small offices or rooms with multipath conditions and human presence. In this case, transmitter antennas with shorter operational range are used. Office environment 2 of the map shown in Fig. 4.5 is used as the experimental area for this experiment.

At the transmitter, the default transmitter antenna (antenna A in Fig. 3.2) with operational range of around 5-6 m is used. 2D positioning tests were performed in an office environment of size 11 m x 5.5m containing multiple metallic and non-metallic obstacles and human presence. This environment consists of metal window frames, outer walls containing steel bars and heavy metallic rods present inside the floor as well as the ceiling. The setup for this experiment is shown in Fig. 4.9.

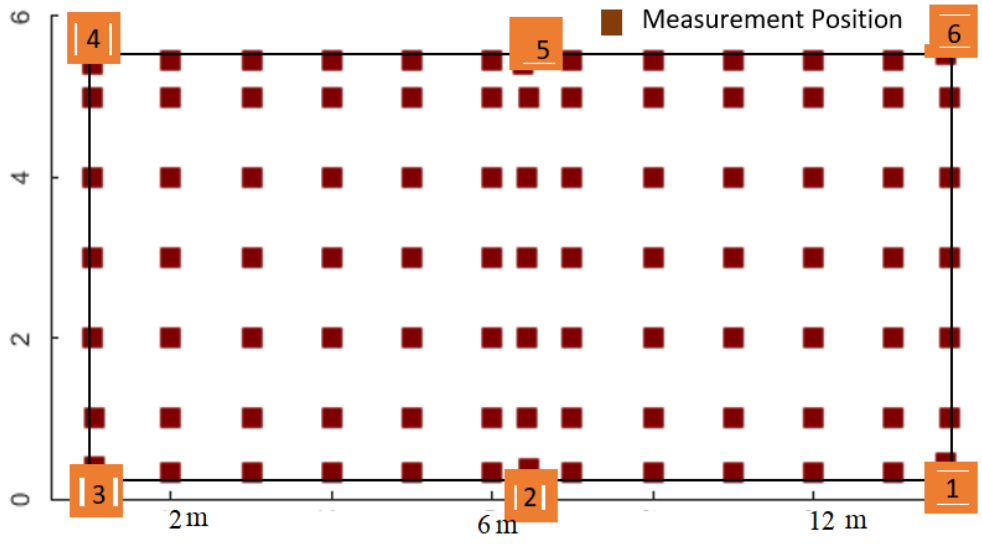

Figure 4.9: Experimental area showing office environment and the setup for the positioning experiment in a small office with DOT system.

During the calibration phase, LF-FSI measurements are recorded at 31 calibration points (Fig. 4.5) while the DOT tag is placed 1.5 m above from the floor with the help of a cardboard stand. Based on these measurements, a mathematical expression for the attenuation model of each activator is obtained. Fig. 4.10 shows the calculated attenuation model for activator 5.

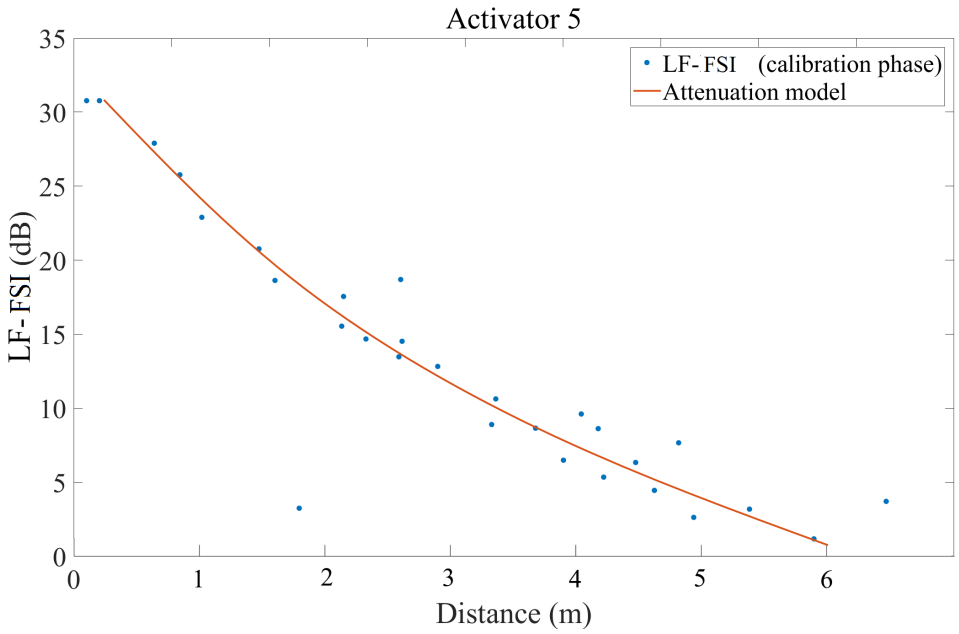

Figure 4.10: Attenuation model for activator 5 in the case of the positioning experiment in a small office with DOT system.

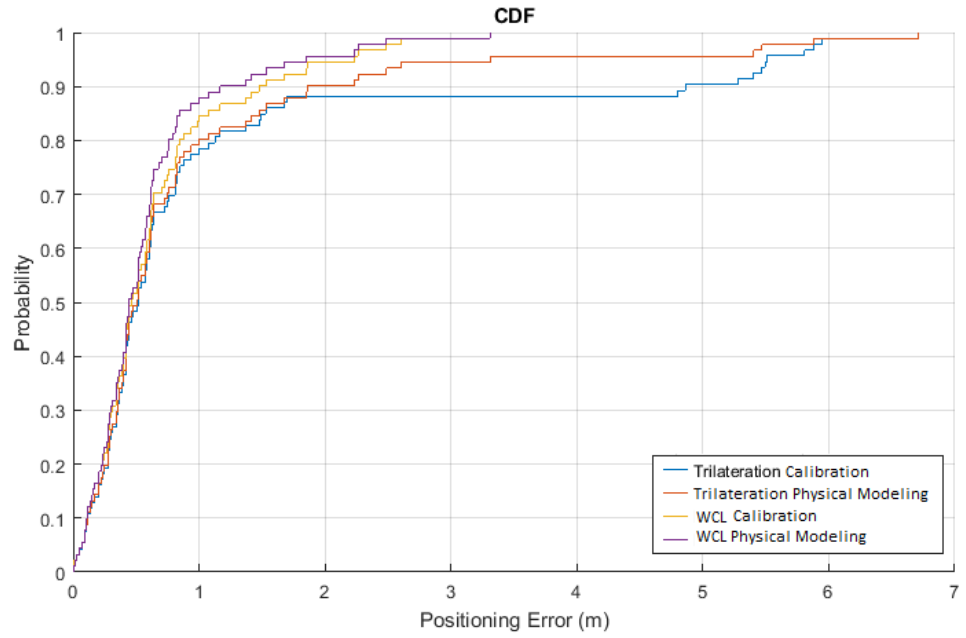

Figure 4.11: CDFs for the 2D positioning error in the case of positioning experiment in a small office with DOT system for different positioning approaches.

Fig. (4.11) compares the CDFs for the 2D positioning error for 2D positioning done with different ranging and positioning approaches in the case of positioning ex-

periment in a small office with DOT system. Trilateration positioning approach with distance estimations obtained with physical modeling approach performs better in this case with positioning error below 1.2 m for 90% of the tests.

4.1.5.1 Positioning Experiment with UHF-RFID Technology

In the case of positioning experiment with the active UHF RFID technology, 2D positioning tests at exact same 352 points are performed for in the case of the DOT system inside the building floor. The system consists of six UHF readers with their wave transmitter antennas installed exactly at the same places as the activators in the case of the DOT system experiment. The height of the UHF readers and active UHF tag is 1.5 m from the ground and the measurement procedure is exactly the same as the DOT system experiment. The coverage offered by the UHF system is superior compared to the DOT system and the entire experimental area can be covered by only four UHF readers installed at four corners of the experimental area. However, in order to compare the system with equal number of base stations, six UHF readers are used. For positioning based on UHF, six UHF-RFID readers and an active UHF-RFID tag operating at 433 MHz band are used. UHF-RSSI value in UHF-RFID experiment corresponds to the strength of the signal transmitted by the active UHF tag at the respective reader. UHF RSSI values are converted to dBm for better representation of power. In both the experiments, information necessary for positioning (e.g. RSSI, tag ID, base station IDs etc.) is collected by the UHF readers and transferred to a computer over the internet and further processing is done in real time.

Six UHF-RFID readers (IP2 readers from ELA Innovation with Wi-Fi connectivity), each attached to an omnidirectional quarter wave UHF antenna (Fig. 4.12 (c)), are used. The UHF-RFID tag shown in Fig. 4.12 is an active tag operating at 433 MHz frequency band. The equipment used for this experiment is also from ELA Innovation.

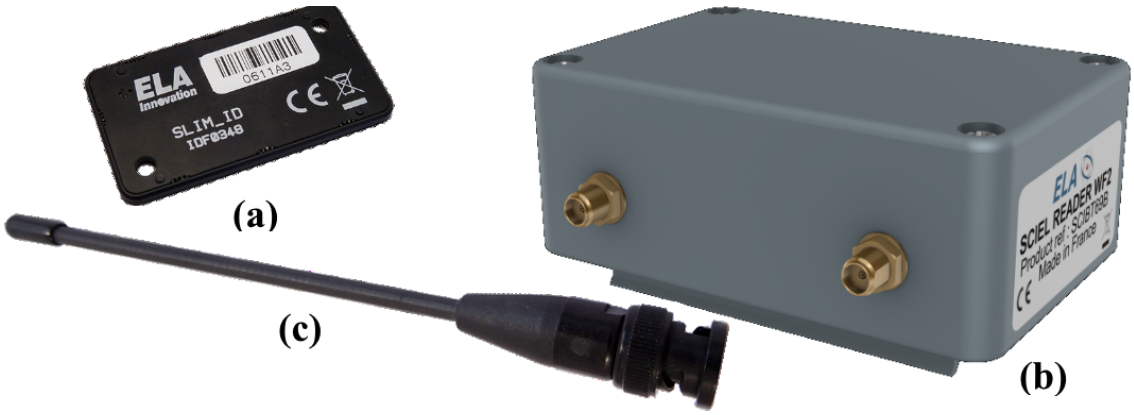

Figure 4.12: UHF-RFID equipment: (a) UHF-RFID tag (b) UHF-RFID reader (c) omnidirectional quarter wave UHF antenna.

Calibration measurements, calculation of attenuation models and calculation of optimum weighting degree, are performed using similar procedures described in the case of DOT system. The value of the optimum weighting degree obtained for this experiment is 2.7 (Fig. 4.13).

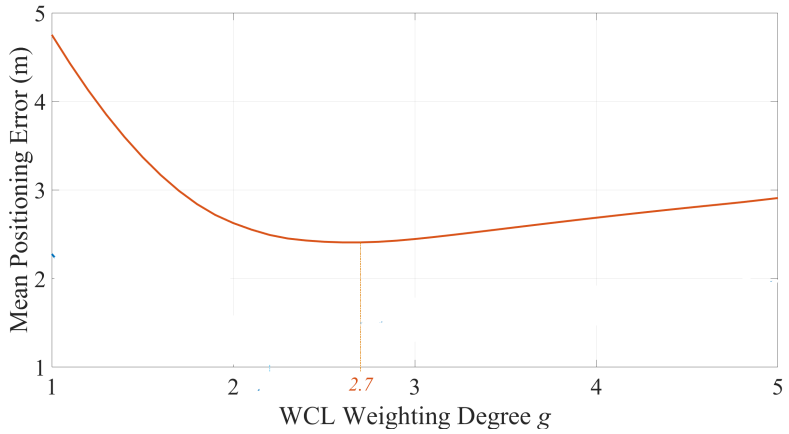

Figure 4.13: Optimal value of weighing degree g for active UHF-RFID technology for building environment

Positioning is performed using WCL algorithm based on estimated distance in case of both the experiments while distance estimation is performed using similar method.

Fig. 4.14 shows the distribution maps of RSSI values captured during UHF-RFID experiment. The magnitudes of RSSI values are displayed as power values in dBm, which are obtained from the actual RSSI values. Comparing the RSSI distribution maps for

both technologies, we can clearly see that the environmental impact on LF-FSI values is very less compared to that on UHF-RSSI values. Attenuation patterns of LF transmitters are more consistent and suitable for more accurate distance estimation while multipath and shadowing effects are clearly visible in case of UHF RSSI patterns. Table 4.3 provides the details about the distance estimation performance of all six UHF readers in the UHF-RFID system.

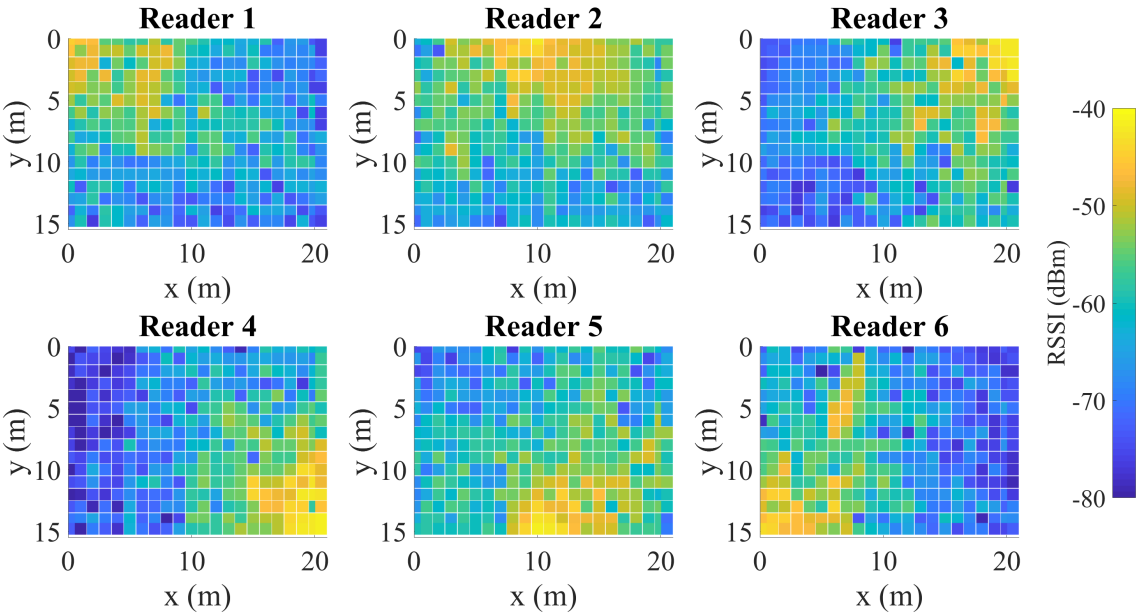

Figure 4.14: RSSI distribution maps for UHF readers used in UHF RFID experiment. Placement of the UHF readers is as shown in Fig. 4.5.

UHF Reader Number	Mean Error in Distance Estimation (m)	Standard Deviation (m)	CDF at 90 %
1	3.15	2.27	6.49
2	2.10	1.68	4.71
3	2.58	1.85	5.01
4	2.16	1.66	4.32
5	2.82	2.15	5.73
6	2.76	2.02	5.91

Table 4.3: Distance estimation performance of UHF-RFID readers

4.1.5.2 Positioning Experiment with UWB Technology

UWB system consists of six UWB anchors installed, as shown in Fig. 4.5 (base stations). Anchors are kept more than 0.15 m away from the walls as per the recommendation from DecaWave to avoid possible errors. The height of the anchors and tag is kept 1.5 m from the ground and the test procedure is exactly the same as described for the experiment inside a building with DOT system.

The UWB positioning system consists of seven EVB1000 evaluation boards Fig. 4.15 form DecaWave, each incorporating DecaWave's DW1000 IEEE802.15.4-2011 UWB compliant Wireless Transceiver IC, STM32F105 ARM Cortex M3 processor, USB interface, LCD display and off board antenna. These boards can be used as UWB anchors (base stations) or as UWB tags. Six UWB anchors and an UWB tag, are used for the positioning test based on UWB. The central operating frequency is set to 3.99 GHz with 110-kbits/s data rate, which is the configuration recommended to achieve maximum range measurement.

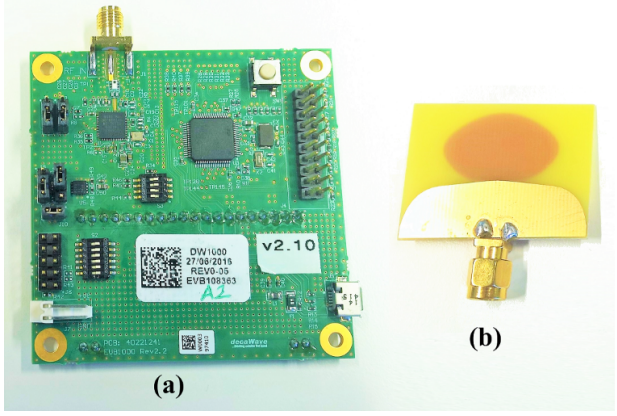

Figure 4.15: UWB equipment: (a) EVB1000 evaluation board from DecaWave (b) UWB Antenna.

UWB Anchor Number	Mean Error in Distance Estimation (m)	Standard Deviation (m)	CDF at 90 %
1	0.5	0.27	0.49
2	0.5	0.18	0.41
3	0.58	0.25	0.51
4	0.46	0.16	0.32
5	0.62	0.15	0.53
6	0.76	0.2	0.41

Table 4.4: Distance estimation performance of UWB anchors

4.1.5.3 2D positioning performance comparison of DOT, UHF-RFID and UWB technologies

In order to compare the distance estimation performance of the three systems, plots of actual distances versus estimated distances for each system are shown in Fig. 4.16. The plot for each system contains combined distance estimation results in the case of all the base stations of that system. Observing the plots, UHF-RFID technology performs worse as it is the most affected by multipath and NLOS conditions. DOT system has the shortest operational range while the distance estimation performance is significantly better compared to UHF-RFID but not quite close to the superior performance of the UWB technology. In the case of UWB technology, estimated distances, most of the times, are larger than the actual distances which is the ideal behavior. Similar to the observations in [160], few range estimations are smaller than the actual distances. In the case of DOT system, the shorter estimated distances are more accurate compared to the larger distance estimations as the quantization error introduced in the LF-FSI measurements increases as the distance between transmitter and receiver is increased.

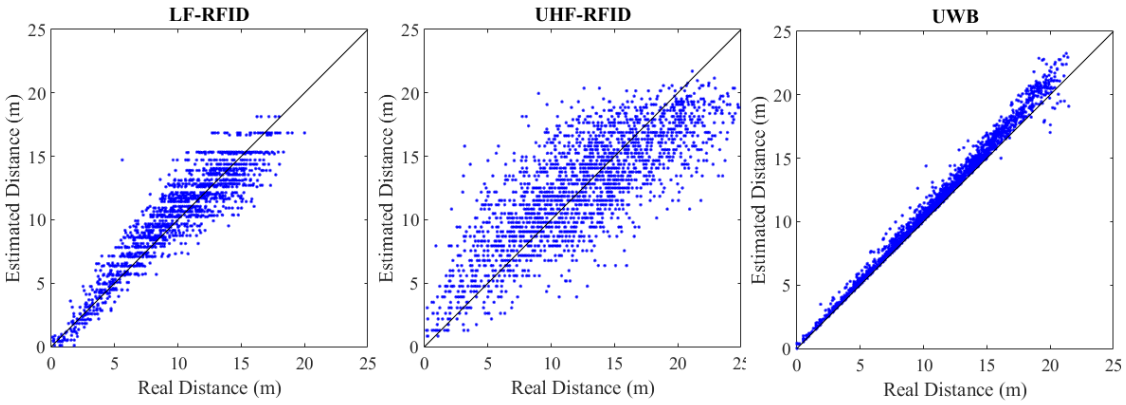

Figure 4.16: Actual versus estimated distances for all base stations in DOT, UHF-RFID and UWB systems.

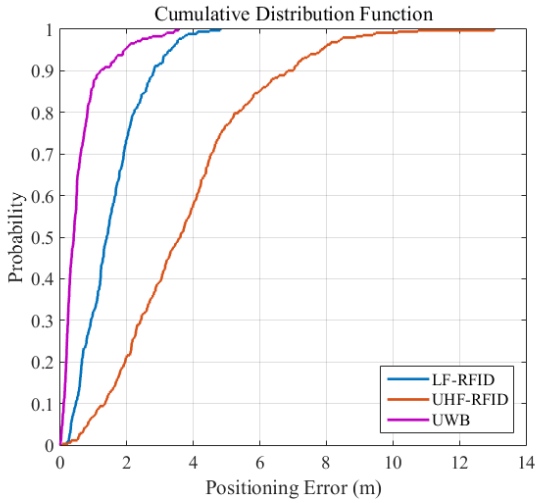

Figure 4.17: Cumulative distribution function for positioning errors of DOT, UHF-RFID and UWB systems

Table 4.5 compares the 2D positioning performance of the three different technologies. Fig. 4.17 shows the cumulative distribution function for positioning errors in the three positioning experiments. Out of the 352 estimated locations, 90% of the locations were estimated with error less than 2.62 m using DOT system and the error is below 5.41 m and 1.1 m in the case of UHF-RFID and UWB technologies. Fig. 4.18 show the magnitude of 2D positioning error in meters at each measurement position of the experimental area for all three experiments. These error maps show the robustness of the DOT system over the entire 315 square-meters area. The performance of UHF-RFID system is worse in the office environment 2 where the density of obstacles and people

is more. On the other hand, performance of DOT is not varied by large margin depending on the environment. WCL algorithm has a systematic error which impacts the positioning accuracy at the edges of the regarding environment [161]. The magnitude of this impact is less for the DOT system because of more accurate distance estimations. Positioning results with UHF-RFID technology is slightly better in the open spaces of the test environment whereas the positioning results with UWB technology are slightly degraded where the signal attenuation due to obstacles is maximum. Positioning errors in the experiment with UWB technology remain below 1 m in most of the spaces in the test environment, including the spaces where obstacles are present. Positioning errors remain below 0.5 m in the spaces where there is low density of obstacles.

-	DOT	UHF-RFID	UWB
Mean error (m)	1.58	2.84	0.58
Standard deviation (m)	0.76	1.81	0.62
CDF at 50% (m)	1.54	2.47	0.41
CDF at 90% (m)	2.62	5.41	1.10
Maximum error (m)	3.75	9.42	3.56

Table 4.5: 2D positioning error performance of DOT system in comparison with positioning based on UHF-RFID and UWB.

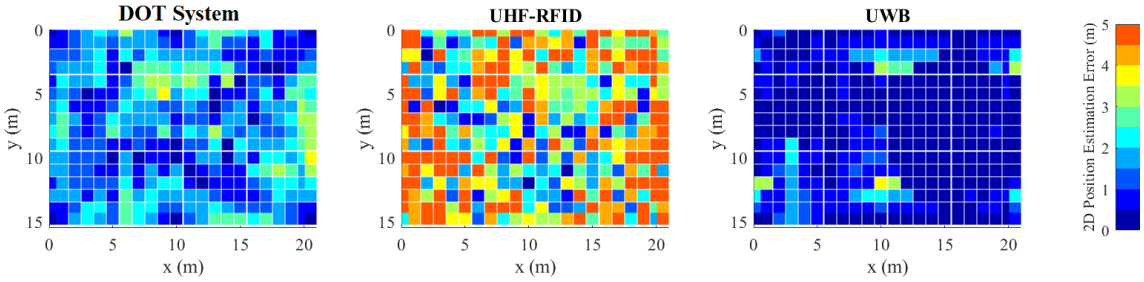

Figure 4.18: 2D Position estimation error map for (a) DOT based positioning and (b) UHF-RFID technology based positioning (c) UWB technology based positioning using four UHF readers in the corners.

Within an environment having surface area of 315 square meters with strong NLOS and multipath conditions and human presence, using simple WCL algorithm based on

estimated distance and trilateration algorithm, an accuracy of 1.58 $\pm$ 0.76 m for 352 position estimations is achieved. Better positioning accuracy is observed with the DOT system compared to the UHF-RFID system (2.94 $\pm$ 1.87 m). UWB system (0.58 $\pm$ 0.62 m) performs better compared to DOT system. It is also interesting to mention that UWB system is considerably costlier than the DOT system. The results proved that the proposed technique is less sensitive to the environment.

4.2 Use cases of DOT system

Ranging and positioning capabilities of DOT system in harsh propagation environments enables various simultaneous use cases. This section discusses the case studies of the DOT system use cases with existing ELA Innovation customers and also the use cases based on the demands from the potential customers.

Characterization of NFMI signal of the DOT system carried out during this thesis work has played important role in highlighting the applicability of DOT system in the design phases or pilot phases of the use cases described in this section. Other than that, work carried out related to these use cases in the context of this thesis involves demonstration and testing of the DOT system with different antenna configurations and measurement setups.

4.2.1 Full track and trace project: Renault

The aim of this project is to improve the efficiency in tracking and transferring the pallets containing the raw material. Bi-frequency-RFID based DOT system is combined with passive RFID technology for this project in order to localize pallets inside a huge vehicle manufacturing and assembly plant. In this case this system improves the efficiency in finding the pallet and provides a cheaper pallet positioning system.

Background

Renault is a French multinational automobile manufacturer with its production facilities all over the world. The full track and trace project aims to keep track of the

real-time locations of the huge number of spare parts in its production facilities. The use case described here considers only the Maubeuge production facility in France with more than 50000 pallets to be tracked with the help of DOT system.

Challenges

The main challenges faced by the production facility is to achieve an efficient and accurate production outcome and the main obstacle to that is the time wasted to accurately locate the large number pallets in the real-time according to production needs and to transfer the spare parts to the respective facility. The solution to keep track of these pallets must face the harsh propagation environments of the facility. Fig. 4.19 shows the target environment containing pallets and other obstacles present around them. The cost of the system is also an important aspect considering the large-scale deployment.

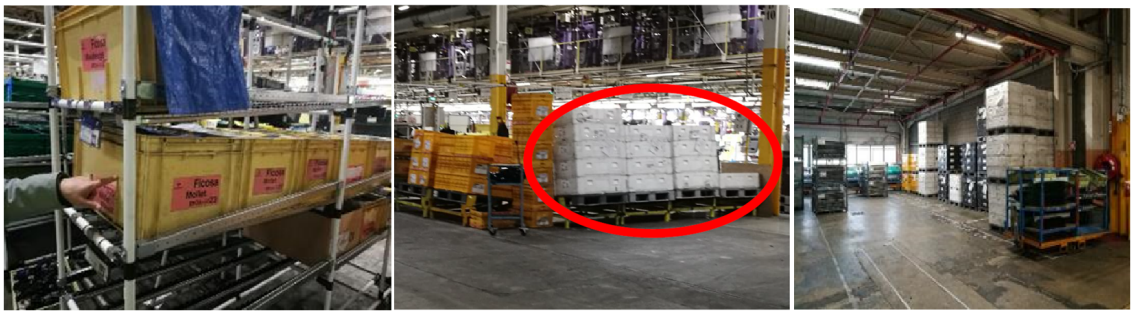

Figure 4.19: Operational environment in the case of pallet tracking system at Renault production facility in Maubeuge

Solution

DOT tags are deployed at the places where the pallets containing different kinds of vehicle parts are stored. The pallet contains a passive UHF RFID tag in form of a sticker. The DOT activator is attached to a forklift used to transfer the pallet. Additionally, the forklift is mounted with a UHF-RFID reader that records the ID of the pallet in front of the forklift. When the DOT tags are within the operating area (5-6 m in radius) of the activator installed on the forklift, they are activated and LF-FSI values are recorded by the RFID reader also present on the forklift. Using these LF-FSI values, position of the forklift is determined based on the distance estimations in real time. This position and

the ID of the palled in front of the forklift is stored in the database and updated when the pallet is moved. As very accurate 2D positioning is not necessary, proximity-based positioning can also be used in several cases where a single activator can cover the entire zone.

Results

Pallet localization system built using the DOT system in addition to UHF-RFID identification solution is able to accurately locate the zone of the pallets which make the pallet tracking and transferring workflow less time consuming and easier. Required localization accuracy target of 2-5 m (zone level) was achieved. The location tracking system has improved the production efficiency since the pallets can be tracked and transferred efficiently saving a significant amount of time and effort.

Next steps

Deployment of the track and trace solution is ongoing as of 2020 within worldwide production plants of Renault and its partners. With the experience of track and trace project, ELA Innovation continues the evolve the DOT system to address different issues regarding the digitalization of factories and compatibility with Industry 4.0 [162].

4.2.2 Passive Keyless Entry (PKE): Demonstrated at RTM Marseille Bus Depot

This project aims to allow the entry doors inside the bus depot to be automatically controlled, therefore improving security, convenient to the driver and saving time compared to the older procedure where the driver used to get down and manually open the door every time.

Background

RTM Marseille offers the public transport service in the city of Marseille with 80 regular lines, RTM has 6 depots, including 3 bus depots, 1 mixed bus or tram depot and

2 metro depots. During the pilot phase of this project, the demonstration of the keyless control of the doors using DOT system was performed.

Challenges

The main challenges faced by the bus depot is to achieve an efficient and secure access to the buses inside the bus depot. The keyless solution must face the harsh propagation environments of the bus depot. Fig. 4.20 shows the target environment with the buses parked in the open and the door with inside parking facility. The cost of the system is also important aspect considering the large-scale deployment.

Figure 4.20: RTM Marseille bus depot and automated door controlled by the DOT system

Solution

In this case the DOT activators were deployed at the top of the big automated doors for the buses. When the DOT tag is in the operational range of the activator, the tag is activated and recorded by the RFID reader which triggers the relay signal controlling the door. During this test, the relay signal for the door was triggered by the dot system when the bus was 1.5 m away from the door. The system was required to set this specific distance for triggering the relay signal because there are other buses passing in front of the door which are not supposed to enter the door. In order to prevents false triggering of the relay signal, and set a strict triggering distance of 1.5 m, a filter was set on LF-

FSI value corresponding to 1.5 m at the RFID reader. In this case the relay signal was only triggered when the LF-FSI value recorded by the tag was greater than the value corresponding to 1.5 m.

Results

ELA Innovation's DOT system was successfully able to open automated doors when the bus containing a DOT tag approached the door for maintenance. In addition to convenient access provided by this system, identification capabilities of DOT tag and the activator allows to block unauthorized access, positioning of buses while parked and also easy employee mustering.

Next steps

This project is still under its pilot phase and ELA Innovation is awaiting the response from RTM after the demonstration.

4.2.3 Pedestrian Collision Warning System inside a manufacturing plant

The aim of this project is to avoid the collisions between the forklifts operating inside a manufacturing plant and the pedestrians inside the facility by sending alarms to both parties when they are inside the specific distance from each other.

Background

In this use case the collision warning system should warn the pedestrian inside a manufacturing plant about the presence of the nearby forklift and also send an alert to the driver of the forklift. Due to confidentiality of this project, the customer name and other details are not included.

Challenges

The main challenges faced by the manufacturing plant in this case to avoid accidents happening inside a manufacturing plants due to various blind spots. The harsh propagation conditions are very challenging for the indoor localization solutions based on RF signals and which are cost friendly.

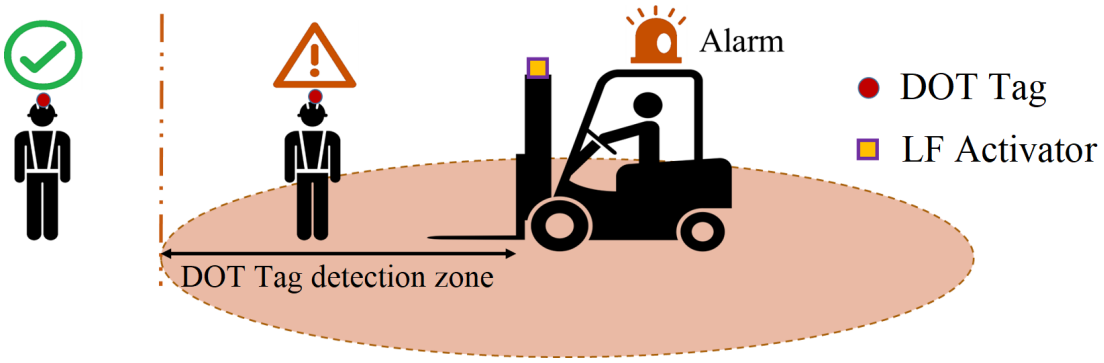

Figure 4.21: Illustration of pedestrian collision warning system tested inside a manufacturing plant using DOT system.

Solution

In this case the activator and the RFID reader are installed on the forklift while the DOT tag is carried by the pedestrian. Whenever the pedestrian is present inside the operational zone of the activator the tag is activated and an alarm is triggered on the tag and also upon reception of the signal from the DOT tag, the RFID reader triggers a relay signal to inform the driver about the presence of one or more pedestrians.

Results

This system successfully triggers the alarm in the case where the pedestrians are inside the danger zone created by the forklift. This avoids the large number of forklift accidents happening inside a manufacturing plants due to various blind spots. Reliability of the DOT system in harsh propagation environment is the highlighting point.

Next steps

The panel antenna used at the LF-Activator on the forklift takes a lot of space and its coverage is affected by large metallic objects. In the future a custom design is planned for the new transmitter antenna using ferrite coils with the target operational range of 15 m. The design of the new antenna will be based on the work carried out during this thesis.

4.3 Conclusion

This chapter presents experimental work related to ranging and positioning performance evaluation of DOT system. Ranging performance of this system is verified in a warehouse environment which is challenging for RF propagation. 2D positioning performance of the proposed system in a challenging indoor environment is evaluated in an environment containing various types of obstacles and it is compared with the performance of UHF-RFID and UWB based positioning system in exactly same environment. Mean positioning accuracy of less than 2 m with good reliability (Table 4.5) in cluttered environment of DOT technology in addition to its identification capability makes it useful for applications such as security, guidance, and asset tracking within smart cities.

Three case studies describing the use cases of the DOT system in different fields are presented. The DOT system improves the efficiency of the workflow in pallet transfer and keyless access applications in addition to secure entry. Additionally, it improves the safety of the workers in the industrial environments in applications where it helps to avoid collisions.

Conclusions and Perspectives

Conclusions

This thesis has developed the theoretical background for a dual-frequency RFID ranging and positioning system (DOT system) based on NFMI signal. The hardware specific to ranging and positioning is based upon the extremely loosely coupled MI resonant coils . Physical modeling for this hardware is presented. Experimental work evaluating the ranging and positioning performance has been presented and the use cases of the system related to ranging and positioning have been discussed.

The DOT system designed for dual-frequency RFID communication pre-existed before the beginning of this work. This work aimed at highlighting the applicability of this system for ranging and positioning purposes. Limited operational range and compactness of the DOT system are the main issues that we have tried to address in this thesis.

The work carried out in this thesis has been aimed to contribute towards the indoor positioning problem in the harsh propagation environments. As an introduction to the indoor positioning problem, an overview of different techniques and technologies used for ranging and indoor positioning has been given in chapter 1 of this thesis. Along with this, the applications of indoor positioning have been discussed. In this chapter, MI technology, which is used by the DOT system for ranging, has been presented and its use cases specific to ranging and positioning are highlighted.

This thesis has documented the essential background information about the DOT system from ELA Innovation, including the pilot research project TROUVE that motivated the further work on this system. The limitations of already existing system are presented. The theory presented in chapter 2 of this thesis begins by presenting the

relevant electromagnetic background regarding the magnetic field generated in the near-field by the helical transmitter coil placed at the origin, physical modeling equations for obtaining the numerical simulation of the magnetic field at any point $P(x, y, z)$, physical modeling equations for obtaining induced voltage across the receiver coil due to this magnetic field and the output voltage of the resonant circuit while considering ferrite core coils at transmitter and the receiver. Due to limitations in modeling the MI coupling between ferrite coils in any receiver orientation, the modeling equation for the output voltage of the resonant circuit is restricted only to the cases where the axes of the coils are parallel to each other.

In chapter 3 characteristics of NFMI signal have been observed with the help of LF-FSI measurements. Different sets of measurements have been recorded in order to observe different aspects such as impact of surrounding environment, human body, ferromagnetic obstacles and orientation of DOT tag. The surrounding environment, human body and non-ferromagnetic obstacles have negligible impact on the NFMI signal generated by the DOT system. Ferromagnetic objects, when placed very close to LF transmitter, affect the tag detection range and LF-FSI captured anywhere inside the operational range of the LF transmitter. This impact reduces as the distance between the transmitter and the ferromagnetic object is increased. After a certain distance from the transmitter, impact on LF-FSI is only observed when the DOT tag is in close proximity of the ferromagnetic object. In this case, if the tag is inside the segment formed by the transmitter and ferromagnetic object, increase in LF-FSI is observed and if it is outside this segment, decrease in LF-FSI is observed. Extension in tag detection range near the walls containing mesh of steel bars is observed when the LF transmitter is very close to such walls. All these measurements are analyzed against the physical modeling equations. An attempt to validate the physical modeling equations with the help of measurements and simulations has been presented in this chapter. For this purpose, transmitter and receiver coils are designed including ferrite core coils. One of the compact ferrite core transmitter coils designed for this experiment increase the operational range of the DOT system to 8.5 m compared to 5.5 m offered by the default compact transmitter antenna of the DOT system.

In chapter 4 of this thesis methodologies used for ranging and positioning based on the DOT system have been discussed. Ranging and 2D positioning performance of the

DOT system is evaluated in different indoor environments with the help of different experiments. In the ranging experiment performed inside a small cluttered warehouse, mean ranging accuracy below 0.2 m was obtained for 25 different test points. 2D positioning experiments were carried out within an environment having surface area of 315 square meters with strong NLOS and multipath conditions and human presence in order to evaluate the positioning performance. Similar experiments were performed using UHF-RFID and UWB technology to benchmark the DOT system against other systems. DOT system with default transmitter antenna (with operational range of 5.5 m) offered mean 2D positioning accuracy below of 0.6 m for 91 position estimations. DOT system with panel antenna (operational rang of 16 m) offered mean 2D positioning accuracy of 1.58 ± 0.76 m for 352 position estimations compared to 2.94 ± 1.87 m offered by UHF-RFID technology and 0.58 ± 0.62 m offered by UWB technology. The DOT system offers acceptable ranging and positioning accuracy within harsh propagation environments in addition to the reliability offered by the NFMI signal, which is less affected by NLOS conditions, multipath and fading in such conditions. In comparison to solutions based on UWB technology which offers more accuracy, the DOT system costs less. The applications where very high accuracy is unnecessary, the DOT system can offer low cost but reliable alternative. Three case studies describing the use cases of the DOT system in different fields have been presented in chapter 4. The DOT system improves the efficiency of the workflow in pallet transfer and keyless access applications in addition to secure entry. Additionally, it improves the safety of the workers in the industrial environments in applications where it helps to avoid collisions.

Perspectives

While this thesis has made contributions towards understanding the problematics of extremely loosely coupled MI based ranging and positioning system, modeling the system and providing guidelines for optimization, only a prototype transmitter antenna has been designed to address the issue of short operational range and compactness of transmitter. Presently, the COTS transmitter antennas used by the DOT system limit the use cases of this system. The default antenna offers limited coverage while the panel antenna with higher operational range is large in form factor and its usage on the mobile

entities such as forklifts is limited. The prototype antennas built based on the work carried out during this thesis offer better tradeoff between the size and operational range. In future, design of the new antenna will be aimed at replacing the panel antenna with a ferrite core antenna small enough to be installed inside the LF activator package and with operational range greater than 12 m.

The LF wakeup receiver used presently on the DOT tag generates only 5-bit LF-FSI valued which limits the ranging and positioning accuracy of the system due to quantization error. In future it will be interesting to look for a different LF wakeup receiver with higher LF-FSI resolution which is cost effective and feasible to replace the current component on the DOT tag. This can considerably improve the ranging and positioning accuracy of the DOT system and highly raise the applicability of this highly reliable system.

This thesis has put forth the physical modeling of a Near Field based extremely loosely coupled MI based ranging and positioning system. However, the modeling is limited by the use of ferrite. In future accurate numerical simulation of the coupling between ferrite cores at any orientation will increase the applicability of the model. The impact of ferromagnetic materials in proximity of the coils is also an interesting future development.

The DOT system has been in use or under consideration for several different use cases due to its acceptable accuracy and cost effectiveness. The work carried out in this thesis will be helpful towards making this system more scalable by increasing its operational range and ease of deployment achieved thanks to compact transmitters.

Appendices

Appendix A

The Trouve Project

An indoor localization guidance based on DOT system is proposed in [163]. In this project, ELA Innovation contributed with a localization solution based on DOT system that can provide information to the voice-guidance system. The description of this project is as follows:

Purpose: Misplacing or losing personal belongings is a concern of everyday life among people of all ages. Older adults with cognitive impairment are significantly more affected by this problem. It is a source of frustration, anxiety, interpersonal conflict and disability in this population. Informal caregivers are greatly impacted by this problem, which compels them to spend a lot of time searching for misplaced items and comforting the person. Assistive technology could thus be of great benefit in this area. However, existing item locator devices do not appear to meet the needs of older adults with cognitive disorders. The TROUVE project aims to conceive and assess an innovative item locator device that effectively addresses their needs, capacities, and goals.

Procedure: The project team conducted a co-design process involving relevant stakeholders (persons with cognitive impairment, informal and formal caregivers, researchers, industry representatives, ethical bodies) using user-tests, focus groups, interviews, and questionnaires. The project plan involved three phases: (1) analysis of end-users' needs, (2) definition of system requirements and iterative prototype development, and (3) prototype assessment.

Findings: The analysis of end-users' needs and the evaluation of existing item locator devices provided us with details about the items which are the most frequently lost or misplaced by older adults at home and their coping strategies to manage these situations.

The analysis of usability problems observed throughout the assessment of existing devices allowed the definition of the system requirements. Prototype assessment showed that spatialized sound can be used to help these users find missing items, and that an item locator device can be part of a more comprehensive assistive and rehabilitation system such as a robot.

Conclusions: An item locator that relies on sensory information (spatialized sound) rather than on conceptual reasoning ("the item is located to your left 4 meters away") appears to be an interesting solution to address the problem of misplacing personal items in elderly with cognitive impairment. Involving end-users and relevant stakeholders throughout the cycle of design and development of assistive technology is an effective method to explore design opportunities and define creative solutions.

Appendix B

Performance Evaluation of Quuppa Positioning System

Quuppa [164, 165] is a Finnish company offering an accurate RTLS solution based on AOA measurement technique using BLE technology. Quuppa relies on its partners and BLE tag manufacturers in order to bring this solution to the end user. Quuppa system offers sub-meter accuracy with lower number of base stations in a particular indoor or outdoor environment compared to other competing technologies. ELA Innovation with its industry grade and long battery life BLE tags collaborates with Quuppa in order to provide RTLS solutions to their customers. In the initial stages of collaboration, it was important to evaluate the performance of Quuppa system and also to better understand the Quuppa system. The base station used in this system, refered as a locator, contains a phased array antenna for AOA measurements. The processing is performed by the positioning engine developed by Quuppa which is installed on local server. Figure B.1 shows the setup and operation of Quuppa system.

2D and 3D positioning test were performed using the BLE tags provided by Quuppa in order to get familiar with the system and to get idea of its capabilities. Figure B.2 shows the setup for the test in a semi-open area on the ground floor of ELA Innovation building with surface area of 80 square meters. The locators offering positioning coverage within 3-5 m radius around it were installed on the ceiling at a height of 3.5 m and calibration procedure was followed. The rectangular experimental area contains a wall along one side and it is open along other 3 sides. There are wooden benches and metallic chairs present in the environment. 2D positioning results of a BLE tag were recorded at 52 different test points, when the tag was placed on a tripod at a height of 1.2 m. 3D

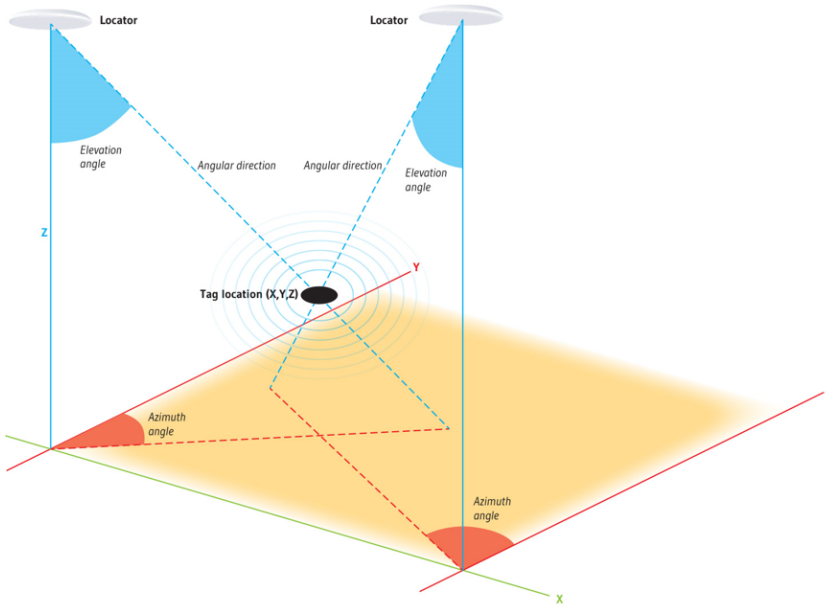

Figure B.1: 3D positioning with the help of two Quuppa locators.

positioning tests were also performed at 12 different test points. Mean 2D positioning accuracy of 0.58 m with a standard deviation of 0.63 m was achieved. Mean positioning accuracy in the case of 3D positioning test was 0.87 m with a standard deviation of 1.12 m.

An attempt was made to perform 2D positioning tests within the indoor space of ELA Innovation. However, the maximum height at which the locators could be installed inside this environment was less than 2.5 m, which is less than the recommended height for installation within an environment prone to multipath. Due to this, the calibration of the locators was difficult and proper installation of the equipment to achieve reliable positioning accuracy was not possible.

In conclusion, the Quuppa system offered sub-meter accuracy within an environment with few surfaces reflecting the signal, when it was properly calibrated. Confined environment with strong multipath and with installation constraints caused problems for the Quuppa system and reliable positioning accuracy could not be achieved. This positioning system is suitable for environments with sufficient height available for installation of locators and can achieve sub-meter positioning accuracy.

Figure B.2: Setup for the positioning tests performed with Quuppa system.

List of Figures

List of Tables

Résumé de la thèse

Les travaux de thèse présentés dans ce manuscrit s'inscrivent dans le cadre d'un partenariat de recherche ANRT-CIFRE [1] entre la société ELA Innovation [2] et deux laboratoires de recherche ESYCOM (UMR 9007 CNRS) [3] et AlliansTIC [4]. En tant que telle, cette thèse CIFFRE a permis de combiner des objectifs de recherche académiques et industriels. Ainsi, les travaux présentés sont en lien direct avec les besoins opérationnels d'ELA Innovation. Ils se concentrent sur le système *Radio Frequency Identification - RFID* à double fréquence, appelé système DOT, qui a été conçu par ELA Innovation avant le début des travaux de cette thèse et constitue aujourd'hui l'un des produits phare de la société. Ce travail avait pour ambition d'approfondir la modélisation du système DOT afin de mettre en évidence et optimiser ses performances et limitations en tant que système de localisation en intérieur.

Au cours des dernières années est apparu un besoin croissant de solutions de suivi et de localisation d'objets communicants à l'intérieur de réseaux de capteurs sans fil (*WSN - Wireless Sensor Network*) dans les environnements tels que les usines, les entrepôts ou les bâtiments publics. En effet, la localisation d'objets ou de personnes peut se révéler critique pour l'optimisation de processus logistiques et industriels (transitique), pour garantir la sécurité de travailleurs dans des tunnels, des mines ou sur des chantiers de construction, ou pour garantir la qualité des soins hospitaliers. Les solutions de navigation par satellite (*Global Navigation Sattelite Systems GNSS*) ont permis de répondre à un grand nombre de problématiques similaires en extérieur et pourraient être des solutions intéressantes. Mais leur précision et leur fiabilité dans des environnements confinés ou intérieurs ne sont pas suffisantes. C'est pourquoi des systèmes de localisation en temps réel (*RTLS - Real-time Location System*) capables d'identifier et trouver, avec précision et en temps réel, l'emplacement d'objets ou de personnes dans des environnement complexes ont été intensivement développés depuis deux décennies.

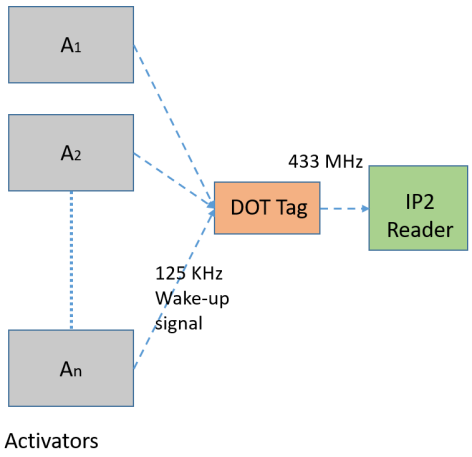

Figure C: Topologie du système DOT

le système DOT

Dans le cadre du projet TROUVE, financé par l'Agence Nationale de la Recherche (ANR) et dont l'objectif était de développer un système de localisation d'objets usuels pour des patients atteints de la maladie d'Alzheimer, ELA innovation a développé le système DOT. Le travail de cette thèse est une extension ce projet de localisation avec l'objectif d'améliorer l'applicabilité du système à des problématiques plus industrielles. Le système DOT se compose de trois éléments principaux, 1) des émetteurs basse fréquence (*Low Frequency - LF*) fonctionnant à 125 kHz appelés Activateurs LF, 2) des balises DOT, contenant un récepteur BF (Basse Fréquence) et un transpondeur Ultra Haute Fréquence (UHF) fonctionnant à 433 MHz et 3) des récepteurs UHF appelés Lecteurs IP2. La topologie du système DOT est illustrée à la Fig. C.

L'activateur LF (Fig. D) se compose d'un circuit d'émission LF avec alimentation 12V et peut être connecté à deux antennes LF externes. Dans ce travail, trois antennes différentes (Fig. E) ont été testées : l'antenne KGEA-BFCR du fabricant Premo initialement utilisée dans le système DOT, un prototype d'antenne ferrite conçu pendant la thèse et une antenne panneau. La transmission du signal LF est intermittente avec une période de récurrence qui peut être configurée supérieure à 200 millisecondes. Les trames transmises par l'activateur LF sont constituées d'un identifiant unique de 11 bits différent pour chaque antenne. La puissance d'émission sur chaque antenne de l'émetteur LF peut être contrôlée en fonction de la portée opérationnelle voulue. Enfin l'activateur LF peut être

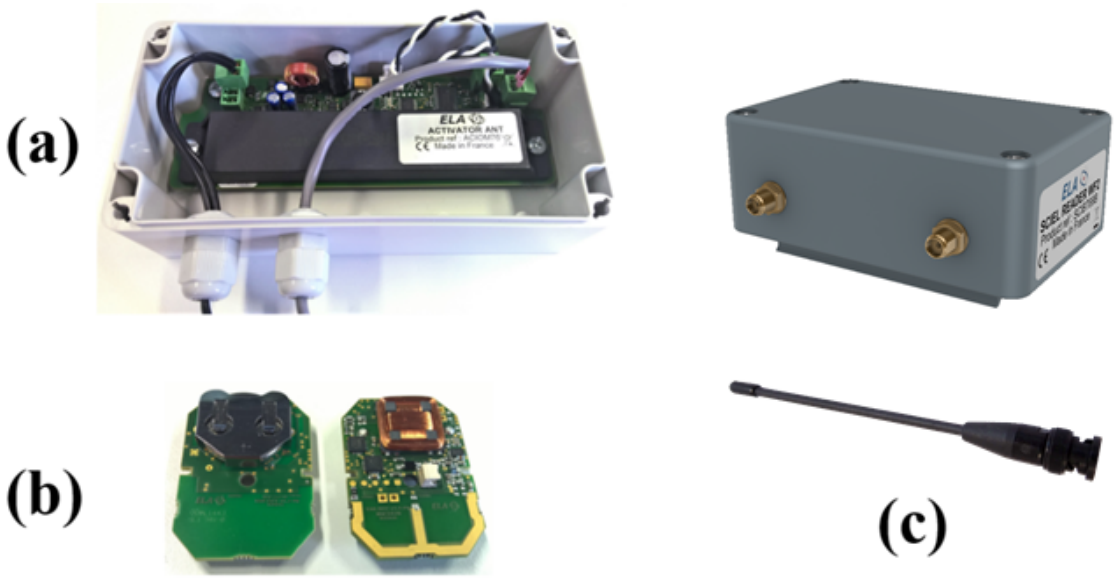

Figure D: Composants du système DOT (a) Activateur LF avec antenne émetteur par défaut (b) Balise DOT (c) Lecteur IP2 avec antenne UHF.

installé de manière fixe ou embarqué à bord d'un véhicule en s'alimentant directement sur la batterie du véhicule.

La balise DOT (Fig. D) est un appareil portable fonctionnant sur batterie avec un petit facteur de forme. Il se compose d'un récepteur de réveil (*Wake-up Receiver - WURx*) LF, d'une unité de commande et d'un transpondeur UHF. Lorsque la balise DOT se trouve à portée de transmission d'un activateur LF et que le signal de cet activateur LF est reçu par le circuit de réveil LF-WURx, la balise DOT s'active et opère une routine logique prédéfinie. Cette routine permet alors de transmettre un signal UHF au Lecteur

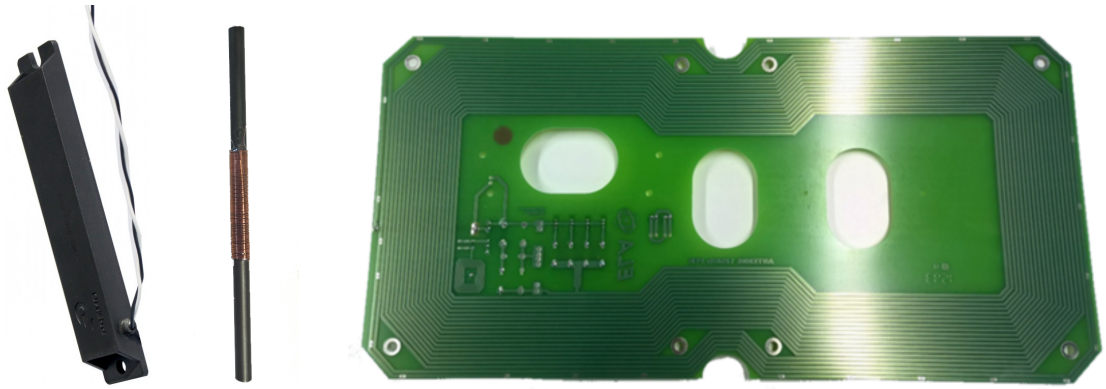

Figure E: Antennes émetteurs BF : (a) antenne par défaut (b) antenne ferrite prototype (c) antenne en boucle de panneau.

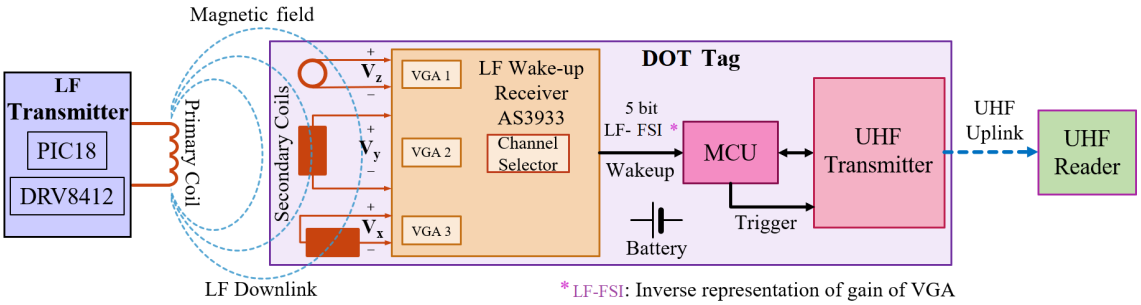

Figure F: Architecture du système DOT.

IP2 contenant l'identificateur de l'antenne de l'activateur LF, l'identificateur de la balise DOT, codé sur 16 bits, et la force du signal LF reçu par la balise DOT appelé indicateur d'intensité de champ LF (*Field Strength Indicator - FSI*).

Le Lecteur IP2 (Fig. D) se compose d'un récepteur UHF et d'un module Lantronix xPico permettant de transférer les données reçues sur différents protocoles TCP/IP (Ethernet, WIFI, USB) jusqu'au système de stockage des données. En d'autres termes, les Lecteurs IP2 sont des passerelles transférant les informations générées par le système DOT vers un serveur ou un ordinateur distant. Le paquet d'informations transmis contient l'identifiant du Lecteur IP2, codé sur 8 bits, l'identifiant de la balise DOT, l'identifiant de l'activateur LF qui a activé ce la balise DOT et la valeur LF-FSI mesurée par la balise DOT. Le Lecteur IP2 est alimenté par une alimentation 12 V (comme l'Activateur LF) et peut donc être installé de manière fixe ou embarquée à bord d'un véhicule.

L'architecture du système est illustrée à la Fig. F. L'activateur BF génère un champ magnétique quasi-statique qui est modulé en amplitude par saut (*Amplitude Shift Keying - ASK*). Ce motif ASK est transmis périodiquement par l'activateur (liaison descendante LF). Une balise DOT dispose de trois antennes de réception orientées dans des plans orthogonaux et connectées au récepteur de réveil BF. Une telle architecture d'antenne, également appelée antenne 3 axes, permet d'utiliser la balise DOT de manière quasi-omnidirectionnelle. Le couplage inductif résonnant entre les antennes d'émetteur et de récepteur induit des tensions électriques aux bornes des antennes de réception. Chaque fois que le récepteur de réveil BF détecte une tension suffisamment forte (supérieure à la sensibilité), la balise DOT est activée (réveil). Lors d'une activation, la balise DOT calcule la valeur LF-FSI (exprimée en dB) qui est la représentation inverse du gain de l'amplificateur à gain variable (*Variable Gain Amplifier - VGA*) présent dans le récepteur

de la balise DOT. Après cette étape, l'émetteur UHF transmet l'identifiant unique de la balise DOT au lecteur UHF ainsi que le LF-FSI (5 bits) et l'identifiant unique de l'activateur par lequel elle a été activée. La modulation ASK est utilisée pour éviter une fausse activation de la balise. Cette architecture réduit considérablement la consommation d'énergie car le récepteur de réveil nécessite une très faible quantité d'énergie pour rester opérationnel tout le temps et la radio UHF n'est fonctionnelle que lorsqu'il y a une activation par un émetteur LF.

Objectifs

La communication entre l'Activateur LF et la balise DOT est basée sur l'Induction Electromagnétique en Champ proche (*Near Field Magneto Inductive - NFMI*), qui est une technologie de communication sans fil à relativement courte portée mais qui offre une très faible consommation d'énergie et un fonctionnement fiable dans des environnements de propagation difficiles. La technologie NFMI utilise le couplage magnéto inductif entre les antennes émettrices et réceptrices qui se comportent alors comme des bobines avec une induction mutuelle autorisant un transfert d'énergie d'un circuit à l'autre via le champ magnétique quasi statique. La tension induite dans la bobine réceptrice est proportionnelle à l'intensité du champ magnétique qu'elle reçoit. Cela permet non seulement de réveiller la balise DOT mais, comme cette intensité décroît avec l'inverse du cube de la distance entre l'antenne de l'émetteur et le récepteur, de relier la valeur du LF-FSI mesurée par tag DOT à la distance entre l'Activateur LF et la balise DOT.

Cependant, la plage de fonctionnement initiale du système DOT est limitée à 5-6 mètres. L'utilisation d'antennes panneau (Fig. E (c)) permet d'augmenter la portée opérationnelle à 15-16 mètres mais leur facteur de forme important rend leur déploiement difficile. D'autre part, la résolution sur la valeur du LF-FSI mesurée par le récepteur LF de la balise DOT, n'est que de 5 bits. Cela signifie que seules 32 valeurs (0-31) de LF-FSI sont utilisables par le système DOT pour évaluer la distance. Cela compromet donc fortement la précision du système DOT pour des applications de télémétrie et de localisation. Les objectifs technologiques principaux de ce travail de recherche sont donc :

1. d'optimiser les portées opérationnelles du système DOT tout en conservant des tailles de bobines d'émetteur et récepteur parmi les plus petites parmi les systèmes RFID bi-fréquence existants.

2. d'optimiser les performances de localisation et de télémétrie du système DOT tout en conservant une complexité architecturale et un coût de production bas.

Modélisation du système

Le problème de la faible portée opérationnelle est commun à de nombreux systèmes basés sur couplage magnéto inductif rapportés dans la littérature. La recherche de meilleures performances en termes de portée et de précision de localisation a conduit les auteurs à proposer des systèmes plutôt complexes et coûteux, avec un nombre important de bobines, parfois de grande taille et/ou avec des méthodes de mesures et du matériel additionnel lourd à mettre en œuvre. Le travail de modélisation réalisé dans cette thèse a permis d'optimiser le système DOT en identifiant le meilleur compromis précision / complexité / coûts / capacité de déploiement et évolutivité.

L'utilisation de bobines multiaxes est nécessaire pour un fonctionnement omnidirectionnel. Bien que cela complique la conception, cela reste modéré et il est possible de conserver une compacité et une simplicité de mise en œuvre très compétitive. Une autre contrainte de conception, imposée par la nécessaire maitrise des coûts, réside dans l'utilisation de composants standards notamment en ce qui concerne les tiges de ferrites et les condensateurs d'accord. Tenant compte de ces contraintes, la modélisation mathématique du système permet d'identifier des règles de conception pour obtenir une précision de télémétrie acceptable. Elle prend en compte l'ensemble des paramètres physiques du système côté émetteur, longueur de tige de ferrite, longueur d'enroulement, inductance de l'enroulement ; comme du côté récepteur : dimensions des bobines, tailles de ferrite, facteur de qualité. Ce sont donc les paramètres d'importance principaux pour l'optimisation d'un système en termes de compacité et de portée.

Le système DOT utilise une bobine d'émetteur hélicoïdale. Cette antenne est caractérisée par son nombre de tours N_{tx}, son rayon a_{tx} sa longueur l_c et le courant sinusoïdal i_{tx} qui la traverse, elle est placée à l'origine comme indiqué sur la figure G. Elle

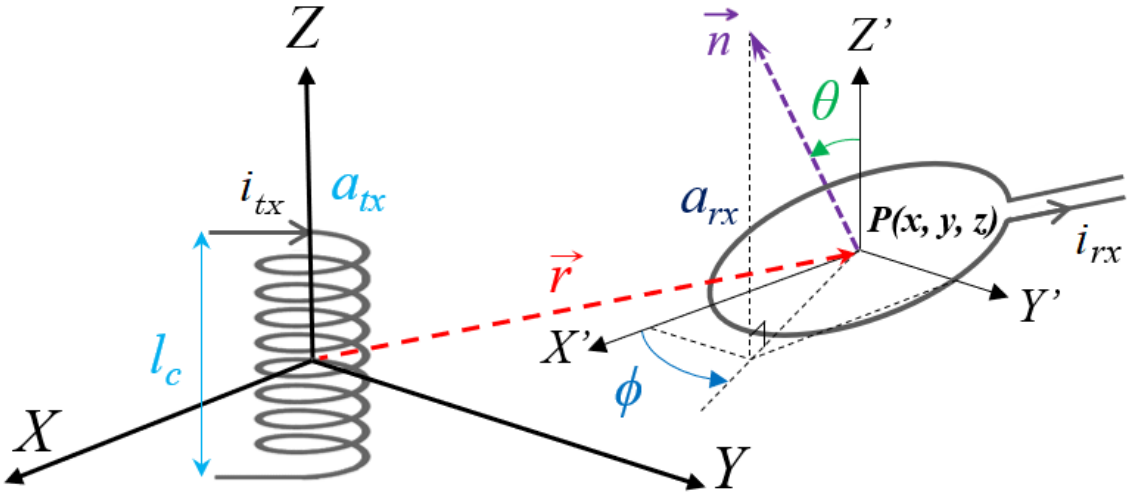

Figure G: Bobine d'émetteur hélicoïdal de rayon a_{tx} à l'origine et bobine de récepteur à un tour de rayon a_{rx} au point P avec son angle d'inclinaison θ par rapport à l'axe Z et son angle azimut ϕ par rapport à l'axe X.

produit un champ magnétique BF qui sera détecté par la bobine de récepteur caractérisée par son rayon a_{rx} et son nombre de tours N_{rx} et placée au point $P(x,y,z)$ à la distance r de l'origine. Le vecteur unitaire normal à la surface de la boucle est noté $\vec{n}$ et est défini par l'angle d'inclinaison θ par rapport à l'axe vertical Z et l'angle d'azimut ϕ par rapport à l'axe horizontal X. Les surfaces orientées A_{tx} et A_{rx} définissent les surfaces actives des antennes de l'émetteur et du récepteur respectivement.

En circuit ouvert, l'amplitude V_{Lrx} de la tension induite au borne de la bobine du récepteur est donnée par (1), où μ_0 est la perméabilité du vide et f_0 est la fréquence de fonctionnement de l'émetteur.

$$V_{Lrx} = \frac{\mu_0 N_{tx} N_{rx} A_{tx} A_{rx} I_{tx} f_0}{2 l_c} \begin{bmatrix} \left(\frac{1}{q^3} - \frac{1}{p^3}\right) x\vec{i} \\ \left(\frac{1}{q^3} - \frac{1}{p^3}\right) y\vec{j} \\ \left(\frac{z+l_c/2}{p^3} - \frac{z-l_c/2}{q^3}\right)\vec{k} \end{bmatrix} \cdot \begin{bmatrix} \sin\theta\cos\phi\vec{i} \\ \sin\theta\sin\phi\vec{j} \\ \cos\theta\vec{k} \end{bmatrix} \tag{1}$$

Où $\vec{i}$, $\vec{j}$ et $\vec{k}$ sont les vecteurs unitaires le long des axes X, Y et Z respectivement et

$$p = \sqrt{x^2 + y^2 + (z + l_c/2)^2}$$

$$q = \sqrt{x^2 + y^2 + (z - l_c/2)^2}$$

Si l'antenne réceptrice est placée dans le plan $X-Y$ ($z=0$), alors l'expression de V_{Lrx} peut être simplifiée :

$$V_{Lrx} = \frac{\mu_0 N_{tx} N_{rx} A_{tx} A_{rx} I_{tx} f_0 \cos\theta}{2\left[r^2 + \frac{l_c^2}{4}\right]^{\frac{3}{2}}} \tag{2}$$

Comme le système DOT utilise des antennes à noyau de ferrite à la fois à l'émetteur et au récepteur, il est important d'en étudier l'impact individuellement. La ferrite est un matériau ferromagnétique avec une perméabilité magnétique élevée et une faible conductivité électrique, utilisé dans les systèmes MI pour augmenter le couplage magnétique entre deux bobines [141]. Dans le cas d'un couplage faible, comme ici, l'utilisation de ferrite est particulièrement intéressante car elle augmente l'inductance mutuelle entre les bobines et donc la portée opérationnelle du système. Lorsqu'une tige de ferrite cylindrique est placée à l'intérieur d'une bobine hélicoïdale, l'inductance de la bobine est augmentée d'un facteur μ_{rod-tx} [142] appelé la perméabilité relative effective et qui est propre au matériau et aux caractéristiques géométriques de la tige. Ainsi l'équation (2) peut être corrigée pour tenir compte de la présence de ferrite dans les bobines d'émetteur et de récepteur en ($\theta=0$) :

$$V_{Lrx} = \frac{\mu_0 \sqrt{\mu_{rod-tx}\mu_{rod-rx}} \cdot N_{tx} A_{tx} N_{rx} A_{rx} f_0 I_{tx}}{2\left[r^2 + \frac{l_c^2}{4}\right]^{\frac{3}{2}}} \tag{3}$$

Cette dernière équation donne une expression exacte du courant induit dans le cas d'intérêt. Cependant, il n'y a pas d'accord général sur le calcul des valeurs de perméabilité relative effective des bobines avec ferrite. Cela limite donc l'utilisation de cette formule pour l'optimisation de la conception.

Une seconde approche analytique est donc proposée et est basée sur un modèle de circuit électrique équivalent. La tension induite est exprimé simplement par :

$$V_{Lrx} = \omega M I_{tx} \tag{4}$$

Où M est l'inductance mutuelle entre la bobine de l'émetteur et du récepteur et

qui peut être exprimée en fonction du coefficient de couplage k ($0 \leq k \leq 1$) et des auto-inductances des bobines d'émetteur et de récepteur L_{tx} et L_{rx} respectivement :

$$k(r) = \frac{{a_{tx}}^{\frac{3}{2}} {a_{rx}}^{\frac{3}{2}}}{\left(\sqrt{r^2 + {a_{rx}}^2}\right)^3} \tag{5}$$

$$M = k\sqrt{L_{tx} \cdot L_{rx}} \tag{6}$$

Ce modèle électrique prend en compte l'impact du noyau ferrite car ses effets sont inclus dans les valeurs des inductances qui peuvent être mesurées facilement. Les deux approches analytiques fournissent des expressions similaires avec notamment une décroissance en $1/r^3$ de la tension induite en fonction de la distance émetteur-récepteur.

$$V_{Lrx} = \frac{2\pi f_0 {a_{tx}}^{\frac{3}{2}} {a_{rx}}^{\frac{3}{2}} \sqrt{L_{tx} \cdot L_{rx}} I_{tx}}{\left[r^2 + {a_{rx}}^2\right]^{\frac{3}{2}}} = \frac{\mu_0 \sqrt{\mu_{rod-tx}\mu_{rod-rx}} \cdot N_{tx} A_{tx} N_{rx} A_{rx} f_0 I_{tx}}{2\left[r^2 + \frac{l_c^2}{4}\right]^{\frac{3}{2}}} \tag{7}$$

Dans le système DOT, la tension aux bornes des bobines n'est pas directement accessible. En effet le récepteur AS3933 fournit une mesure du LF-FSI (FSI_{LF}) qui peut en revanche être exprimée par :

$$FSI_{LF} = 10log\left(\frac{V_{out}}{V_{ref}}\right) \tag{8}$$

Avec V_{out} la tension induite aux bornes de l'antenne sélectionnée et V_{ref}=0,226 mVpp la sensibilité du récepteur. En utilisant le modèle du circuit équivalent et en faisant l'hypothèse que $a_{rx} = 8\text{ mm} \ll r$, on peut établir la relation entre le LF-FSI et la distance émetteur récepteur selon :

$$FSI_{LF} = 10log\left(\frac{2\pi f_0 {a_{tx}}^{\frac{3}{2}} {a_{rx}}^{\frac{3}{2}} \sqrt{L_{tx} \cdot L_{rx}} I_{tx} Q_{rx}}{V_{ref} r^3}\right) \tag{9}$$

La figure H présente une comparaison entre le modèle analytique et les mesures expérimentales obtenues en utilisant trois modèles antennes d'émetteur différentes et

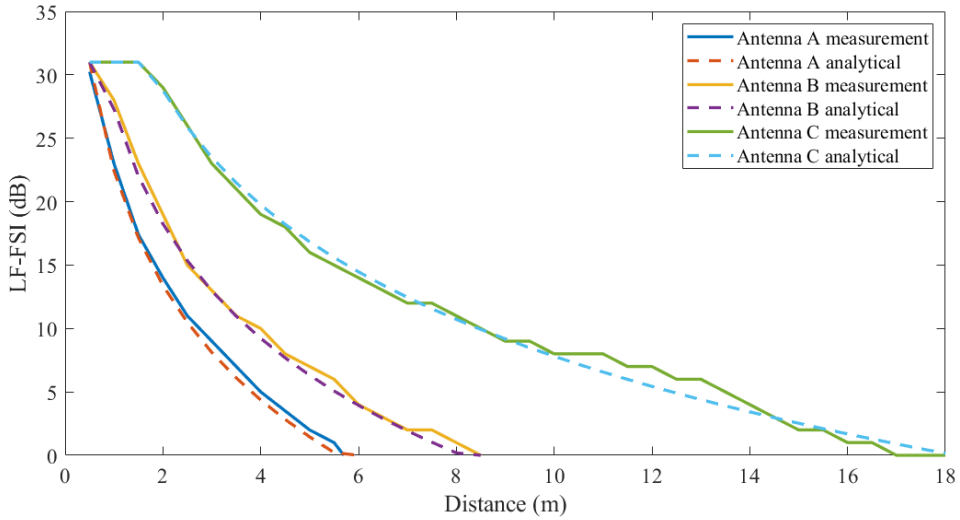

Figure H: Modèle d'atténuation LF-FSI pour antennes émetteurs A, B et C.

dans des conditions de propagation directe (sans réflexion ni obstacles). L'antenne A (figure E (a)) correspond à l'antenne commerciale standard originellement utilisée dans le sytème DOT (antenne KGEA-BFCR du fabricant Premo). L'antenne B est un prototype réalisé au cours de cette thèse et constitué d'un enroulement de cuivre (figure E (b)) autour d'une tige ferrite de 140 mm. Enfin l'antenne C (figure E (c)) est une antenne panneau également conçue au cours de cette thèse et constituée de N boucles de cuivre sur un PCB.

La correspondance entre les prédictions analytiques et les résultats expérimentaux est très satisfaisante. L'antenne C permet d'augmenter de façon importante la portée du système, de 6 à 18 m, grâce à une inductance mutuelle avec la bobine du récepteur fortement accrue. Cependant, il faut noter que le récepteur AS3933 sature pour un LF-FSI supérieur à 30 induisant un plateau dans la plage 0-2m pour le système DOT avec l'antenne C : il ne sera pas possible d'estimer précisément la distance émetteur récepteur dans cette plage et il sera préférable d'utiliser les antenne A ou B pour les applications correspondantes. D'autre part, les valeurs de LF-FSI générées par le récepteur AS3933 sont des valeurs entières entre 0 et 31 car codées sur 5 bits uniquement. Cela induit des erreurs de quantification qui impacteront aussi la précision des mesures de distance.

Estimation de distance

La modélisation analytique a permis d'établir la relation entre la distance émetteur récepteur et le LF-FSI. Cependant, la validité de ce modèle n'est rigoureusement vérifiée que dans des conditions idéales de propagation du signal magnétique, ce qui est rarement le cas en pratique. En effet, la modélisation analytique néglige l'impact des phénomènes de réflexion, de diffusion et de réception de trajets multiples car le signal magnéto inductif BF est théoriquement peu impacté par ces effets.

Il est donc nécessaire de comparer la méthode d'estimation de distance basée sur l'utilisation directe de la formule analytique avec une méthode empirique basée sur l'étalonnage et la calibration. Cette dernière méthode consiste à mesurer le LF-FSI du signal entre un activateur et un DOT pour différentes distances et directions connues dans l'environnement de propagation réel. Il est ainsi possible de reconstruire, en utilisant la méthode des moindres carrés, la courbe d'atténuation du LF-FSI en fonction des positions respectives de l'émetteur et du récepteur tout en tenant compte des caractéristiques spécifiques d'atténuation de l'environnement considéré. Cette courbe peut ensuite être directement utilisée pour estimer la distance.

La méthode analytique consiste à inverser l'équation 9 pour exprimer la distance émetteur récepteur en fonction du LF-FSI et d'utiliser les valeurs mesurées de ce dernier paramètre ainsi que les valeurs des paramètres géométriques et matériaux connus pour estimer cette distance :

$$\hat{r} = \sqrt[3]{\frac{2\pi f_0 {a_{tx}}^{\frac{3}{2}} {a_{rx}}^{\frac{3}{2}} \sqrt{L_{tx} \cdot L_{rx}} I_{tx} Q_{rx}}{V_{ref} 10^{\frac{FSI_{LF}}{10}}}} \tag{10}$$

Le récepteur AS3933 sélectionne la valeur LF-FSI la plus élevée parmi les trois canaux correspondant à trois bobines orthogonales d'antenne 3 axes. De cette façon, la complexité du système est considérablement réduite. Cependant, cette approche introduit certaines limites sur l'estimation de la distance. Lorsque le système DOT est analysé pour différentes orientations de l'antenne 3 axes à l'aide de simulations, on constate que cette approche de faible complexité fournit une bonne approximation du fonctionnement omidirectionnel. Ainsi, (9) peut être utilisé dans certaines limites afin de modéliser le

système DOT sans sacrifier la précision de l'estimation de la distance lorsque l'orientation de l'étiquette est inconnue.

Fig I (d) montre la comparaison entre la performance globale de l'estimation de la distance du système à l'aide de méthodes de calibration et de modélisation. Pour l'estimation de distance de 25 positions, l'erreur moyenne obtenue est de 0,21±0,16 m avec la méthode de télémétrie par étalonnage et de 0,18±0,13 m, donc meilleure avec la méthode analytique. L'erreur d'estimation de distance est inférieure à 0,41 m pour 90 % des estimations pour la méthode de télémétrie par étalonnage et inférieure à 0,37 m pour la méthode de modélisation analytique. Ces différences s'expliquent en partie par la faible résolution du recepteur AS9333 sur la valeur du LF-FSI. En effet, les erreurs induites par la quantification des valeurs de LF-FSI limitent la précision globale une première fois lors de l'ajustement par la méthode des moindres carrés et une seconde fois lors de la mesure réelle de la distance d'intérêt.

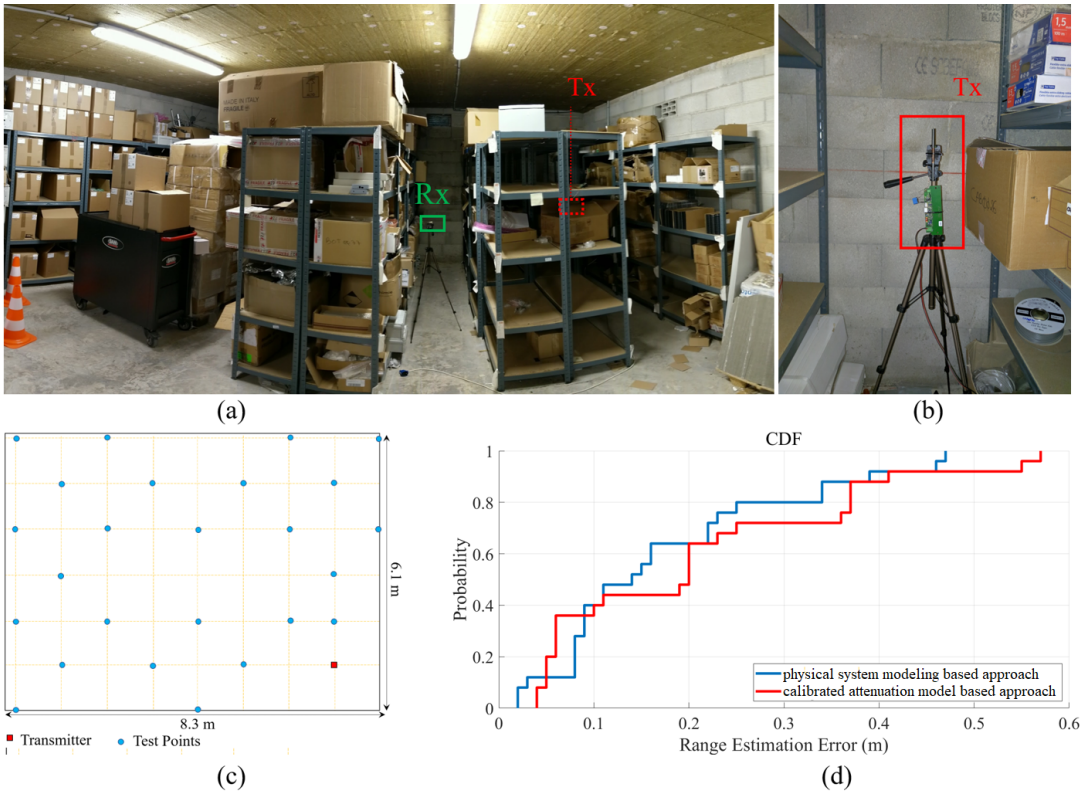

Figure I: (a) Environnement dans lequel l'expérience de télémétrie est réalisée (b) Émetteur BF avec antenne Tx3 (c) Configuration pour l'expérience d'estimation de la distance. (d) Fonction de distribution cumulative pour les erreurs d'estimation de la distance.

Performances de positionnement 2D

La modélisation analytique et les investigations expérimentales en champ libre ont permis d'optimiser et de caractériser les performances d'un système d'estimation de distance basé sur le système DOT. Cependant, le réel objectif de cette thèse concerne l'optimisation et la caractérisation d'un système de positionnement 2D basés sur le DOT et opéré dans des conditions proches du réel. Les derniers travaux de cette thèse ont donc consisté à comparer les performances d'un tel système à celles offertes par des systèmes de positionnement 2D commerciaux basés sur deux autres technologies de localisation 2D. Deux systèmes de références ont été choisis : le premier basé sur des dispositifs RFID Ultra Haute Fréquence (UHF) et l'autre sur des dispositifs *Ultra Wide Band* (UWB). Cette comparaison a été réalisée dans un environnement de propagation proche de conditions applicatives réelles avec la présence de personnes et d'obstacles métalliques et non métalliques.

L'estimation de la position 2D met en jeux des algorithmes dits "de positionnement" permettant de calculer la position de l'objet (DOT) à partir des mesures de distances entre l'objet et au moins trois points fixes (Activator LF). Il existe plusieurs algorithmes de positionnement dont deux sont plus particulièrement utilisés ici : l'algorithme de trilatération et l'algorithme des barycentres pondérés. L'algorithme de trilatération consiste à chercher l'intersection entre trois cercles au minimum centrés respectivement sur des points fixes de références. Lorsque plus de trois valeurs de mesure de distance sont disponibles, il est possible d'améliorer la précision de cet algorithme en prenant la position moyenne entre les positions estimées par chaque combinaison possible de trois points de référence. L'algorithme des barycentres pondérés consiste à identifier la position de l'objet à celle du barycentre pondéré des points de référence avec des poids correspondant respectivement aux distances mesurées. L'algorithme de trilatération offre l'avantage d'une meilleure robustesse aux erreurs de quantification de la mesure de distance. Cependant, lorsque ces dernières sont négligeables, l'algorithme des barycentres donne généralement des résultats plus précis.

L'ensemble du premier étage du bâtiment d'ELA Innovation, d'une superficie totale d'environ 315 m^2 a été choisi pour ces essais. Cet environnement se compose de plusieurs

pièces séparées par des cloisons intérieures, et comporte notamment des fenêtres à cadres métalliques, des murs extérieurs contenant des armatures métalliques et de grandes poutres métalliques soutenant le plancher et le plafond. Cet espace peut être subdivisé en différents sous espaces tels que les bureaux, la réserve et l'atelier, comme le montre la figure J. Dans la zone appelée environnement de bureau 1, la densité de personnes, d'ordinateurs, d'équipements électriques et autres objets métalliques est moindre comparée à l'environnement de bureau 2. La réserve avec une superficie d'environ 25 mètres carrés, contient plusieurs racks métalliques où sont rangés des composant électroniques et différents produits RFID tels que des tags, des lecteurs et des antennes. La densité de métal y est donc très élevée. L'atelier contient plusieurs machines et outils métalliques et est typiquement occupé par un grand nombre d'opérateurs.

Le système RFID UHF utilisé pour cette étude comparative est basée sur des tags RFID actif développés et commercialisés par ELA sous la dénomination commerciale COIN ID et les mêmes lecteurs RFID que le système DOT, les lecteurs IP2. Dans cette solution de localisation, les mesures de distances sont obtenues via la mesure du RSSI et l'utilisation d'une courbe d'atténuation étalonnée *in situ*. Les positions sont déterminées par la méthode des barycentres.

Le système UWB utilisé correspond au kit d'évaluation DW1000 commercialisé par la société Decawave. Il comprend des ancres (points fixes) qui transmettent des impulsions RF à des tags qui retransmettent ces impulsions vers les ancres dès réception. Les ancres mesurent le temps d'aller retour du signal et estiment la distance parcourue à l'aide de la vitesse de propagation. Pour ce systèmes les deux algorithmes de positionnement sont utilisés.

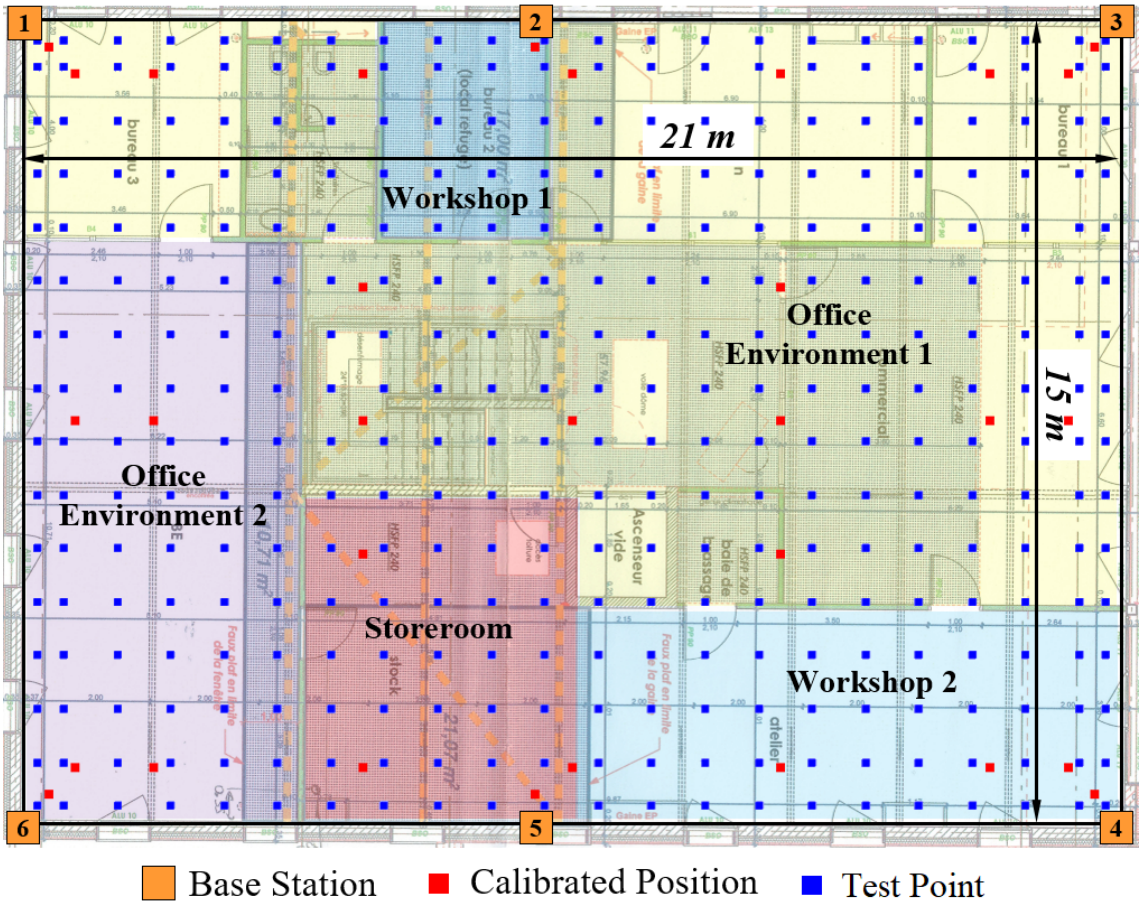

Figure J: Zone expérimentale montrant différents environnements et positions des stations de base pour le positionnement des expériences à l'intérieur d'un bâtiment.

La table 4.1 présente les résultats obtenus pour les trois systèmes de positionnement 2D considérés, en terme d'erreur de positionnement et la figure K montre la fonction de répartition cumulative des erreurs de positionnement. Sur les 352 positions estimées, 90% ont été estimées avec une erreur inférieure à 2,62 m en utilisant le système DOT, 5,41 m pour le système RFID et 1,1 m pour le système UWB. Il est intéressant de noter que cette comparaison des technologies est ici principalement liée à la sensibilité de chacune des technologies aux conditions non idéales de propagation. En particulier les performances du système DOT et du systèmes RFID sont beaucoup plus proches en conditions idéales de propagation. D'autre part, la précision du système DOT est principalement limitée par la résolution du recepteur AS933 sur la valeur du LF-FSI. L'utilisation d'un autre récepteur avec une résolution d'au moins 10 bits permettrait d'atteindre des précisions inférieures à 1 m.

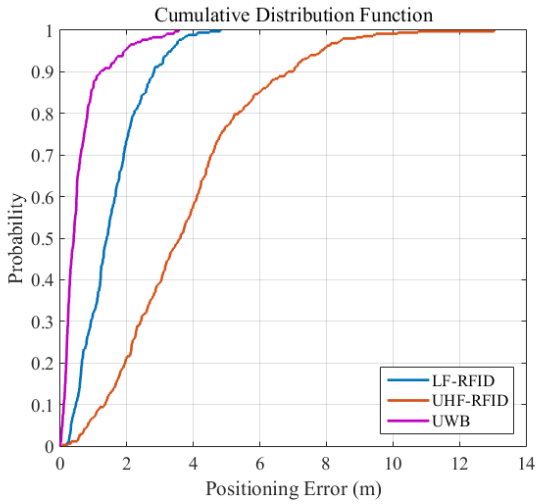

Figure K: Fonction de distribution cumulative pour les erreurs de positionnement des systèmes DOT, UHF-RFID et UWB

-	DOT	UHF-RFID	UWB
Erreur moyenne (m)	1.58	2.84	0.58
Écart-type (m)	0.76	1.81	0.62
CDF à 50% (m)	1.54	2.47	0.41
CDF à 90% (m)	2.62	5.41	1.10
Erreur maximale (m)	3.75	9.42	3.56

Table 4.1: Erreur de positionnement 2D du système DOT par rapport au positionnement basé sur UHF-RFID et UWB.

Expérimentation du système DOT sur des cas d'utilisation de clients

Au cours de ce travail, le système DOT a été testé pour différents cas d'utilisation de clients ELA tels qu'un suivi temps-réel de palettes des palettes (expérimentation avec l'entreprise Renault), un système d'entrée sans clé (*Passive Keyless Entry - PKE*) testé dans un dépôt de bus avec la régie des transports méropolitain de Marseille (RTM) et un système de prévention des de collisions engins-piétons dans les usines. Ces applications

utilisent les capacités d'estimation de distance du système DOT.

Le projet de suivi des palettes a pour objectif de tracer en temps réel les emplacements du grand nombre de pièces de rechange dans les installations de production. L'expérimentation a porté sur l'usine de production de Maubeuge en France avec plus de 50000 palettes à suivre à l'aide du système DOT associé à une solution d'identification UHF-RFID. La cible de précision de localisation requise de 2 à 5 m (niveau de la zone) a été atteinte. Le système a permis d'améliorer l'efficacité de la production grâce au suivi et au transfert efficace des palettes.

Au cours de la phase pilote du projet d'entrée sans clé du RTM de Marseille, une démonstration de la commande sans clé des portes à l'aide du système DOT a été effectuée, l'objectif étant de permettre l'ouverture des portes sans que les conducteurs n'aient à descendre des bus comme c'est le cas actuellement. Les activateurs DOT ont été déployés en haut des grandes portes automatisées. Lorsque une balise DOT est dans la plage de fonctionnement de l'activateur, la balise est activée et enregistrée par le lecteur RFID qui déclenche le contrôle du signal de relais la porte. Le déclenchement doit être effectué lorsque le bus est à 1,5m de la porte de façon à éviter que d'autres bus passant devant la porte n'activent le système par erreur. Le système DOT a réussi à répondre à cette spécification. En plus de simplifier l'accès au dépôt pour les conducteurs, le système DOT permet de bloquer les accès non autorisés et de positionner les bus en stationnement.

Le système DOT a aussi été testé dans le cadre d'un projet visant à éviter les collisions entre les chariots élévateurs exploités à l'intérieur d'une usine de fabrication et les piétons à l'intérieur de l'installation. l'activateur et le lecteur RFID sont installés sur le chariot élévateur et les tags DOT sont portés par les piétons. Le système anti-collision envoie des alarmes aux deux parties lorsque la distance les séparant est infére ieure à une valeur spécifique. Le système DOT déclenche avec succès l'alarme lorsque les piétons se trouvent à l'intérieur de la zone de danger créée par le chariot élévateur. Cela permet d'éviter le grand nombre d'accidents de chariot élévateur se produisant à l'intérieur d'une usine de fabrication en raison de divers angles morts. La fiabilité du système DOT dans un environnement de propagation difficile est le facteur important de ce projet.

Conclusion

Les travaux de thèse présentés dans ce manuscrit ont donc permis d'étudier théoriquement, d'optimiser et d'évaluer les performances d'un système de localisation 2D, baptisé système DOT et basé sur le couplage magnéto inductif faible et basse fréquence d'antennes magnétiques (bobines). Les deux objectifs principaux qui étaient d'augmenter la portée opérationnelle et la précision du système tout en conservant des caractéristiques de compacité, de coûts et de simplicité de mise en œuvre, ont pu être atteints grâce à une méthodologie basée sur la modélisation analytique et la vérification expérimentale. Plus précisément les principales contributions de ce travail sont :

1. La modélisation analytique du couplage inductif dans des systèmes à couplage extrêmement faible,
2. L'identification de règles de conception des antennes magnétiques mise en jeu par le système afin d'accroître la portée opérationnelle et améliorer la compacité,
3. L'étude expérimentale et théorique de l'influence de la présence d'objets ferromagnétiques dans l'environnement de propagation et les règles de conception associées à la minimisation de ces effets,
4. L'évaluation expérimentale et théorique de l'influence de l'orientation du récepteur dans le cadre d'antennes magnétiques 3D intégrées dans une électronique de pilotage simplifiée,
5. L'évaluation des performances du système présenté pour la localisation 2D et la comparaison à des solutions existantes basées sur les technologies UHF et UWB.

L'ensemble des ces résultats permettent finalement d'identifier les principales voies d'amélioration du système DOT pour le futur. Notamment, l'antenne de l'activateur pourrait être remplacée par une antenne avec un cœur en ferrite, proche de celle proposée dans ce manuscrit sous forme de prototype. Cela permettrait de conserver une compacité proche du système actuel tout en offrant une portée opérationnelle de l'ordre de 12 m comparable à celle offerte par les larges antennes panneaux.

Pour ce faire, il sera nécessaire d'approfondir la modélisation analytique du système, par exemple, à l'aide de modèles numériques capables de rendre compte de façon plus précise de l'influence de la présence de ferrite et notamment de son orientation. Le développement de ces modèles numériques permettra également de mieux prendre en compte les perturbations du champ magnétique dues à la présence de matériaux ferromagnétiques dans l'environnement de propagation. Enfin, l'utilisation d'un LF-WURx capable de mesurer des valeurs de LF-FSI avec une résolution meilleure que celle offerte par le composant actuel (5 bits) permettrait d'améliorer très sensiblement la précision de mesure de distance. En effet, cette limitation de résolution est le principal facteur limitant dans le système DOT actuel avec une précision de 40 cm. L'utilisation d'un LF-FSI codé sur 16 bits devrait permettre d'atteindre des précisions de l'ordre de 10 cm.

En tenant compte de ces optimisations restantes, le système DOT et plus généralement les système de localisation 2D basé sur le couplage magnéto inductif basse fréquence de deux bobines constitue un candidat particulièrement pertinent pour répondre aux cas d'usages nécessitant des fonctions de localisation ultra précise (sub 10 cm), faibles coûts, compactes et à portée limitée (12 m).

References

[1] Cifre. http://www.anrt.asso.fr/fr/cifre-7843. Accessed: March 2020.

[2] Ela innovation. https://elainnovation.com/. Accessed: March 2020.

[3] Laboratoire ESYCOM (UMR 9007 CNRS). http://esycom.u-pem.fr/. Accessed: March 2020.

[4] Laboratoire AlliansTIC. https://www.efrei.fr/innovation-recherche/le-laboratoire-de-recherche-allianstic/. Accessed: March 2020.

[5] Agence nationale de la recherche. https://anr.fr/. Accessed: March 2020.

[6] Amitangshu Pal and Krishna Kant. NFMI: connectivity for short-range IoT applications. *Computer*, 52(2):63–67, 2019.

[7] Yanying Gu, Anthony Lo, and Ignas Niemegeers. A survey of indoor positioning systems for wireless personal networks. *IEEE Communications Surveys & Tutorials, 11 (1), 2009*, 2009.

[8] Michailas Romanovas, Vadim Goridko, Lasse Klingbeil, Mohamed Bourouah, Ahmed Al-Jawad, Martin Traechtler, and Yiannos Manoli. Pedestrian indoor localization using foot mounted inertial sensors in combination with a magnetometer, a barometer and RFID. In *Progress in Location-Based Services*, pages 151–172. Springer, 2013.

[9] Michael Brown, James Pinchin, and Chris Hide. Opening indoors: the advent of indoor positioning. In *Contemporary ergonomics and human factors 2013: Proceedings of the International Conference on Ergonomics and Human Factors*, pages 35–43, 2013.

[10] Farid Benbadis, Timur Friedman, M Dias De Amorim, and Serge Fdida. GPS-free-free positioning system for wireless sensor networks. In *Second IFIP International Conference on Wireless and Optical Communications Networks, 2005. WOCN 2005.* Pages 541–545. IEEE, 2005.

[11] Yunhao Liu, Zheng Yang, Xiaoping Wang, and Lirong Jian. Location, localization, and localizability. *Journal of Computer Science and Technology*, 25(2):274–297, 2010.

[12] Mai A Al-Ammar, Suheer Alhadhrami, Abdulmalik Al-Salman, Abdulrahman Alarifi, Hend S Al-Khalifa, Ahmad Alnafessah, and Mansour Alsaleh. Comparative survey of indoor positioning technologies, techniques, and algorithms. In *2014 International Conference on Cyberworlds*, pages 245–252. IEEE, 2014.

[13] Faheem Zafari, Athanasios Gkelias, and Kin K Leung. A survey of indoor localization systems and technologies. *IEEE Communications Surveys & Tutorials*, 21(3):2568–2599, 2019.

[14] Jeffrey Hightower and Gaetano Borriello. Location systems for ubiquitous computing. *computer*, 34(8):57–66, 2001.

[15] Andreas Braun, Henning Heggen, and Reiner Wichert. CapFloor–a flexible capacitive indoor localization system. In *International Competition on Evaluating AAL Systems through Competitive Benchmarking*, pages 26–35. Springer, 2011.

[16] Robert J Orr and Gregory D Abowd. The smart floor: a mechanism for natural user identification and tracking. In *CHI'00 extended abstracts on Human factors in computing systems*, pages 275–276, 2000.

[17] Kyoung Nam Ha, Kyung Chang Lee, and Suk Lee. Development of PIR sensor based indoor location detection system for smart home. In *2006 SICE-ICASE International Joint Conference*, pages 2162–2167. IEEE, 2006.

[18] Matthew S Gast. *Building applications with iBeacon: proximity and location services with Bluetooth low energy*. " O'Reilly Media, Inc.", 2014.

[19] Miodrag Bolic, Majed Rostamian, and Petar M Djuric. Proximity detection with RFID: a step toward the internet of things. *IEEE Pervasive Computing*, 14(2):70–76, 2015.

[20] Nirupama Bulusu, John Heidemann, Deborah Estrin, et al. GPS-less low-cost outdoor localization for very small devices. *IEEE personal communications*, 7(5):28–34, 2000.

[21] Christine Laurendeau and Michel Barbeau. Relative span weighted localization of uncooperative nodes in wireless networks. In *International Conference on Wireless Algorithms, Systems, and Applications*, pages 358–367. Springer, 2009.

[22] Jan Blumenthal, Frank Reichenbach, and Dirk Timmermann. Position estimation in ad hoc wireless sensor networks with low complexity. In *Joint 2nd workshop on positioning, navigation and communication*, pages 41–49, 2005.

[23] Stephan Schuhmann, Klaus Herrmann, Kurt Rothermel, Jan Blumenthal, and Dirk Timmermann. Improved weighted centroid localization in smart ubiquitous environments. In *International Conference on Ubiquitous Intelligence and Computing*, pages 20–34. Springer, 2008.

[24] Ralf Behnke and Dirk Timmermann. AWCL: adaptive weighted centroid localization as an efficient improvement of coarse grained localization. In *2008 5th Workshop on Positioning, Navigation and Communication*, pages 243–250. IEEE, 2008.

[25] Herbert L Groginsky. Position estimation using only multiple simultaneous range measurements. *IRE Transactions on Aeronautical and Navigational Electronics*, (3):178–187, 1959.

[26] Javier O Roa, Antonio Ramón Jiménez, F Seco, José Carlos Prieto, and J Ealo. Optimal placement of sensors for trilateration: regular lattices vs meta-heuristic solutions. In *International Conference on Computer Aided Systems Theory*, pages 780–787. Springer, 2007.

[27] Robert J Mailloux. Phased array theory and technology. *Proceedings of the IEEE*, 70(3):246–291, 1982.

[28] Kamol Kaemarungsi and Prashant Krishnamurthy. Properties of indoor received signal strength for WLAN location fingerprinting. In *The First Annual International Conference on Mobile and Ubiquitous Systems: Networking and Services, 2004. MOBIQUITOUS 2004.* Pages 14–23. IEEE, 2004.

[29] Stephen P Tarzia, Peter A Dinda, Robert P Dick, and Gokhan Memik. Indoor localization without infrastructure using the acoustic background spectrum. In *Proceedings of the 9th international conference on Mobile systems, applications, and services*, pages 155–168, 2011.

[30] Farhang Vedadi and Shahrokh Valaee. Automatic visual fingerprinting for indoor image-based localization applications. *IEEE Transactions on Systems, Man, and Cybernetics: Systems*, 2017.

[31] Martin Azizyan, Ionut Constandache, and Romit Roy Choudhury. Surroundsense: mobile phone localization via ambience fingerprinting. In *Proceedings of the 15th annual international conference on Mobile computing and networking*, pages 261–272, 2009.

[32] Paramvir Bahl and Venkata N Padmanabhan. RADAR: an in-building RF-based user location and tracking system. In *Proceedings IEEE INFOCOM 2000. Conference on Computer Communications. Nineteenth Annual Joint Conference of the IEEE Computer and Communications Societies (Cat. No. 00CH37064)*, volume 2, pages 775–784. Ieee, 2000.

[33] Chao-Lin Wu, Li-Chen Fu, and Feng-Li Lian. WLAN location determination in e-home via support vector classification. In *IEEE International Conference on Networking, Sensing and Control, 2004*, volume 2, pages 1026–1031. IEEE, 2004.

[34] Laslo Gogolak, Silvester Pletl, and Dragan Kukolj. Indoor fingerprint localization in WSN environment based on neural network. In *2011 IEEE 9th International Symposium on Intelligent Systems and Informatics*, pages 293–296. IEEE, 2011.

[35] Luis W Alvarez. Dead reckoning range finding device for cart, 1984. US Patent 4,480,310.

[36] Helena Leppäkoski, Jussi Collin, and Jarmo Takala. Pedestrian navigation based on inertial sensors, indoor map, and WLAN signals. *Journal of Signal Processing Systems*, 71(3):287–296, 2013.

[37] Hui Liu, Houshang Darabi, Pat Banerjee, and Jing Liu. Survey of wireless indoor positioning techniques and systems. *IEEE Transactions on Systems, Man, and Cybernetics, Part C (Applications and Reviews)*, 37(6):1067–1080, 2007.

[38] Rudolph Emil Kalman. A new approach to linear filtering and prediction problems, 1960.

[39] Greg Welch, Gary Bishop, et al. An introduction to the kalman filter, 1995.

[40] Pierre-Yves Gilliéron, Ivan Spassov, Bertrand Merminod, et al. Indoor navigation enhanced by map-matching. *European Journal of navigation*, 3(3):6–13, 2005.

[41] Mohammed A Quddus, Washington Y Ochieng, and Robert B Noland. Current map-matching algorithms for transport applications: state-of-the art and future research directions. *Transportation research part c: Emerging technologies*, 15(5):312–328, 2007.

[42] Abdelmoula Bekkali, Horacio Sanson, and Mitsuji Matsumoto. RFID indoor positioning based on probabilistic RFID map and kalman filtering. In *Third IEEE International Conference on Wireless and Mobile Computing, Networking and Communications (WiMob 2007)*, pages 21–21. IEEE, 2007.

[43] Marco Altini, Davide Brunelli, Elisabetta Farella, and Luca Benini. Bluetooth indoor localization with multiple neural networks. In *IEEE 5th International Symposium on Wireless Pervasive Computing 2010*, pages 295–300. IEEE, 2010.

[44] Ruey-Hsuan Lee, Jen-Chieh Wu, Shao-Hsuan Chang, Sheng-Fuh Chang, Chia-Chan Chang, and Yi-Ming Chen. Radar design for wireless indoor positioning applications. In *2013 European Microwave Conference*, pages 846–849. IEEE, 2013.

[45] Mengyun Liu, Ruizhi Chen, Deren Li, Yujin Chen, Guangyi Guo, Zhipeng Cao, and Yuanjin Pan. Scene recognition for indoor localization using a multi-sensor fusion approach. *Sensors*, 17(12):2847, 2017.

[46] Davide Macagnano and Giuseppe Thadeu Freitas De Abreu. Algebraic approach for robust localization with heterogeneous information. *IEEE Transactions on Wireless Communications*, 12(10):5334–5345, 2013.

[47] Can Wang, Kang Li, Guoyuan Liang, Haoyao Chen, Sheng Huang, and Xinyu Wu. A heterogeneous sensing system-based method for unmanned aerial vehicle indoor positioning. *Sensors*, 17(8):1842, 2017.

[48] Jingbin Liu, Ruizhi Chen, Ling Pei, Robert Guinness, and Heidi Kuusniemi. A hybrid smartphone indoor positioning solution for mobile LBS. *Sensors*, 12(12):17208–17233, 2012.

[49] Mark A Weissberger. An initial critical summary of models for predicting the attenuation of radio waves by trees. Technical report, ELECTROMAGNETIC COMPATIBILITY ANALYSIS CENTER ANNAPOLIS MD, 1982.

[50] Kaveh Pahlavan and Allen H Levesque. *Wireless information networks*, volume 93. John Wiley & Sons, 2005.

[51] Santiago Mazuelas, Francisco A Lago, David González, Alfonso Bahillo, Juan Blas, Patricia Fernandez, Ruben M Lorenzo, and Evaristo J Abril. Dynamic estimation of optimum path loss model in a RSS positioning system. In *2008 IEEE/ION Position, Location and Navigation Symposium*, pages 679–684. IEEE, 2008.

[52] Majid Hosseini, Hassan Chizari, Chai Kok Soon, and Rahmat Budiarto. RSS-based distance measurement in underwater acoustic sensor networks: an application of the lambert w function. In *2010 4th International Conference on Signal Processing and Communication Systems*, pages 1–4. IEEE, 2010.

[53] Qinghua Wang, Ilangko Balasingham, Miaomiao Zhang, and Xin Huang. Improving RSS-based ranging in LOS-NLOS scenario using GMMs. *IEEE Communications Letters*, 15(10):1065–1067, 2011.

[54] Nasir Saeed, Waqas Ahmad, and Dost Muhammad Saqib Bhatti. Localization of vehicular ad-hoc networks with RSS based distance estimation. In *2018 International Conference on Computing, Mathematics and Engineering Technologies (iCoMET)*, pages 1–6. IEEE, 2018.

[55] Hetal P Mistry and Nital H Mistry. RSSI based localization scheme in wireless sensor networks: a survey. In *2015 Fifth International Conference on Advanced Computing & Communication Technologies*, pages 647–652. IEEE, 2015.

[56] Yishuang Geng, Haokun Deng, et al. Modeling the effect of human body on TOA ranging for indoor human tracking with wrist mounted sensor. In *2013 16th International Symposium on Wireless Personal Multimedia Communications (WPMC)*, pages 1–6. IEEE, 2013.

[57] Bradford W Parkinson, Per Enge, Penina Axelrad, and James J Spilker Jr. *Global Positioning System: Theory and applications, Volume II*. American Institute of Aeronautics and Astronautics, 1996.

[58] Danwei Wang, Ramprashanth Kannan, Liu Wei, and Bertrand Tay. Time of flight based two way ranging for real time locating systems. In *2010 IEEE Conference on Robotics, Automation and Mechatronics*, pages 199–205. IEEE, 2010.

[59] Chih-Yu Wen, Robin D Morris, and William A Sethares. Distance estimation using bidirectional communications without synchronous clocking. *IEEE Transactions on Signal Processing*, 55(5):1927–1939, 2007.

[60] Sinan Gezici, Zhi Tian, Georgios B Giannakis, Hisashi Kobayashi, Andreas F Molisch, H Vincent Poor, and Zafer Sahinoglu. Localization via ultra-wideband radios: a look at positioning aspects for future sensor networks. *IEEE signal processing magazine*, 22(4):70–84, 2005.

[61] Fauzia Ahmad, Moeness G Amin, and Pawan Setlur. Through-the-wall target localization using dual-frequency CW radars. In *Sensors, and Command, Control, Communications, and Intelligence (C3I) Technologies for Homeland Security and Homeland Defense V*, volume 6201, 62010H. International Society for Optics and Photonics, 2006.

[62] Xin Li, Yimin Zhang, and Moeness G Amin. Multifrequency-based range estimation of RFID tags. In *2009 IEEE International Conference on RFID*, pages 147–154. IEEE, 2009.

[63] Tarig Ballal and Chris J Bleakley. Phase-difference ambiguity resolution for a single-frequency signal. *IEEE Signal Processing Letters*, 15:853–856, 2008.

[64] Martin Woolley. Bluetooth core specification v5.1. In Bluetooth, 2019.

[65] Kaishun Wu, Jiang Xiao, Youwen Yi, Dihu Chen, Xiaonan Luo, and Lionel M Ni. CSI-based indoor localization. *IEEE Transactions on Parallel and Distributed Systems*, 24(7):1300–1309, 2012.

[66] Zheng Yang, Zimu Zhou, and Yunhao Liu. From RSSI to CSI: indoor localization via channel response. *ACM Computing Surveys (CSUR)*, 46(2):1–32, 2013.

[67] Jiang Xiao, Kaishun Wu, Youwen Yi, and Lionel M Ni. FIFS: fine-grained indoor fingerprinting system. In *2012 21st international conference on computer communications and networks (ICCCN)*, pages 1–7. IEEE, 2012.

[68] Xuyu Wang, Lingjun Gao, Shiwen Mao, and Santosh Pandey. DeepFi: deep learning for indoor fingerprinting using channel state information. In *2015 IEEE wireless communications and networking conference (WCNC)*, pages 1666–1671. IEEE, 2015.

[69] Robert K Crane. *Propagation handbook for wireless communication system design*. CRC press, 2003.

[70] Esmond Mok and Günther Retscher. Location determination using WiFi fingerprinting versus WiFi trilateration. *Journal of Location Based Services*, 1(2):145–159, 2007.

[71] Ramsey Faragher and Rob Harle. SmartSLAM-an efficient smartphone indoor positioning system exploiting machine learning and opportunistic sensing. In *ION GNSS*, volume 13, pages 1–14, 2013.

[72] Hongbo Zhang, Hongwei Du, Qiang Ye, and Chuang Liu. Utilizing CSI and RSSI to achieve high-precision outdoor positioning: a deep learning approach. In *ICC 2019-2019 IEEE International Conference on Communications (ICC)*, pages 1–6. IEEE, 2019.

[73] Chung-Wei Ou, Chin-Jung Chao, Fa-Shian Chang, Shun-Min Wang, Guan-Xun Liu, Min-Ren Wu, Kai-Yi Cho, Lih-Tyng Hwang, and Yi-Ying Huan. A ZigBee position technique for indoor localization based on proximity learning. In *2017 IEEE International Conference on Mechatronics and Automation (ICMA)*, pages 875–880. IEEE, 2017.

[74] Mare Srbinovska, Cvetan Gavrovski, and Vladimir Dimcev. Localization estimation system using measurement of RSSI based on ZigBee standard. In *Conference Proceedings of the 17th International Scientific and Applied Science Conference (Electronics 2008)*, pages 48–50, 2008.

[75] Ramsey Faragher and Robert Harle. Location fingerprinting with bluetooth low energy beacons. *IEEE journal on Selected Areas in Communications*, 33(11):2418–2428, 2015.

[76] Vicente Cantón Paterna, Anna Calveras Auge, Josep Paradells Aspas, and Maria Alejandra Perez Bullones. A bluetooth low energy indoor positioning system with channel diversity, weighted trilateration and kalman filtering. *Sensors*, 17(12):2927, 2017.

[77] Klaus Finkenzeller. *RFID handbook: fundamentals and applications in contactless smart cards, radio frequency identification and near-field communication*. John Wiley & Sons, 2010, pages 11–28.

[78] Part 1: active and passive RFID: two distinct, but complementary, technologies for real-time supply chain visibility. `http://www.thetrackit.com/Library.php`. Accessed: March 2020.

[79] Feng-juan Zhu, Zong-heng Wei, Bin-jie Hu, Jian-guang Chen, and Zi-min Guo. Analysis of indoor positioning approaches based on active RFID. In *2009 5th International Conference on Wireless Communications, Networking and Mobile Computing*, pages 1–4. IEEE, 2009.

[80] Qing Fu and Guenther Retscher. Active RFID trilateration and location fingerprinting based on RSSI for pedestrian navigation. *The Journal of Navigation*, 62(2):323–340, 2009.

[81] Robert J Fontana. Recent system applications of short-pulse ultra-wideband (UWB) technology. *IEEE Transactions on microwave theory and techniques*, 52(9):2087–2104, 2004.

[82] Abdulrahman Alarifi, AbdulMalik Al-Salman, Mansour Alsaleh, Ahmad Alnafessah, Suheer Al-Hadhrami, Mai A Al-Ammar, and Hend S Al-Khalifa. Ultra wideband indoor positioning technologies: analysis and recent advances. *Sensors*, 16(5):707, 2016.

[83] Matteo Ridolfi, Samuel Van de Velde, Heidi Steendam, and Eli De Poorter. Analysis of the scalability of UWB indoor localization solutions for high user densities. *Sensors*, 18(6):1875, 2018.

[84] Nel Samama. *Global positioning: Technologies and performance*, volume 7. John Wiley & Sons, 2008, pages 309–342.

[85] Liwen Dai, Jinling Wang, Chris Rizos, and Shaowei Han. Pseudo-satellite applications in deformation monitoring. *GPS solutions*, 5(3):80–87, 2002.

[86] Alexandre Vervisch Picois and Nel Samama. Near-far interference mitigation for pseudolites using double transmission. *IEEE Transactions on Aerospace and Electronic Systems*, 50(4):2929–2941, 2014.

[87] Rikard Eriksson and Vlad Badea. Indoor navigation with pseudolites (fake GPS sat.) 2005.

[88] Janne Haverinen and Anssi Kemppainen. Global indoor self-localization based on the ambient magnetic field. *Robotics and Autonomous Systems*, 57(10):1028–1035, 2009.

[89] Yuta Nakashima, Ryosuke Kaneto, and Noboru Babaguchi. Indoor positioning system using digital audio watermarking. *IEICE TRANSACTIONS on Information and Systems*, 94(11):2201–2211, 2011.

[90] Faheem Ijaz, Hee Kwon Yang, Arbab Waheed Ahmad, and Chankil Lee. Indoor positioning: a review of indoor ultrasonic positioning systems. In *2013 15th International Conference on Advanced Communications Technology (ICACT)*, pages 1146–1150. IEEE, 2013.

[91] Andy Ward, Alan Jones, and Andy Hopper. A new location technique for the active office. *IEEE Personal communications*, 4(5):42–47, 1997.

[92] Nissanka B Priyantha, Anit Chakraborty, and Hari Balakrishnan. The cricket location-support system. In *Proceedings of the 6th annual international conference on Mobile computing and networking*, pages 32–43, 2000.

[93] Kaikai Liu, Xinxin Liu, and Xiaolin Li. Guoguo: enabling fine-grained indoor localization via smartphone. In *Proceeding of the 11th annual international conference on Mobile systems, applications, and services*, pages 235–248, 2013.

[94] Robert Harle. A survey of indoor inertial positioning systems for pedestrians. *IEEE Communications Surveys & Tutorials*, 15(3):1281–1293, 2013.

[95] Ye-Sheng Kuo, Pat Pannuto, Ko-Jen Hsiao, and Prabal Dutta. Luxapose: indoor positioning with mobile phones and visible light. In *Proceedings of the 20th annual international conference on Mobile computing and networking*, pages 447–458, 2014.

[96] Roy Want, Andy Hopper, Veronica Falcao, and Jonathan Gibbons. The active badge location system. *ACM Transactions on Information Systems (TOIS)*, 10(1):91–102, 1992.

[97] Ernesto Martín Gorostiza, José Luis Lázaro Galilea, Franciso Javier Meca Meca, David Salido Monzú, Felipe Espinosa Zapata, and Luis Pallarés Puerto. Infrared sensor system for mobile-robot positioning in intelligent spaces. *Sensors*, 11(5):5416–5438, 2011.

[98] Sebastian Tilch and Rainer Mautz. Development of a new laser-based, optical indoor positioning system. *International Archives of the Photogrammetry, Remote Sensing and Spatial Information Sciences*, 38(5):575–580, 2010.

[99] Jean Armstrong, Y Ahmet Sekercioglu, and Adrian Neild. Visible light positioning: a roadmap for international standardization. *IEEE Communications Magazine*, 51(12):68–73, 2013.

[100] Huy Q Tran and Cheolkeun Ha. Fingerprint-based indoor positioning system using visible light communication—a novel method for multipath reflections. *Electronics*, 8(1):63, 2019.

[101] Keon Young Yi, Dae Young Kim, and Kwang Moo Yi. Development of a localization system based on vlc technique for an indoor environment. *Journal of Electrical Engineering & Technology*, 10(1):436–442, 2015.

[102] Antoni Rogalski. Infrared detectors: an overview. *Infrared physics & technology*, 43(3-5):187–210, 2002.

[103] Burhan Gulbahar and Ozgur B Akan. A communication theoretical modeling and analysis of underwater magneto-inductive wireless channels. *IEEE Transactions on Wireless Communications*, 11(9):3326–3334, 2012.

[104] Traian E Abrudan, Zhuoling Xiao, Andrew Markham, and Niki Trigoni. Distortion rejecting magneto-inductive three-dimensional localization (MagLoc). *IEEE Journal on Selected Areas in Communications*, 33(11):2404–2417, 2015.

[105] Thomas D Barkand, Nicholas W Damiano, and Wesley A Shumaker. Through-the-earth, two-way, mine emergency, voice communication systems. In *Conference Record of the 2006 IEEE Industry Applications Conference Forty-First IAS Annual Meeting*, volume 2, pages 955–958. IEEE, 2006.

[106] Andrew Markham and Niki Trigoni. Magneto-inductive networked rescue system (MINERS): taking sensor networks underground. In *Proceedings of the 11th international conference on Information Processing in Sensor Networks*, pages 317–328. ACM, 2012.

[107] Xueliang Huo, Jia Wang, and Maysam Ghovanloo. A magneto-inductive sensor based wireless tongue-computer interface. *IEEE transactions on neural systems and rehabilitation engineering*, 16(5):497–504, 2008.

[108] K-N An, MC Jacobsen, LJ Berglund, and EYS Chao. Application of a magnetic tracking device to kinesiologic studies. *Journal of biomechanics*, 21(7):613–620, 1988.

[109] Johann B Hummel, Michael R Bax, Michael L Figl, Yan Kang, Calvin Maurer Jr, Wolfgang W Birkfellner, Helmar Bergmann, and Ramin Shahidi. Design and application of an assessment protocol for electromagnetic tracking systems. *Medical physics*, 32(7Part1):2371–2379, 2005.

[110] Huiru Zheng, Norman D Black, and Nigel D Harris. Position-sensing technologies for movement analysis in stroke rehabilitation. *Medical and biological engineering and computing*, 43(4):413–420, 2005.

[111] Indira Chatterjee, Yong-Gong Gu, and Om P Gandhi. Quantification of electromagnetic absorption in humans from body-mounted communication transceivers. *IEEE transactions on vehicular technology*, 34(2):55–62, 1985.

[112] Niels Kuster and Quirino Balzano. Energy absorption mechanism by biological bodies in the near field of dipole antennas above 300 MHz. *IEEE Transactions on vehicular technology*, 41(1):17–23, 1992.

[113] Brian K Lickfelt. Method to track vehicle key near vehicle for smart entry, April 2012. US Patent App. 12/907,198.

[114] Riad Ghabra and Craig Elder. Passive entry passive start systems employing consumer mobile devices as portable remote control units, October 2018. US Patent 10,091,633.

[115] Baldassare Di Bartolo. *Classical Theory of Electromagnetism: with Companion Solution Manual Second Edition*. World Scientific Publishing Company, 2004, pages 170–171.

[116] Christos G Christodoulou and Parveen F Wahid. *Fundamentals of antennas: concepts and applications*, volume 50. SPIE Press, 2001, pages 13–14.

[117] Occupational Safety and Cincinnati Technical Center Health Administration. Electromagnetic radiation and how it affects your instruments. *Near-Field vs. Far-Field*, 1990.

[118] John David Jackson. Classical electrodynamics 3rd edition. *Cited on*:181–183, 1998.

[119] John J Sojdehei, Paul N Wrathall, and Donald F Dinn. Magneto-inductive (MI) communications. In *MTS/IEEE Oceans 2001. An Ocean Odyssey. Conference Proceedings (IEEE Cat. No. 01CH37295)*, volume 1, pages 513–519. IEEE, 2001.

[120] Traian E Abrudan, Orfeas Kypris, Niki Trigoni, and Andrew Markham. Impact of rocks and minerals on underground magneto-inductive communication and localization. *IEEE Access*, 4:3999–4010, 2016.

[121] Steven R Best. Optimizing the receiving properties of electrically small HF antennas. *URSI Radio Science Bulletin*, 2016(359):13–29, 2016.

[122] Slawomir Tumanski. Induction coil sensors—a review. *Measurement Science and Technology*, 18(3):R31, 2007.

[123] European Telecommunications Standards Institute. European standard ETSI EN 300 330 v2.1.1.

[124] Frederick H Raab, Ernest B Blood, Terry O Steiner, and Herbert R Jones. Magnetic position and orientation tracking system. *IEEE Transactions on Aerospace and Electronic systems*, (5):709–718, 1979.

[125] Christian Metzger, Alexander Ilic, Philippe Bourquin, Florian Michahelles, and Elgar Fleisch. Distance-sensitive high frequency RFID systems. In *2008 Third International Conference on Pervasive Computing and Applications*, volume 2, pages 729–734. IEEE, 2008.

[126] Kenichi Ohara, Yuji Abe, Tomohito Takubo, Yasushi Mae, Tamio Tanikawa, and Tatsuo Arai. Range estimation technique using received signal strength indication on low frequency waves. *Journal of Robotics and Mechatronics*, 23(4):466–474, 2011.

[127] Valter Pasku, Alessio De Angelis, Marco Dionigi, Antonio Moschitta, Guido De Angelis, and Paolo Carbone. Analysis of nonideal effects and performance in magnetic positioning systems. *IEEE Transactions on Instrumentation and Measurement*, 65(12):2816–2827, 2016.

[128] P Ripka and J Humr. Inductive distance sensor for biomedical applications. In *SENSORS, 2008 IEEE*, pages 1230–1232. IEEE, 2008.

[129] Andrew Markham, Niki Trigoni, Stephen A Ellwood, and David W Macdonald. Revealing the hidden lives of underground animals using magneto-inductive tracking. In *Proceedings of the 8th ACM Conference on Embedded Networked Sensor Systems*, pages 281–294. ACM, 2010.

[130] DD Arumugam, JD Griffin, DD Stancil, and DS Ricketts. Two-dimensional position measurement using magnetoquasistatic fields. In *2011 IEEE-APS Topical Conference on Antennas and Propagation in Wireless Communications*, pages 1193–1196. IEEE, 2011.

[131] Darmindra D Arumugam, Joshua D Griffin, Daniel D Stancil, and David S Ricketts. Three-dimensional position and orientation measurements using magnetoquasistatic fields and complex image theory [measurements corner]. *IEEE Antennas and Propagation Magazine*, 56(1):160–173, 2014.

[132] Arie Sheinker, Boris Ginzburg, Nizan Salomonski, Lev Frumkis, and Ben-Zion Kaplan. Localization in 2D using beacons of low frequency magnetic field. *IEEE Journal of Selected Topics in Applied Earth Observations and Remote Sensing*, 6(2):1020–1030, 2012.

[133] Valter Pasku, Alessio De Angelis, Marco Dionigi, Guido De Angelis, Antonio Moschitta, and Paolo Carbone. A positioning system based on low-frequency magnetic fields. *IEEE Transactions on Industrial Electronics*, 63(4):2457–2468, 2015.

[134] Arie Sheinker, Boris Ginzburg, Nizan Salomonski, Lev Frumkis, and Ben-Zion Kaplan. Localization in 3-D using beacons of low frequency magnetic field. *IEEE transactions on instrumentation and measurement*, 62(12):3194–3201, 2013.

[135] Niki Trigoni. Underground localization in 3-D using magneto- inductive tracking. *IEEE Sensors Journal*, 12, 2012.

[136] Jörg Blankenbach and Abdelmoumen Norrdine. Position estimation using artificial generated magnetic fields. In *2010 International Conference on Indoor Positioning and Indoor Navigation*, pages 1–5. IEEE, 2010.

[137] Vighnesh Gharat, Geneviève Baudoin, Elizabeth Colin, and Damien Richard. Low frequency RFID system for identification and localization in smart cities-comparison with uhf rfid. *International Journal of RF Technologies*, 8(4):191–211, 2017.

[138] Eric A Prigge and Jonathan P How. Signal architecture for a distributed magnetic local positioning system. *IEEE sensors journal*, 4(6):864–873, 2004.

[139] Bo H Choi, Eun S Lee, Ji H Kim, and Chun T Rim. 7m-off-long-distance extremely loosely coupled inductive power transfer systems using dipole coils. In *2014 IEEE Energy Conversion Congress and Exposition (ECCE)*, pages 858–563. IEEE, 2014.

[140] Gustavo Theodoro Laskoski, Sérgio Francisco Pichorim, and Paulo José Abatti. Distance measurement with inductive coils. *IEEE Sensors Journal*, 12(6):2237–2242, 2012.

[141] JD Brunett and VV Liepa. Near field measurement of LF loop transmitters. In *2004 International Symposium on Electromagnetic Compatibility (IEEE Cat. No. 04CH37559)*, volume 2, pages 367–371. IEEE, 2004.

[142] Evgueni Kaverine, Sebastien Palud, Franck Colombel, and Mohamed Himdi. Investigation on an effective magnetic permeability of the rod-shaped ferrites. *Progress In Electromagnetics Research*, 65:43–48, 2017.

[143] Klaus Finkenzeller. *RFID handbook: fundamentals and applications in contactless smart cards, radio frequency identification and near-field communication*. John Wiley & Sons, 2010, pages 68–70.

[144] R Belmans and K Hameyer. Electrical energy. basics and applications; elektrische energie. fundamenten en toepassingen, 1999.

[145] *RSSI to Voltage Conversion*. (AS3933). Application Note v1-01. ams. July 2011.

[146] Niaz Ahmed, Y Rosa Zheng, and David Pommerenke. Theoretical modeling of multi-coil channels in near field magneto-inductive communication. In *2015 IEEE 82nd Vehicular Technology Conference (VTC2015-Fall)*, pages 1–5. IEEE, 2015.

[147] Orfeas Kypris, Traian E Abrudan, and Andrew Markham. Magnetic induction-based positioning in distorted environments. *IEEE Transactions on Geoscience and Remote Sensing*, 54(8):4605–4612, 2016.

[148] Johnson Ihyeh Agbinya. Investigation of near field inductive communication system models, channels and experiments. *Progress In Electromagnetics Research*, 49:129–153, 2013.

[149] Computer simulation technology–EMCoS antenna VLab. `https://www.emcos.com/?products=emcos-antenna-vla`. Accessed: March 2020.

[150] Walton C Gibson. *The method of moments in electromagnetics*. CRC press, 2014.

[151] *SMD 3D Coil - 3-Axis Transponder Inductor*. (3DC15F). General Catalogue. Premo. 2018.

[152] Ansys Q3D extractor. `https://www.ansys.com/products/electronics/ansys-q3d-extractor`. Accessed: March 2020.

[153] Tim Williams. *EMC for product designers*. Newnes, 2016.

[154] LTspice. `https://www.analog.com/en/design-center/design-tools-and-calculators/ltspice-simulator.html`. Accessed: March 2020.

[155] Tapan K Sarkar, Zhong Ji, Kyungjung Kim, Abdellatif Medouri, and Magdalena Salazar-Palma. A survey of various propagation models for mobile communication. *IEEE Antennas and propagation Magazine*, 45(3):51–82, 2003.

[156] Paula Tarrio, Ana M Bernardos, and Jose R Casar. An RSS localization method based on parametric channel models. In *2007 International Conference on Sensor Technologies and Applications (SENSORCOMM 2007)*, pages 265–270. IEEE, 2007.

[157] Kaj Madsen, Hans Bruun Nielsen, and Ole Tingleff. Methods for non-linear least squares problems, 2004.

[158] Andreas Fink and Helmut Beikirch. Analysis of RSS-based location estimation techniques in fading environments. In *2011 International Conference on Indoor Positioning and Indoor Navigation*, pages 1–6. IEEE, 2011.

[159] Abdelmoumen Norrdine. An algebraic solution to the multilateration problem. In *Proceedings of the 15th international conference on indoor positioning and indoor navigation, Sydney, Australia*, volume 1315, 2012.

[160] Antonio Ramón Jiménez Ruiz and Fernando Seco Granja. Comparing Ubisense, Bespoon, and Decawave UWB location systems: indoor performance analysis. *IEEE Transactions on instrumentation and Measurement*, 66(8):2106–2117, 2017.

[161] Andreas Fink and Helmut Beikirch. Refinement of weighted centroid localization using a regular infrastructure topology. In *2014 International Conference on Indoor Positioning and Indoor Navigation (IPIN)*, pages 501–510. IEEE, 2014.

[162] Heiner Lasi, Peter Fettke, Hans-Georg Kemper, Thomas Feld, and Michael Hoffmann. Industry 4.0. *Business & information systems engineering*, 6(4):239–242, 2014.

[163] P Lopes, M Pino, G Carletti, S Hamidi, S Legué, H Kerhervé, S Benveniste, G Andéol, P Bonsom, S Reingewirtz, et al. Co-conception process of an innovative assistive device to track and find misplaced everyday objects for older adults with cognitive impairment: the TROUVE project. *IRBM*, 37(2):52–57, 2016.

[164] Quuppa intelligent locating system. `https://quuppa.com/technology/overview/`. Accessed: March 2020.

[165] Kimmo Kalliola and Quuppa Oy. Locating anything anywhere, 2013.

Titre: Système magnéto-inductif d'estimation de distance en champ proche très faiblement couplé : modélisation et applications

Mots Clés : Estimation de distance, BF, *NFMI*, systèmes très faiblement couplé, champs magnétiques quasi-statiques, mesures d'intensité de champ magnétique.

Résumé : L'estimation de distances, basée sur la mesure de l'intensité de couplage magnéto-inductif entre deux bobines, est fortement limitée en étendue de mesure et trouve donc peu d'applications pratiques. Toutefois, ce principe de mesure est simple à mettre en œuvre, faible coût et peu consommateur d'énergie. L'utilisation de bobines plus grandes peut permettre d'étendre la zone de mesure mais va à l'encontre des besoins courants de miniaturisation et de simplicité de déploiement. Cette thèse se concentre donc sur la modélisation analytique et l'investigation expérimentales de tels systèmes afin d'optimiser leur étendue de mesure, leur précision, leur complexité et leur coût tout en concevant des facteurs de forme et des autonomies énergétiques compétitifs.

Title: Extremely Loosely Coupled Near-Field Magneto-Inductive Ranging System: Modeling and Applications

Keywords: Ranging, LF, NFMI, extremely loosely coupled systems, quasi-static magnetic fields, magnetic field strength measurements.

Abstract: Distance estimation or ranging, based on the measurement of the magneto inductive coupling intensity between the two coils, is highly limited in terms of operational range and therefore has few practical applications. However, this kind of ranging remains simple to implement, low cost and energy efficient. The use of larger coils can increase the operating range, but it goes against the common needs of miniaturization and ease-of-deployment. This thesis therefore focuses on the analytical modeling and experimental investigation of such systems in order to optimize their operational range, accuracy, complexity and cost while maintaining competitive form factors and energy consumption.